# Chapter 5

# Corundum Oxide Passivation of Aluminium and Steel

## 5.1 Abstract

Atomic scale computer simulation was used to predict the mechanisms and energies associated with the accommodation of an extensive range of aliovalent and isovalent dopants in three host oxides with the corundum structure. These host oxides are known to form at least part of the corrosion product on the most common industrial materials (aluminium and steels) in typical operating environments. Comparison of calculated mechanism energetics predict that divalent ions are charge compensated by oxygen vacancies and tetravalent ions by cation vacancies. At equilibrium, defects resulting from extrinsic dopant solution dominate intrinsic processes, except for the largest dopant cations. Solution reaction energies increase markedly with increasing dopant radius so that only dopant cations with ion sizes very similar to the lattice will exhibit any substantial solubility. As such even at ppm levels, large ions may be expected to come out of solution and form a second phase.

## 5.2 Introduction

In this chapter the approach laid out in chapter 4 is extended to a more complex set of systems. Thus, the extent to which this methodology can be applied to major industrial applications is tested.

The majority of metallic artifacts are produced from either aluminium or steel. A detailed understanding of the corrosion products formed on these materials is of great interest. In the case of aluminium, a passive $\alpha$-$Al_2O_3$ film forms which exhibits strong bonding with the surface and imparts good corrosion resistance [68]. Stainless steel forms an oxide surface with a structure which is still debated but undoubtedly provides effective protection [69]. In the case of iron and low chromium steels various iron oxides form but impart at best only modest corrosion protection [70].

A scenario where these metals all form a cohesive corundum oxide is considered. In addition to aluminium alloys this, is ultimately the case in many Fe-Cr alloys in the absence of water at high temperature. However, a continuous $Cr_2O_3$ scale is only formed when the Cr content is above 18 wt% [71]. Below this content the scale contains iron oxides that include $\alpha$-$Fe_2O_3$ [72], as is the case in iron and low chromium steels [73].

Using computer simulation, solution mechanisms and relative equilibrium concentrations for possible alloy additions into the perfect lattices of $\alpha$-$Al_2O_3$, $\alpha$-$Cr_2O_3$ and $\alpha$-$Fe_2O_3$ are predicted. This data allows a qualitative understanding of the relative importance of different impurity additions on the formation of those ionic defects (vacancies or interstitials) which, in a passive layer, could be responsible for ion transport. Furthermore, prediction of which impurity ions, at their equilibrium concentrations, will generate more vacancies or interstitial ions than the corresponding intrinsic reactions are made. Since impurities will be present via diffusion or film growth from the underlying alloy which is being protected, it is vital to understand how important such defect impurities are in these components of the

passive surface and, in particular, compare these three bulk oxides.

In contrast to chapter 4, simulation of migration activation energies and mechanisms in the host lattices was not attempted. Such a study could be undertaken separately and would complement the currently available literature. It should be noted that experience gained with the $NiF_2$ system suggests that such a study would be no small undertaking.

### 5.2.1 Crystallography

The host lattices considered are $\alpha$-$Al_2O_3$, $\alpha$-$Cr_2O_3$ and $\alpha$-$Fe_2O_3$. All exhibit the hexagonal corundum structure (space group $R\overline{3}c$) shown in figure 5.1. In this structure cations occupy the 12$c$ sites and oxygen ions the 18$e$ sites. An important 6b interstitial site exists between alternate pairs of cations, seen at the centre of the cation column in figure 5.1. Two positional parameters $u$ and $v$ are needed to define the structure and are given in table 5.1.

**Table 5.1:** Host corundum lattice parameters, calculated and experimental [74–76].

| Parameter | | $Al_2O_3$ | $Cr_2O_3$ | $Fe_2O_3$ |
|---|---|---|---|---|
| a (Å) | *expt.* | 4.76050 | 4.9570 | 5.0206 |
| | *calc.* | 4.784 | 5.038 | 5.051 |
| c (Å) | *expt.* | 13.003 | 13.5923 | 13.7196 |
| | *calc.* | 12.9956 | 13.328 | 13.345 |
| Vol. (Å$^3$) | *expt.* | 255.467 | 289.242 | 299.491 |
| | *calc.* | 255.054 | 292.992 | 294.921 |
| $u$ | | 0.352 | 0.3475 | 0.355 |
| $v$ | | 0.306 | 0.306 | 0.300 |

### 5.2.2 Defects and Transport in Corundum Oxides

The significance of the defect and transport properties of surface oxides to the corrosion resistance of alloys has been widely recognised in the literature [73, 77–82], with much of

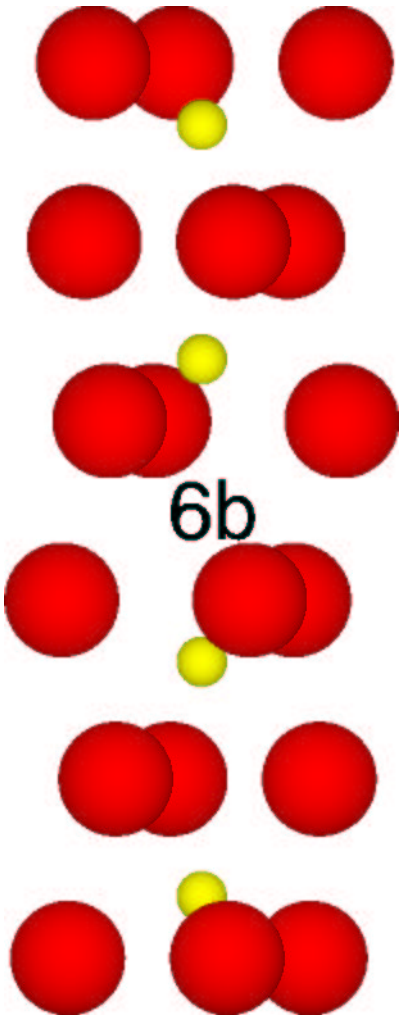


**Figure 5.1:** Representation of the corundum structure, large red spheres represent oxygen ions on 18*e* sites and small yellow spheres $M^{3+}$ cations on 12*c* sites. The 6*b* site is also identified.

the older work reviewed by Kofstad [83]. Several computational studies have also been conducted in this area [37, 63, 84–88], some of which have considered impurity defects. Here such work is extended by modelling the behaviour of a wide range of possible dopant cation species (for the time being potentially aggressive $Cl^-$ or $S^{2-}$ ions have not been considered, although these could eventually also be modelled). Since modelling studies ideally complement experimental work, the literature is first reviewed.

#### 5.2.2.1 Defects and Transport in $\alpha$-$Al_2O_3$

Even in quite recent studies the defect chemistry of $\alpha$-$Al_2O_3$ has not been resolved. Experimental and theoretical studies concerning the dominant intrinsic disorder are found to be inconclusive [37, 63, 89, 90]. Where a preference is stated it is for Schottky disorder [84, 91] but usually only by a small margin. All studies agree, however, that the cation Frenkel process is of sufficiently high energy that it does not to play an important role. Thus, it seems impractical to separate the Schottky and Anion Frenkel processes. It seems likely that the conclusion of El-Aiat and Kröger [89], which states that it is not possible, experimentally, to categorically differentiate between these mechanisms, is probably valid. No appreciable nonstoichiometry is observed in $\alpha$-$Al_2O_3$ [83].

Studies of oxygen self-diffusion [92–94] as well as aluminium self-diffusion [77–79] show that Al is the more mobile species. Aluminium ions are thought to diffuse via a vacancy mechanism. The incorporation of dopants has also been studied with respect to their effect on oxygen self-diffusion. Crawley *et al.* [92] maintain that there is no dopant effect but Lagerlöf *et al.* [95, 96] and Haneda *et al.* [97] find that magnesium doping increases the diffusion rate while titanium doping decreases it. Interestingly Perot-Ervas *et al.* [77] claim that, at high $p_{O_2}$, titanium doping is compensated by the formation of aluminium vacancies, in agreement with previous studies by Mohapatra and Kröger [98] and Rassmussen and Kingery [99]. The charge compensating defect accompanying

solution of $Mg^{2+}$ is less clear with both oxygen vacancies and aluminium interstitials having been considered by some [100] but only oxygen vacancies by others [97]. The possibility of magnesium interstitial compensation has been proposed from modelling studies [37].

#### 5.2.2.2 Defects and Transport in $\alpha$-$Cr_2O_3$

Crawford and Vest [101] suggest that $\alpha$-$Cr_2O_3$ is an intrinsic electronic conductor at high temperatures and a structural defect controlled conductor at low temperatures. $\alpha$-$Cr_2O_3$ is not thought to exhibit any great nonstoichiometry although experiments have proved difficult. The atomistic simulation study of Lawrence *et al.* [86] predict that either Schottky or anion Frenkel disorder dominates, depending on whether they use an empirical or non-empirical potential set.

The literature suggests that Cr is the mobile species [80, 101, 102], however, the mechanism is disputed (compare [102] with [80]). Interestingly Hagel and Seybolt [81] determined that doping of $\alpha$-$Cr_2O_3$ with $CeO_2$ or $Y_2O_3$ has very little effect on cation diffusion rates. While $Y^{3+}$ is an isovalent dopant, $Ce^{4+}$ ions would require charge compensation in a $\alpha$-$Cr_2O_3$ lattice. On the other hand, it may be that in $\alpha$-$Cr_2O_3$ the cerium ion assumes a 3+ charge state.

#### 5.2.2.3 Defects and Transport in $\alpha$-$Fe_2O_3$

While it is generally accepted that $\alpha$-$Fe_2O_3$ is an intrinsic-semiconductor at high temperature [103], it also exhibits nonstoichiometry associated with oxygen vacancy formation [104]. Thus, the dominant defect type depends upon $p_{O_2}$ and temperature. For example, at high temperature Hoshino and Peterson [105] initially report lattice defects to be more important than intrinsic electronic defects. However, they later changed their conclusions [106] in line with Chang and Wagner [103], who found that intrinsic electronic defects dominate at high temperature.

It is reported that the diffusivity of cations decreases with increasing $p_{O_2}$ [103, 106] which leads to the conclusion that cation interstitial diffusion is responsible for lattice transport [82, 83, 103, 105, 106]. The charge state of the migrating species is debatable since it has been suggested that the interstitial ion migrates as $Fe_i^{\bullet\bullet}$ in preference to $Fe_i^{\bullet\bullet\bullet}$ [105, 106]. There also appears to be great variation in the absolute values of diffusivity and activation enthalpy for self-diffusion [103, 106] although Atkinson and Taylor [82] have applied corrections to published data, achieving good agreement across several types of experimental methodology. Some investigators comment on variations in results between samples thought to be due to different impurity concentrations [105, 106].

Although the review of the literature presented here is brief, it is clear that these three isostructural oxides present a remarkably complex defect chemistry. The aim is therefore to provide a set of defect energies for selected dopant cations that predict how the solution mechanisms will change as a function of dopant cation radius. Such general trends, rather than absolute energies, will be particularly amenable to experimental investigation.

### 5.2.3 Simulation

The simulations were carried out using the CASCADE [59] simulation code and the methodology used is discussed in chapter 3. As such, this chapter follows a similar framework to chapter 4. Most short-range potential parameters for host and dopant ions were taken from the literature as detailed in chapter 3. The validity of the potentials in reproducing the lattice parameters of the host oxides is seen in table 5.1.

## 5.3 Defect Chemistry

### 5.3.1 Defect Process Model and Equations

Possible intrinsic defect process reactions are required. Additionally, possible reactions that describe solution of a range of 2+, 3+ and 4+ cation binary oxides into the host corundum lattices must also be determined. Solution is assumed to proceed via cation substitution onto a cation 12c site. For the 2+ and 4+ cations ionic charge compensation is required and this is considered via several available mechanisms. Both isolated and neutral defect clusters are investigated in charge compensated solution mechanisms.

Reactions 5.1-5.10 detail the important defect processes for these systems where M denotes the host lattice cation ($Al^{3+}$, $Cr^{3+}$ or $Fe^{3+}$). The intrinsic Schottky (reaction 5.1), interstitial (reaction 5.2), anion Frenkel (reaction 5.3) and cation Frenkel (reaction 5.4) processes are considered. The isovalent solution process (reaction 5.5) is used for 3+ cation incorporation where no charge compensation is required. In the case of 2+ aliovalent cation solution three compensation processes are considered: dopant interstitial (reaction 5.6), interstitial (reaction 5.7) and vacancy (reaction 5.8). For 4+ aliovalent cation solution two compensation processes are considered: interstitial (reaction 5.9) and vacancy (reaction 5.10).

**Intrinsic Defect Reactions:**

$$2M_M^{\times} + 3O_O^{\times} \rightleftharpoons 2V_M''' + 3V_O^{\bullet\bullet} + M_2O_3 \tag{5.1}$$

$$M_2O_3 \rightleftharpoons 2M_i^{\bullet\bullet\bullet} + 3O_i'' \tag{5.2}$$

$$O_O^{\times} \rightleftharpoons V_O^{\bullet\bullet} + O_i'' \tag{5.3}$$

$$M_M^{\times} \rightleftharpoons V_M''' + M_i^{\bullet\bullet\bullet} \tag{5.4}$$

The process in reaction 5.2 is not normally considered as an intrinsic defect mecha-

nism as it is a combination of the other three mechanisms. However since it was explicitly included by El-Aiat and Kröger [89] when they studied intrinsic defects in α-$Al_2O_3$ it is included here for completeness. (Results in table 5.6 shows that the predicted energy for reaction 5.2 is actually similar to that for the cation Frenkel reaction 5.4.)

For the next sets of reactions each is described with respect to isolated defects followed by the same reaction assuming neutral defect cluster formation.

**Isovalent Solution Reaction:**

$$C_2O_3 + 2M_M^\times \rightleftharpoons 2C_M^\times + M_2O_3 \tag{5.5}$$

**Aliovalent Solution Reactions:**

$$\begin{aligned} 3BO + 2M_M^\times &\rightleftharpoons 2B_M' + B_i^{\bullet\bullet} + M_2O_3 \\ &\rightleftharpoons \{2B_M' : B_i^{\bullet\bullet}\}^\times + M_2O_3 \end{aligned} \tag{5.6}$$

$$\begin{aligned} 3BO + 3M_M^\times &\rightleftharpoons 3B_M' + M_i^{\bullet\bullet\bullet} + M_2O_3 \\ &\rightleftharpoons \{3B_M' : M_i^{\bullet\bullet\bullet}\}^\times + M_2O_3 \end{aligned} \tag{5.7}$$

$$\begin{aligned} 2BO + 2M_M^\times + O_O^\times &\rightleftharpoons 2B_M' + V_O^{\bullet\bullet} + M_2O_3 \\ &\rightleftharpoons \{2B_M' : V_O^{\bullet\bullet}\}^\times + M_2O_3 \end{aligned} \tag{5.8}$$

$$\begin{aligned} 2DO_2 + 2M_M^\times &\rightleftharpoons 2D_M^\bullet + O_i'' + M_2O_3 \\ &\rightleftharpoons \{2D_M^\bullet : O_i''\}^\times + M_2O_3 \end{aligned} \tag{5.9}$$

$$\begin{aligned} 3DO_2 + 4M_M^\times &\rightleftharpoons 3D_M^\bullet + V_M''' + 2M_2O_3 \\ &\rightleftharpoons \{3D_M^\bullet : V_M'''\}^\times + 2M_2O_3 \end{aligned} \tag{5.10}$$

The various defect equilibria detailed above allow a simple assessment of the general effect aliovalent dopants will have on the intrinsic defect concentrations. This is summarised in tables 5.2 and 5.3. Of course, exactly which mechanism dominates will depend

on the relative solution energies for each mechanism. Defect clusters, also detailed above, may also play an important role in determining the most favourable mechanism. Computer simulations are thus specifically designed to evaluate such energies.

**Table 5.2:** Relative change in concentration of important defects due to incorporation of 2+ ions.

| Equation | Dopant Species | | Intrinsic Species | | | |
|---|---|---|---|---|---|---|
| | $B'_M$ | $B_i^{\bullet\bullet}$ | $M_i^{\bullet\bullet\bullet}$ | $V_M'''$ | $O_i''$ | $V_O^{\bullet\bullet}$ |
| 5.6 | ↑ | ↑ | - | - | - | - |
| 5.7 | ↑ | - | ↑ | ↓ | ↓ | ↑ |
| 5.8 | ↑ | - | ↑ | ↓ | ↓ | ↑ |

**Table 5.3:** Relative change in concentration of important defects due to incorporation of 4+ ions.

| Equation | Dopant Species | | Intrinsic Species | | | |
|---|---|---|---|---|---|---|
| | $D_M^{\bullet}$ | $D_i^{\bullet\bullet}$ | $M_i^{\bullet\bullet\bullet}$ | $V_M'''$ | $O_i''$ | $V_O^{\bullet\bullet}$ |
| 5.9 | ↑ | - | ↓ | ↑ | ↑ | ↓ |
| 5.10 | ↑ | - | ↓ | ↑ | ↑ | ↓ |

Table 5.2 details the expected change in defect concentrations if the concentration of divalent solution defects, $B'_M$, increases. In reaction 5.6 the intrinsic defect concentrations are unchanged since compensation is by dopant interstitials, $B_i^{\bullet\bullet}$. Thus, the dopant interstitial concentration is expected to increase. In equation 5.7 compensation is via host cation interstitials. Consequently, the cation Frenkel equilibrium will act to reduce the cation vacancy concentration; leading to the Schottky equilibrium acting to increase the oxygen vacancy concentration; and finally, via the Schottky equilibrium, the oxygen interstitial concentration is reduced. In equation 5.8 compensation is via oxygen vacancies. Consequently, the anion Frenkel equilibrium will act to reduce the oxygen interstitial concentration and also the Schottky equilibrium will act to decrease the cation vacancy concentration; subsequently the cation Frenkel reaction will act to increase the

cation interstitial concentration.

Table 5.2 details the expected change in defect concentration if the concentration of tetravalent solution defects, $D_M^{\bullet}$, increases. In reaction 5.9 compensation is via oxygen interstitials. Consequently, the anion Frenkel equilibrium acts to reduce the oxygen vacancy concentration; leading to an increase in the cation vacancy concentration, via the Schottky equilibrium; and finally the cation Frenkel equilibrium will act to reduce the cation interstitial concentration. In equation 5.10 compensation is via cation vacancies which will act to decrease the cation interstitial concentration, via the cation Frenkel equilibrium, and also reduce the oxygen vacancy concentration, through the Schottky equilibrium; this will in turn increase the oxygen interstitial concentration via the anion Frenkel equilibrium.

Naturally dopants of the same valence have the same mechanistic effect on the intrinsic defect equilibria. Thus, an important question is whether these extrinsic defect processes will dominate the intrinsic defect processes. This depends on the magnitude of the solution energy processes compared to the energies of the intrinsic defect processes.

### 5.3.2 Normalisation of Defect Reaction Energies

One stated aim of this study is to predict, for each dopant, the mechanism by which it is incorporated into the lattice, assuming equilibrium (but without, at this stage, recourse to compensation via electronic defects). It is therefore not sufficient to report the total intrinsic energies for reactions 5.1-5.4 or the total solution energies for reactions 5.6-5.10. In each case, the reaction energies must be normalised by a factor derived from a mass action analysis [63, 64].

Consider first the intrinsic Schottky disorder, reaction 5.1, the corresponding mass action equation is,

$$[V_M^{\prime\prime\prime}]^2[V_O^{\bullet\bullet}]^3 = e^{\frac{-\Delta H_{sh}}{kT}} \tag{5.11}$$

where $\Delta H_{sh}$ is the predicted energy for reaction 5.1, $k$ is the Boltzmann constant and $T$ is the temperature. Note that terms such as the concentration of oxygen sites, $[O_O^{\times}]$, are all approximately unity and have therefore not been included for brevity. If the Schottky reaction is dominant then the electroneutrality condition is,

$$3[V_M'''] = 2[V_O^{\bullet\bullet}] \tag{5.12}$$

Substitution of equation 5.12 into equation 5.11 yields,

$$[V_M'''] = \left(\frac{2}{3}\right)^{\frac{3}{5}} e^{\frac{-\Delta H_{sh}}{5kT}} \tag{5.13}$$

and,

$$[V_O^{\bullet\bullet}] = \left(\frac{3}{2}\right)^{\frac{2}{5}} e^{\frac{-\Delta H_{sh}}{5kT}} \tag{5.14}$$

The Schottky energy is therefore normalised by a factor 5 (as is the intrinsic interstitial reaction 5.2). Similarly anion Frenkel disorder, reaction 5.3, is normalised by a factor 3 (as is the cation Frenkel reaction 5.4).

The analysis for solution reactions 5.6-5.10 is similar. For example, solution of $B^{2+}$ ions via reaction 5.8 yields the corresponding mass action equation,

$$[B_M']^2[V_O^{\bullet\bullet}] = e^{\frac{-\Delta H_{sol(5.8)}}{kT}} \tag{5.15}$$

where $\Delta H_{sol(5.8)}$ is the predicted energy for reaction 5.8. If this is the dominant solution mechanism then the electroneutrality condition is,

$$[B_M'] = 2[V_O^{\bullet\bullet}] \tag{5.16}$$

Substitution of equation 5.16 into equation 5.15 yields,

$$[B_M'] = 2e^{\frac{-\Delta H_{sol(5.8)}}{3kT}} \tag{5.17}$$

and,

$$[V_O^{\bullet\bullet}] = 4^{\frac{-1}{3}} e^{\frac{-\Delta H_{sol(5.8)}}{3kT}} \tag{5.18}$$

Therefore the predicted energy for reaction 5.8 must be normalised by a factor of 3. Similar analysis yields factors of 3 for reaction 5.6 and 4 for reaction 5.7.

When considering solution of tetravalent, $D^{4+}$, ions, reaction 5.10 yields the corresponding mass action reaction,

$$[D_M^{\bullet}]^3[V_M^{'''}] = e^{\frac{-\Delta H_{sol(5.10)}}{kT}} \tag{5.19}$$

where $\Delta H_{sol(5.10)}$ is the predicted energy for reaction 5.10. If this is the dominant solution mechanism then the electroneutrality condition is,

$$[D_M^{\bullet}] = 3[V_M^{'''}] \tag{5.20}$$

Substitution of equation 5.20 into equation 5.19 yields,

$$[D_M^{\bullet}] = 3^{\frac{1}{4}} e^{\frac{-\Delta H_{sol(5.10)}}{4kT}} \tag{5.21}$$

and,

$$[V_M^{'''}] = 3^{\frac{-3}{4}} e^{\frac{-\Delta H_{sol(5.10)}}{4kT}} \tag{5.22}$$

so that reaction 5.10 is normalised by a factor of 4. Through similar analysis reaction 5.9 is normalised by a factor of 3.

Finally for isovalent solution of $C^{3+}$ ions, a mass action analysis yields a normalisation factor of 2.

### 5.3.3 Cluster Geometries

For all the clusters studied, substitutional defects surround a single compensating defect (see reactions 5.6-5.10). These five aliovalent mechanisms give rise to four sets of cluster arrangements which are detailed A-D in table 5.4. The alphanumeric geometry codes can be used in conjunction with table 5.5 to fully define the spatial coordinates of all the defects in any given cluster. Wychoff style coordinates are given in table 5.5 so that these clusters

may be easily reproduced in any corundum lattice. The origin for these coordinates is the 6b interstitial site.

#### 5.3.3.1 Divalent Dopant Interstitial Clusters

In this solution mechanism a dopant interstitial will compensate the solution of two divalent substitutional defects, $\{2B'_M{:}B_i^{\bullet\bullet}\}$. The interstitial, $B_i^{\bullet\bullet}$ ion, is at (0,0,0) and the compensated substitutional ions, $B'_M$, are arranged as in geometry listing A of table 5.4.

#### 5.3.3.2 Divalent Interstitial Clusters

In this solution mechanism a host cation interstitial ion will compensate the solution of three divalent substitutional defects, $\{3B'_M{:}M_i^{\bullet\bullet\bullet}\}$. The interstitial ion, $M_i^{\bullet\bullet\bullet}$, is at (0,0,0) and the compensated substitutional ions, $B'_M$, are arranged as in geometry listing B of table 5.4.

#### 5.3.3.3 Divalent Vacancy Clusters

In this solution mechanism a host oxygen vacancy will compensate the solution of two divalent substitutional defects, $\{2B'_M{:}V_O^{\bullet\bullet}\}$. The vacancy, $V_O^{\bullet\bullet}$, is at ($v$,0,$\frac{1}{4}$) and the compensated substitutional ions, $B'_M$, are arranged as in geometry listing C of table 5.4.

#### 5.3.3.4 Tetravalent Interstitial Clusters

In this solution mechanism a host oxygen interstitial ion will compensate the solution of two tetravalent substitutional defects, $\{2D_M^{\bullet}{:}O_i''\}$. The interstitial ion, $O_i''$, is at (0,0,0) and the compensated substitutional ions, $D_M^{\bullet}$, are arranged as in geometry listing A of table 5.4.

**Table 5.4:** Tables of cluster geometry in the corundum $M_2O_3$.

| Geometry A | |
|---|---|
| Cluster | Geometry |
| 1-1a | B1-C1 |
| 1-2a | B1-B2 |
| 1-2b | B1-B3 |
| 1-3a | B1-C2 |
| 1-3b | B1-A3 |
| 1-4a | B1-A1 |
| 1-4b | B1-D1 |
| 2-2a | B2-B3 |
| 2-2b | B2-B4 |
| 2-2c | B3-B5 |
| 2-3a | B2-C2 |
| 2-3b | B2-C4 |
| 2-3c | B3-A3 |
| 2-3d | B3-A5 |
| 2-4a | B2-A1 |
| 2-4b | B2-D1 |
| 3-3a | C2-C4 |
| 3-3b | C2-A3 |
| 3-3c | C2-A5 |
| 3-4a | C2-A1 |
| 3-4b | C2-D1 |
| 4-4a | A1-D1 |

| Geometry B | |
|---|---|
| Cluster | Geometry |
| 1-1-2a | B1-C1-B2 |
| 1-1-3a | B1-C1-C2 |
| 1-2-2a | B1-B2-B3 |
| 1-2-2b | B1-B2-B5 |
| 1-2-2c | B1-B2-B4 |
| 1-2-2d | B1-B3-B5 |
| 1-2-3a | B1-B2-C2 |
| 1-2-3b | B1-B2-C4 |
| 1-2-3c | B1-B2-A3 |
| 1-2-3d | B1-B2-A5 |
| 1-2-3e | B1-B3-C2 |
| 1-2-3f | B1-B4-C4 |
| 1-2-3g | B1-B5-A3 |
| 1-2-3h | B1-B6-A5 |
| 1-3-3a | B1-C2-C4 |
| 1-3-3b | B1-A3-A5 |
| 1-3-3c | B1-C2-A3 |
| 1-3-3d | B1-C2-A5 |
| 2-2-2a | B2-B3-B4 |
| 2-2-2b | B2-B3-B5 |
| 2-2-2c | B2-B4-B6 |
| 2-2-3a | B2-B3-C2 |
| 2-2-3b | B2-B3-C4 |
| 2-2-3c | B2-B3-C6 |
| 2-2-3d | B2-B3-A3 |

| Geometry B continues | |
|---|---|
| Cluster | Geometry |
| 2-2-3e | B2-B3-A5 |
| 2-2-3f | B2-B3-A7 |
| 2-2-3g | B2-B4-C2 |
| 2-2-3h | B2-B4-C6 |
| 2-2-3i | B2-B4-A3 |
| 2-2-3j | B2-B4-A5 |
| 2-2-3k | B2-B5-C2 |
| 2-2-3l | B2-B5-C4 |
| 2-2-3m | B2-B5-A3 |
| 2-2-3n | B2-B5-A5 |
| 2-3-3a | B2-C2-C4 |
| 2-3-3b | B2-C4-C6 |
| 2-3-3c | B2-A3-A5 |
| 2-3-3d | B2-A3-A7 |
| 2-3-3e | B2-C2-A3 |
| 2-3-3f | B2-C2-A5 |
| 2-3-3g | B2-C4-A3 |
| 2-3-3h | B2-C4-A5 |
| 2-3-3i | B2-C4-A7 |
| 2-3-3j | B2-C6-A3 |
| 3-3-3a | B2-C4-C6 |
| 3-3-3b | A3-A5-A7 |
| 3-3-3c | C2-C4-A3 |
| 3-3-3d | C2-C4-A5 |

| Geometry C | |
|---|---|
| Cluster | Geometry |
| 1-1a | C2-C7 |
| 1-2a | C2-C1 |
| 1-2b | C2-D1 |
| 1-3a | C2-C3 |
| 1-3b | C2-C6 |
| 1-4a | C2-D2 |
| 1-4b | C2-B7 |
| 2-2a | C1-D1 |
| 2-3a | C1-C3 |
| 2-3b | C1-C6 |
| 2-4a | C1-D2 |
| 2-4b | C1-B7 |
| 3-3a | C3-C6 |
| 3-4a | C3-D2 |
| 3-4b | C3-B7 |
| 4-4a | D2-B7 |

| Geometry D | |
|---|---|
| Cluster | Geometry |
| 1-2-2a | D1-C2-C4 |
| 1-2-3a | D1-C2-B3 |
| 1-2-3b | D1-C2-B5 |
| 2-2-2a | C2-C4-C6 |
| 2-2-3a | C2-C4-B3 |
| 2-2-3b | C2-C4-B5 |
| 2-3-3a | C2-B3-B5 |
| 2-3-3b | C2-B3-B7 |
| 3-3-3a | B3-B5-B7 |

**Table 5.5:** Position of substitutional defect sites relative to a 6b interstitial site at (0,0,0).

| Tag | Position | | |
|---|---|---|---|
| A1 | 0 | 0 | -u |
| A2 | $\frac{1}{3}$ | $\frac{2}{3}$ | u-$\frac{2}{3}$ |
| A3 | $\frac{2}{3}$ | $\frac{1}{3}$ | $\frac{1}{6}$-u |
| A4 | $\frac{1}{3}$ | -$\frac{1}{3}$ | u-$\frac{2}{3}$ |
| A5 | -$\frac{1}{3}$ | -$\frac{2}{3}$ | $\frac{1}{6}$-u |
| A6 | -$\frac{2}{3}$ | -$\frac{1}{3}$ | u-$\frac{2}{3}$ |
| A7 | -$\frac{1}{3}$ | $\frac{1}{3}$ | $\frac{1}{6}$-u |
| B1 | 0 | 0 | u-$\frac{1}{2}$ |
| B2 | $\frac{1}{3}$ | $\frac{2}{3}$ | $\frac{1}{3}$-u |
| B3 | $\frac{2}{3}$ | $\frac{1}{3}$ | u-$\frac{1}{3}$ |
| B4 | $\frac{1}{3}$ | -$\frac{1}{3}$ | $\frac{1}{3}$-u |
| B5 | -$\frac{1}{3}$ | -$\frac{2}{3}$ | u-$\frac{1}{3}$ |
| B6 | -$\frac{2}{3}$ | -$\frac{1}{3}$ | $\frac{1}{3}$-u |
| B7 | -$\frac{1}{3}$ | $\frac{1}{3}$ | u-$\frac{1}{3}$ |
| C1 | 0 | 0 | $\frac{1}{2}$-u |
| C2 | $\frac{1}{3}$ | $\frac{2}{3}$ | u-$\frac{1}{6}$ |
| C3 | $\frac{2}{3}$ | $\frac{1}{3}$ | $\frac{2}{3}$-u |
| C4 | $\frac{1}{3}$ | -$\frac{1}{3}$ | u-$\frac{1}{6}$ |
| C5 | -$\frac{1}{3}$ | -$\frac{2}{3}$ | $\frac{2}{3}$-u |
| C6 | -$\frac{2}{3}$ | -$\frac{1}{3}$ | u-$\frac{1}{6}$ |
| C7 | -$\frac{1}{3}$ | $\frac{1}{3}$ | $\frac{2}{3}$-u |
| D1 | 0 | 0 | u |
| D2 | $\frac{1}{3}$ | $\frac{2}{3}$ | $\frac{5}{6}$-u |
| D3 | $\frac{2}{3}$ | $\frac{1}{3}$ | $\frac{1}{6}$+u |
| D4 | $\frac{1}{3}$ | -$\frac{1}{3}$ | $\frac{5}{6}$-u |
| D5 | -$\frac{1}{3}$ | -$\frac{2}{3}$ | $\frac{1}{6}$+u |
| D6 | -$\frac{2}{3}$ | -$\frac{1}{3}$ | $\frac{5}{6}$-u |
| D7 | -$\frac{1}{3}$ | $\frac{1}{3}$ | $\frac{1}{6}$+u |

#### 5.3.3.5 Tetravalent Vacancy Clusters

In this solution mechanism a host cation vacancy will compensate the solution of three tetravalent substitutional defects, $\{3D_M^{\bullet}{:}V_M^{///}\}$. The vacancy, $V_M^{///}$, is at (0,0,$\frac{1}{2}$-u) and the compensated substitutional ions, $D_M^{\bullet}$, are arranged as in geometry listing D of table 5.4.

## 5.4 Results and Discussion

### 5.4.1 Intrinsic Defect Equilibria

The normalised intrinsic defect reaction energies, reported in table 5.6, suggest that all these disorder reactions are relatively high energy processes. The Schottky reaction has marginally the lowest energy in $\alpha$-$Al_2O_3$ while the anion Frenkel reaction is marginally lower energy in $\alpha$-$Cr_2O_3$ and $\alpha$-$Fe_2O_3$. Unfortunately, given the small relative difference between these energies, it would be practically impossible to differentiate between reactions experimentally, the same conclusion drawn by El-Aiat and Kröger [89] when studying $\alpha$-$Al_2O_3$.

**Table 5.6:** Normalised $M_2O_3$ lattice intrinsic equilibria energies.

| Energy (eV) | Equation | $Al_2O_3$ | $Cr_2O_3$ | $Fe_2O_3$ |
|---|---|---|---|---|
| Schottky | 5.1 | 5.15 | 5.59 | 5.82 |
| interstitial | 5.2 | 7.26 | 7.08 | 7.15 |
| anion Frenkel | 5.3 | 5.54 | 5.34 | 5.43 |
| cation Frenkel | 5.4 | 7.22 | 7.80 | 8.07 |

## 5.4.2 Extrinsic Defect Behaviour

### 5.4.2.1 Presentation of Extrinsic Results

The number of simulations required to assess possible mechanisms is significant, (approximately 2,500) and this level of detail is presented in tables. However, when unfavourable mechanisms are excluded this condenses to a more manageable dataset which is presented graphically. Consequently discussions will concentrate on figures 5.2, 5.3 and 5.4 which present this concise data. The detail in the tables is useful since it allows comparison of different cluster geometries, identifying the lowest energy configuration.

**Solution Energy Graphs.** The lowest energy mechanism results of calculations, for the isolated and clustered case, are presented graphically as normalised solution energy vs. dopant cation radii in figures 5.2, 5.3 and 5.4. In each case subfigure (a) gives results for solution via isolated defects and subfigure (b) gives results for solution via the formation of neutral clusters. In these figures the dopant cation size is plotted along the $x$-axis and the solution energies are plotted along the $y$-axis. Figure 5.2 shows results for $\alpha$-$Al_2O_3$, figure 5.3 for $\alpha$-$Cr_2O_3$ and figure 5.4 for $\alpha$-$Fe_2O_3$. As a guide to the eye, a quadratic trend-line is fitted to the data for each mechanism.

In these figures squares (■) denote dopant interstitial compensation, circles (●) denote interstitial compensation and inverted triangles (▼) denote vacancy compensation. The colour blue represents 2+ cation solution results and red represents 4+ cation results. The colour black and the asterisk (*) represents 3+ cation solution which does not require compensation.

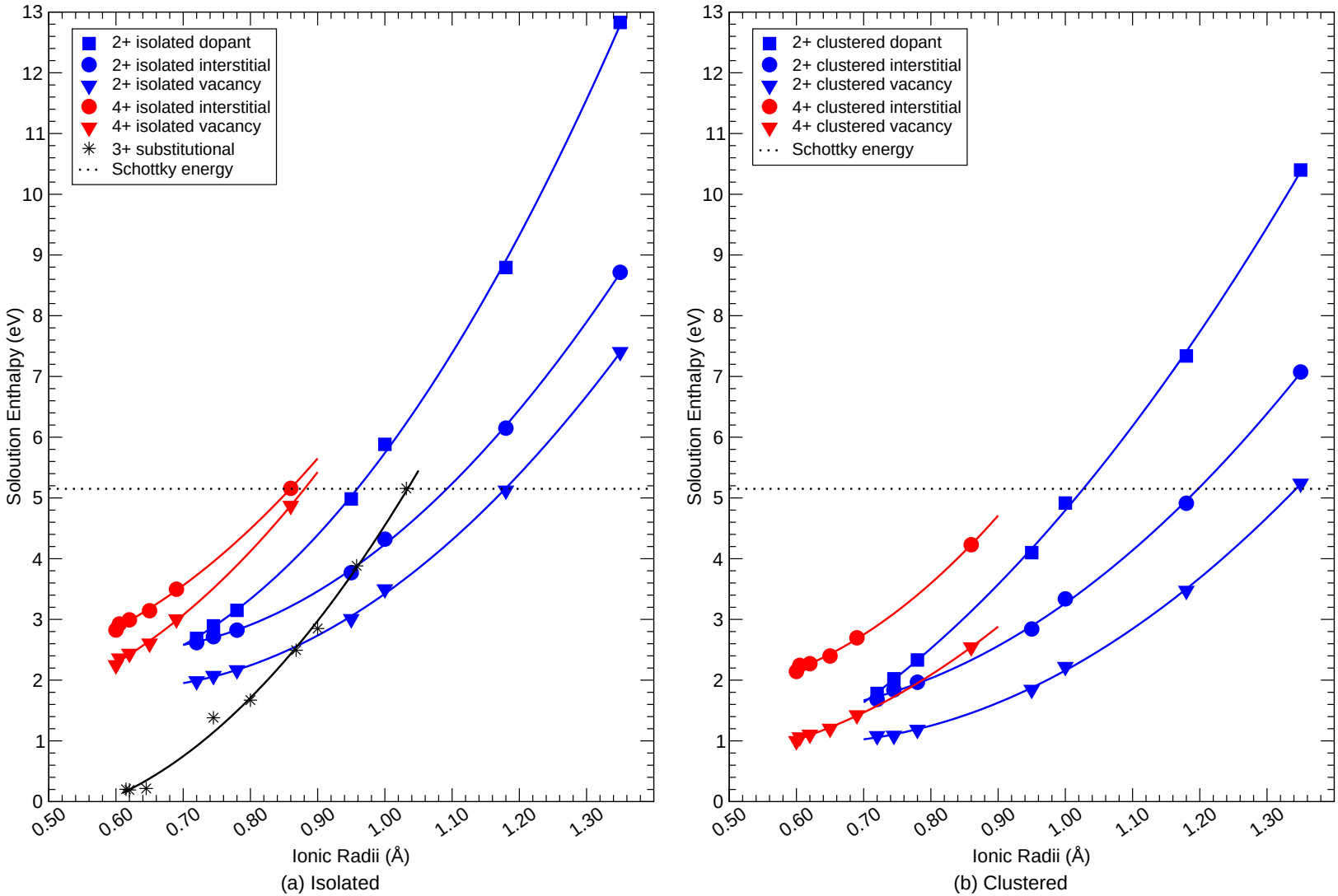


**Figure 5.2:** Normalised solution energetics of $Al_2O_3$.

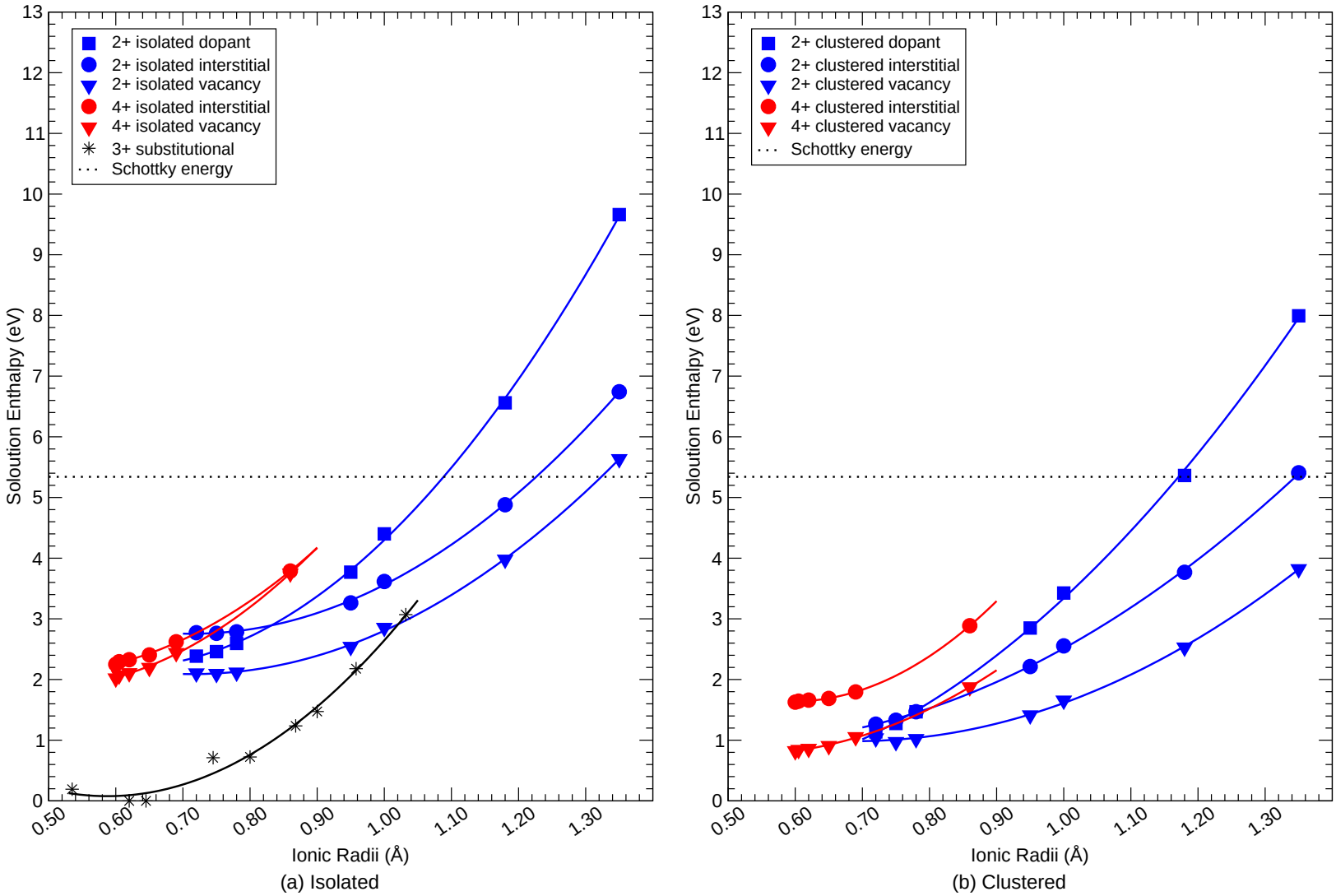


**Figure 5.3:** Normalised solution energetics of $Cr_2O_3$.

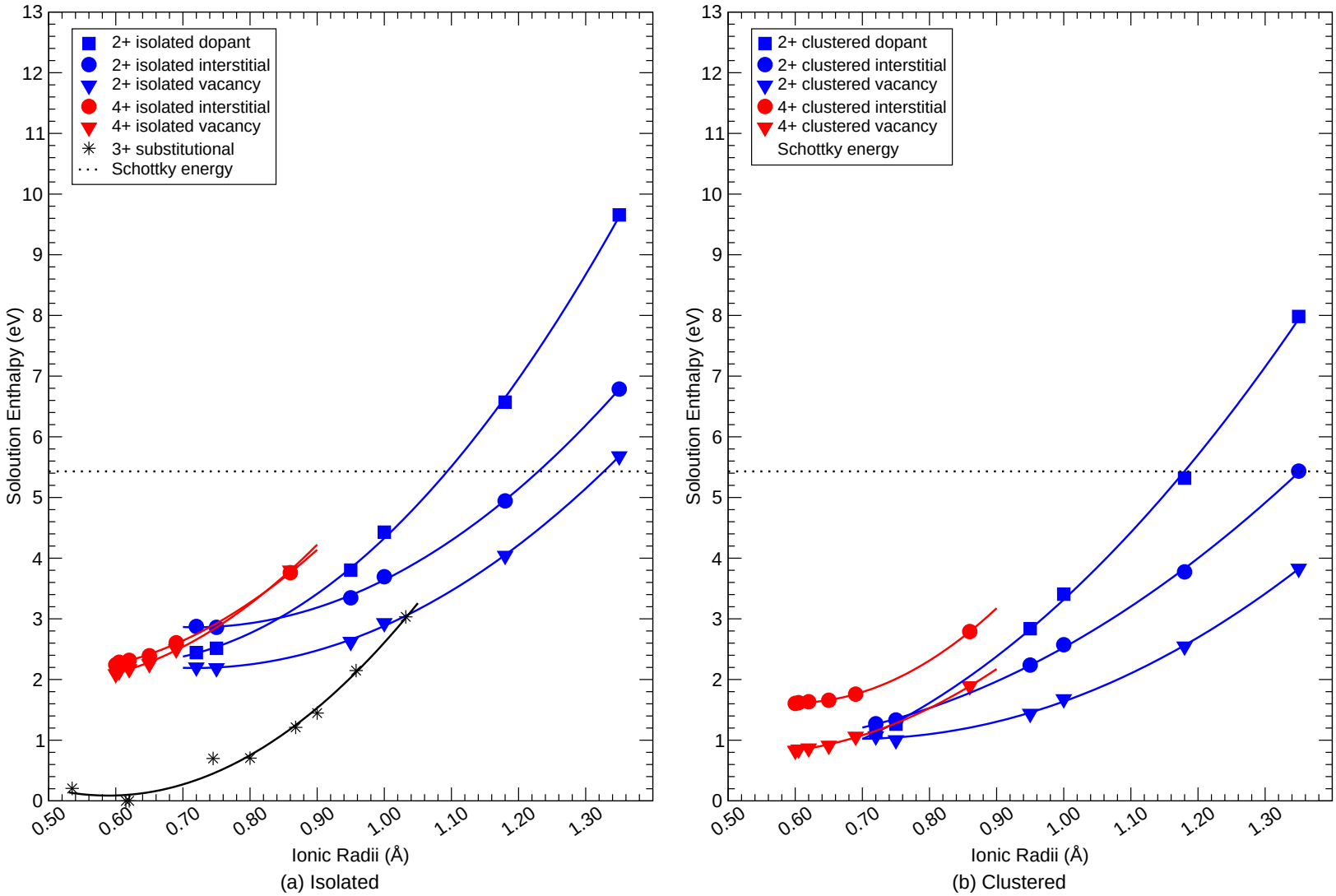


**Figure 5.4:** Normalised solution energetics of $Fe_2O_3$.

**Solution Energy Tables.** In the isovalent case no compensation is required and the situation is simple. Individual components of the reaction sum are given in table 5.7 and normalised solution energies are given in table 5.8. (Thus, this data is plotted in figures 5.2a, 5.3a and 5.4a).

In the aliovalent case the situation is much more complex. Two valences are simulated (2+ and 4+) and since clustering is a possibility both the isolated and clustered cases are considered.

For divalent solution in $\alpha$-$Al_2O_3$, isolated components of the reaction sum are given in table 5.9 and detailed data for divalent solution mechanisms are presented in tables 5.10-5.18. For divalent solution in $\alpha$-$Cr_2O_3$, isolated components of the reaction sum are given in table 5.19 and detailed data for divalent solution mechanisms are presented in tables 5.20-5.28. For divalent solution in $\alpha$-$Fe_2O_3$, isolated components of the reaction sum are given in table 5.29 and detailed data for divalent solution mechanisms are presented in tables 5.30-5.38.

For tetravalent solution in $\alpha$-$Al_2O_3$, isolated components of the reaction sum are given in table 5.39 and detailed data for tetravalent solution mechanisms are presented in tables 5.40-5.45. For tetravalent solution in $\alpha$-$Cr_2O_3$, isolated components of the reaction sum are given in table 5.46 and detailed data for tetravalent solution mechanisms are presented in tables 5.47-5.52. For tetravalent solution in $\alpha$-$Fe_2O_3$, isolated components of the reaction sum are given in table 5.53 and detailed data for tetravalent solution mechanisms are presented in tables 5.54-5.59.

Each mechanism is detailed in three tables. The first gives the cluster energy, with the equivalent isolated defect sum highlighted at the top of the table. The second gives the solution energy for each cluster, with the equivalent isolated solution energy highlighted at the top of each table. The third gives the binding energy, which is the difference between the isolated and clustered solution energies given in the solution energy table. The most

favourable (lowest energy) solution result, which becomes a point plotted in figures 5.2, 5.3 or 5.4, is embolded in the solution energy tables. This corresponds to the highest binding energy result which is embolded in the binding energy tables.

Not all cluster calculations completed successfully. In some cases a persistent negative curvature (*pnc*) occurred during the minimisation (indicating an unstable cluster configuration). These 'null' results are indicated by *pnc* in the tables.

**Table 5.7:** Isolated oxide lattice and substitutional energies for trivalent cations in host corundum lattices.

| $C_M^{\times}$ Cation | Cation Radii (Å) | $M_2O_3$ Lattice En. (eV) | Substitutional Energy (eV) $\alpha$-$Al_2O_3$ | $\alpha$-$Cr_2O_3$ | $\alpha$-$Fe_2O_3$ |
|---|---|---|---|---|---|
| $Al^{3+}$ | 0.535 | -159.65 | - | -3.36 | -3.34 |
| $Cr^{3+}$ | 0.615 | -152.54 | 3.76 | - | 0.01 |
| $Ga^{3+}$ | 0.620 | -152.66 | 3.69 | -0.06 | -0.05 |
| $Fe^{3+}$ | 0.645 | -152.57 | 3.76 | -0.01 | - |
| $Sc^{3+}$ | 0.745 | -146.20 | 8.11 | 3.88 | 3.88 |
| $In^{3+}$ | 0.800 | -141.14 | 10.93 | 6.43 | 6.42 |
| $Yb^{3+}$ | 0.868 | -136.92 | 13.86 | 9.05 | 9.04 |
| $Y^{3+}$ | 0.900 | -135.50 | 14.93 | 9.99 | 9.98 |
| $Sm^{3+}$ | 0.958 | -131.86 | 17.78 | 12.52 | 12.50 |
| $La^{3+}$ | 1.032 | -128.13 | 20.92 | 15.27 | 15.25 |

**Table 5.8:** Solution energies for trivalent cations in host corundum lattices.

| $C_M^{\times}$ Cation | Cation Radii (Å) | Solution Energy (eV) $\alpha$-$Al_2O_3$ | $\alpha$-$Cr_2O_3$ | $\alpha$-$Fe_2O_3$ |
|---|---|---|---|---|
| $Al^{3+}$ | 0.535 | - | 0.192 | 0.206 |
| $Cr^{3+}$ | 0.615 | 0.204 | - | 0.000 |
| $Ga^{3+}$ | 0.620 | 0.193 | 0.000 | 0.001 |
| $Fe^{3+}$ | 0.645 | 0.217 | 0.000 | - |
| $Sc^{3+}$ | 0.745 | 1.381 | 0.711 | 0.699 |
| $In^{3+}$ | 0.800 | 1.671 | 0.724 | 0.705 |
| $Yb^{3+}$ | 0.868 | 2.493 | 1.236 | 1.212 |
| $Y^{3+}$ | 0.900 | 2.850 | 1.473 | 1.447 |
| $Sm^{3+}$ | 0.958 | 3.881 | 2.178 | 2.147 |
| $La^{3+}$ | 1.032 | 5.156 | 3.069 | 3.033 |

**Table 5.9:** Isolated interstitial defect, substitutional defect and oxide lattice energies (eV) for divalent cations in α-$Al_2O_3$

| Divalent Cation | $Mg^{2+}$ | $Co^{2+}$ | $Fe^{2+}$ | $Cd^{2+}$ | $Ca^{2+}$ | $Sr^{2+}$ | $Ba^{2+}$ |
|---|---|---|---|---|---|---|---|
| Cation Radii (Å) | 0.72 | 0.75 | 0.780 | 0.95 | 1.00 | 1.18 | 1.35 |
| iso $B_i^{\bullet\bullet}$ | -15.04 | -13.42 | -12.45 | -6.63 | -4.30 | 2.05 | 9.20 |
| iso $B_M^{\prime}$ | 29.41 | 30.80 | 31.43 | 35.53 | 37.38 | 42.31 | 47.62 |
| Lattice En. | -41.31 | -40.05 | -39.56 | -36.72 | -35.61 | -33.12 | -31.23 |

**Table 5.10:** Cluster energies (eV) for divalent cation solution in α-$Al_2O_3$ via neutral dopant interstitial compensation.

| Divalent Cation | $Mg^{2+}$ | $Co^{2+}$ | $Fe^{2+}$ | $Cd^{2+}$ | $Ca^{2+}$ | $Sr^{2+}$ | $Ba^{2+}$ |
|---|---|---|---|---|---|---|---|
| Cation Radii (Å) | 0.72 | 0.75 | 0.780 | 0.95 | 1.00 | 1.18 | 1.35 |
| Isolated | 43.79 | 48.19 | 50.41 | 64.44 | 70.46 | 86.66 | 104.44 |
| 1-1a | 41.07 | 45.58 | 47.96 | 62.54 | 68.55 | 84.47 | 101.44 |
| 1-2a | 41.63 | 46.02 | 48.33 | 62.57 | 68.50 | 82.30 | 97.70 |
| 1-2b | 41.64 | 46.06 | 48.35 | 62.50 | 68.42 | 84.05 | 98.08 |
| 1-3a | 41.70 | 46.13 | 48.44 | 62.79 | 68.82 | 82.72 | 98.75 |
| 1-3b | 41.90 | 46.26 | 48.54 | 62.59 | 68.47 | 84.02 | 100.61 |
| 1-4a | 41.54 | 45.76 | 48.03 | 61.78 | 67.57 | 82.86 | 99.39 |
| 1-4b | 41.28 | 45.68 | 48.00 | 62.30 | 68.35 | 84.51 | 98.82 |
| 2-2a | 42.19 | 46.45 | 48.59 | 62.05 | 67.79 | 83.04 | 98.14 |
| 2-2b | 42.02 | 46.33 | 48.48 | 62.02 | 67.84 | 83.27 | 99.73 |
| 2-2c | 42.02 | 46.33 | 48.48 | 62.02 | 67.83 | 83.27 | 99.73 |
| 2-3a | 42.60 | 46.92 | 49.07 | 62.62 | 68.41 | 83.71 | 97.15 |
| 2-3b | 42.23 | 46.57 | 48.77 | 62.60 | 68.53 | 84.32 | 100.94 |
| 2-3c | 42.60 | 46.92 | 49.07 | 62.62 | 68.41 | 83.71 | 97.17 |
| 2-3d | 42.23 | 46.57 | 48.77 | 62.60 | 68.53 | 84.32 | 100.94 |
| 2-4a | 41.77 | 46.04 | 48.23 | 61.91 | 67.80 | 83.56 | 100.60 |
| 2-4b | 41.81 | 46.09 | 48.30 | 62.04 | 67.97 | 83.81 | 101.03 |
| 3-3a | 42.54 | 46.90 | 49.12 | 63.15 | 69.16 | 84.99 | 98.30 |
| 3-3b | 42.53 | 46.91 | 49.14 | 63.23 | 69.25 | 85.31 | 98.70 |
| 3-3c | 42.48 | 46.85 | 49.07 | 63.15 | 69.17 | 85.32 | 98.39 |
| 3-4a | 41.99 | 46.31 | 48.54 | 62.52 | 68.55 | 84.78 | 98.75 |
| 3-4b | 42.26 | 46.58 | 48.82 | 62.80 | 68.77 | 84.49 | 101.60 |
| 4-4a | 41.52 | 45.79 | 48.03 | 61.94 | 67.98 | 84.27 | 102.34 |

**Table 5.11:** Solution energies (eV) for divalent cations in $\alpha$-$Al_2O_3$ via neutral dopant interstitial compensation (reaction 5.6).

| Divalent Cation | $Mg^{2+}$ | $Co^{2+}$ | $Fe^{2+}$ | $Cd^{2+}$ | $Ca^{2+}$ | $Sr^{2+}$ | $Ba^{2+}$ |
|---|---|---|---|---|---|---|---|
| Cation Radii (Å) | 0.72 | 0.75 | 0.780 | 0.95 | 1.00 | 1.18 | 1.35 |
| Isolated | 2.69 | 2.89 | 3.15 | 4.98 | 5.88 | 8.79 | 12.83 |
| 1-1a | **1.78** | **2.02** | **2.33** | 4.35 | 5.25 | 8.06 | 11.83 |
| 1-2a | 1.97 | 2.17 | 2.46 | 4.36 | 5.23 | **7.34** | 10.58 |
| 1-2b | 1.97 | 2.18 | 2.46 | 4.34 | 5.20 | 7.92 | 10.71 |
| 1-3a | 1.99 | 2.21 | 2.49 | 4.44 | 5.33 | 7.48 | 10.93 |
| 1-3b | 2.06 | 2.25 | 2.53 | 4.37 | 5.22 | 7.91 | 11.55 |
| 1-4a | 1.94 | 2.08 | 2.36 | **4.10** | **4.92** | 7.53 | 11.15 |
| 1-4b | 1.85 | 2.06 | 2.35 | 4.27 | 5.18 | 8.07 | 10.95 |
| 2-2a | 2.15 | 2.31 | 2.54 | 4.19 | 4.99 | 7.59 | 10.73 |
| 2-2b | 2.10 | 2.27 | 2.51 | 4.18 | 5.01 | 7.66 | 11.26 |
| 2-2c | 2.10 | 2.27 | 2.51 | 4.18 | 5.01 | 7.66 | 11.26 |
| 2-3a | 2.29 | 2.47 | 2.70 | 4.38 | 5.20 | 7.81 | **10.40** |
| 2-3b | 2.17 | 2.35 | 2.60 | 4.37 | 5.24 | 8.01 | 11.66 |
| 2-3c | 2.29 | 2.47 | 2.70 | 4.38 | 5.20 | 7.81 | 10.41 |
| 2-3d | 2.17 | 2.35 | 2.60 | 4.37 | 5.24 | 8.01 | 11.66 |
| 2-4a | 2.02 | 2.18 | 2.42 | 4.14 | 5.00 | 7.76 | 11.55 |
| 2-4b | 2.03 | 2.19 | 2.45 | 4.19 | 5.05 | 7.84 | 11.69 |
| 3-3a | 2.27 | 2.46 | 2.72 | 4.55 | 5.45 | 8.24 | 10.78 |
| 3-3b | 2.27 | 2.47 | 2.73 | 4.58 | 5.48 | 8.34 | 10.92 |
| 3-3c | 2.25 | 2.45 | 2.70 | 4.55 | 5.45 | 8.35 | 10.81 |
| 3-4a | 2.09 | 2.27 | 2.53 | 4.34 | 5.24 | 8.16 | 10.93 |
| 3-4b | 2.18 | 2.36 | 2.62 | 4.44 | 5.32 | 8.07 | 11.88 |
| 4-4a | 1.93 | 2.09 | 2.36 | 4.15 | 5.05 | 8.00 | 12.13 |

**Embolded** results indicate the lowest solution energy geometry.

**Table 5.12:** Binding energies (eV) for neutral clusters in $\alpha$-$Al_2O_3$: dopant interstitial compensation of 2+ cations (reaction 5.6).

| Divalent Cation | $Mg^{2+}$ | $Co^{2+}$ | $Fe^{2+}$ | $Cd^{2+}$ | $Ca^{2+}$ | $Sr^{2+}$ | $Ba^{2+}$ |
|---|---|---|---|---|---|---|---|
| Cation Radii (Å) | 0.72 | 0.75 | 0.780 | 0.95 | 1.00 | 1.18 | 1.35 |
| 1-1a | **2.72** | **2.61** | **2.45** | 1.90 | 1.91 | 2.19 | 3.00 |
| 1-2a | 2.16 | 2.16 | 2.08 | 1.87 | 1.96 | **4.37** | 6.73 |
| 1-2b | 2.15 | 2.13 | 2.06 | 1.93 | 2.04 | 2.61 | 6.36 |
| 1-3a | 2.09 | 2.06 | 1.97 | 1.64 | 1.64 | 3.94 | 5.69 |
| 1-3b | 1.89 | 1.93 | 1.87 | 1.84 | 1.99 | 2.64 | 3.83 |
| 1-4a | 2.25 | 2.43 | 2.38 | **2.65** | **2.90** | 3.80 | 5.05 |
| 1-4b | 2.50 | 2.51 | 2.41 | 2.13 | 2.12 | 2.16 | 5.62 |
| 2-2a | 1.60 | 1.74 | 1.82 | 2.39 | 2.67 | 3.62 | 6.30 |
| 2-2b | 1.76 | 1.86 | 1.93 | 2.41 | 2.63 | 3.39 | 4.71 |
| 2-2c | 1.76 | 1.86 | 1.93 | 2.41 | 2.63 | 3.39 | 4.71 |
| 2-3a | 1.19 | 1.26 | 1.34 | 1.81 | 2.06 | 2.95 | **7.29** |
| 2-3b | 1.55 | 1.62 | 1.64 | 1.83 | 1.94 | 2.34 | 3.49 |
| 2-3c | 1.19 | 1.26 | 1.34 | 1.81 | 2.06 | 2.95 | 7.26 |
| 2-3d | 1.55 | 1.62 | 1.64 | 1.83 | 1.94 | 2.34 | 3.49 |
| 2-4a | 2.01 | 2.15 | 2.18 | 2.53 | 2.66 | 3.10 | 3.83 |
| 2-4b | 1.98 | 2.10 | 2.11 | 2.39 | 2.50 | 2.85 | 3.40 |
| 3-3a | 1.24 | 1.29 | 1.29 | 1.29 | 1.30 | 1.67 | 6.13 |
| 3-3b | 1.26 | 1.28 | 1.27 | 1.21 | 1.22 | 1.35 | 5.74 |
| 3-3c | 1.31 | 1.34 | 1.34 | 1.29 | 1.29 | 1.34 | 6.05 |
| 3-4a | 1.79 | 1.88 | 1.87 | 1.92 | 1.92 | 1.89 | 5.69 |
| 3-4b | 1.53 | 1.61 | 1.59 | 1.64 | 1.69 | 2.18 | 2.84 |
| 4-4a | 2.26 | 2.40 | 2.38 | 2.49 | 2.48 | 2.39 | 2.10 |

**Embolded** results indicate the highest binding energy geometry.

**Table 5.13:** Cluster energies (eV) for divalent cation solution in α-$Al_2O_3$ via neutral interstitial compensation.

| Divalent Cation | $Mg^{2+}$ | $Co^{2+}$ | $Fe^{2+}$ | $Cd^{2+}$ | $Ca^{2+}$ | $Sr^{2+}$ | $Ba^{2+}$ |
|---|---|---|---|---|---|---|---|
| Cation Radii (Å) | 0.72 | 0.75 | 0.780 | 0.95 | 1.00 | 1.18 | 1.35 |
| Isolated | 46.20 | 50.37 | 52.25 | 64.56 | 70.10 | 84.88 | 100.81 |
| 1-1-2a | 42.46 | 46.87 | 49.25 | 63.95 | 70.09 | 85.74 | 102.19 |
| 1-1-3a | 42.55 | 46.88 | 49.17 | 63.38 | 69.34 | 84.66 | 100.96 |
| 1-2-2a | 42.88 | 47.11 | 49.23 | 62.53 | 68.22 | 83.24 | 97.85 |
| 1-2-2b | 42.78 | 47.06 | 49.22 | 62.84 | 68.70 | 83.64 | 99.73 |
| 1-2-2c | 42.70 | 46.94 | 49.09 | 62.50 | 68.25 | 82.50 | 97.78 |
| 1-2-2d | 42.76 | 47.05 | 49.19 | 62.72 | 68.58 | 84.22 | 99.89 |
| 1-2-3a | 43.10 | 47.33 | 49.41 | 62.57 | 68.24 | 82.49 | 97.70 |
| 1-2-3b | 42.74 | 46.98 | 49.11 | 62.49 | 68.27 | 82.91 | 98.60 |
| 1-2-3c | 43.14 | 47.31 | 49.42 | 62.62 | 68.27 | 83.21 | 99.05 |
| 1-2-3d | 42.91 | 47.08 | 49.16 | 62.25 | 67.88 | 82.73 | 98.47 |
| 1-2-3e | 42.86 | 47.11 | 49.23 | 62.56 | 68.32 | *pnc* | 98.73 |
| 1-2-3f | 43.10 | 47.33 | 49.41 | 62.57 | 68.24 | 82.49 | 97.70 |
| 1-2-3g | 42.98 | 47.18 | 49.27 | 62.41 | 68.09 | 83.16 | 99.25 |
| 1-2-3h | 43.08 | 47.24 | 49.32 | 62.33 | 67.91 | 82.61 | 98.16 |
| 1-3-3a | 42.87 | 47.08 | 49.18 | 62.41 | 68.18 | 82.85 | 98.69 |
| 1-3-3b | 43.26 | 47.35 | 49.38 | 62.09 | 67.59 | 82.13 | 97.58 |
| 1-3-3c | 43.04 | 47.21 | 49.27 | 62.28 | 67.92 | 82.88 | 98.90 |
| 1-3-3d | 42.98 | 47.14 | 49.20 | 62.19 | 67.82 | 82.76 | 98.73 |
| 2-2-2a | 43.17 | 47.22 | 49.04 | 60.86 | 66.17 | 80.16 | 94.89 |
| 2-2-2b | 43.06 | 47.16 | 49.02 | 61.12 | 66.58 | 81.10 | 96.64 |
| 2-2-2c | 42.86 | 46.98 | 48.83 | 60.87 | 66.36 | 80.95 | 96.54 |
| 2-2-3a | 43.63 | 47.69 | 49.46 | 61.06 | 66.26 | 79.93 | 94.25 |
| 2-2-3b | 43.38 | 47.45 | 49.31 | 61.32 | 66.69 | 80.85 | 95.75 |
| 2-2-3c | 43.19 | 47.27 | 49.12 | 61.13 | 66.55 | 80.88 | 96.13 |
| 2-2-3d | 43.83 | 47.88 | 49.72 | 61.66 | 66.97 | 80.98 | 95.71 |
| 2-2-3e | 43.17 | 47.24 | 49.09 | 61.06 | 66.46 | 80.71 | 95.81 |
| 2-2-3f | 43.29 | 47.35 | 49.18 | 61.04 | 66.37 | 80.44 | 95.31 |
| 2-2-3g | 43.38 | 47.49 | 49.30 | 61.17 | 66.54 | 80.77 | 95.88 |
| 2-2-3h | 43.04 | 47.15 | 49.00 | 61.12 | 66.61 | 81.22 | 96.85 |
| 2-2-3i | 43.32 | 47.41 | 49.26 | 61.20 | 66.57 | 80.69 | 95.50 |
| 2-2-3j | 43.23 | 47.33 | 49.21 | 61.35 | 66.81 | 81.31 | 96.71 |

*(continued on next page)*

*(continued from previous page)*

| Divalent Cation | $Mg^{2+}$ | $Co^{2+}$ | $Fe^{2+}$ | $Cd^{2+}$ | $Ca^{2+}$ | $Sr^{2+}$ | $Ba^{2+}$ |
|---|---|---|---|---|---|---|---|
| Cation Radii (Å) | 0.72 | 0.75 | 0.780 | 0.95 | 1.00 | 1.18 | 1.35 |
| 2-2-3k | 43.43 | 47.55 | 49.39 | 61.48 | 66.94 | 81.51 | 97.25 |
| 2-2-3l | 43.17 | 47.28 | 49.16 | 61.39 | 66.90 | 81.63 | 97.54 |
| 2-2-3m | 43.30 | 47.42 | 49.31 | 61.57 | 67.07 | 81.71 | 97.38 |
| 2-2-3n | 43.43 | 47.55 | 49.39 | 61.48 | 66.94 | 81.51 | 97.25 |
| 2-3-3a | 43.60 | 47.68 | 49.48 | 61.31 | 66.66 | 80.83 | 95.90 |
| 2-3-3b | 43.27 | 47.36 | 49.21 | 61.27 | 66.73 | 81.26 | 96.80 |
| 2-3-3c | 43.47 | 47.55 | 49.41 | 61.51 | 66.95 | 81.40 | 96.77 |
| 2-3-3d | 43.57 | 47.64 | 49.50 | 61.48 | 66.86 | 81.08 | 96.09 |
| 2-3-3e | 43.81 | 47.90 | 49.72 | 61.62 | 66.96 | 81.05 | 95.94 |
| 2-3-3f | 43.53 | 47.63 | 49.44 | 61.32 | 66.69 | 80.93 | 96.07 |
| 2-3-3g | 43.46 | 47.55 | 49.43 | 61.57 | 67.03 | 81.50 | 96.86 |
| 2-3-3h | 43.24 | 47.34 | 49.20 | 61.36 | 66.87 | 81.55 | 97.32 |
| 2-3-3i | 43.28 | 47.38 | 49.22 | 61.23 | 66.65 | 81.03 | 96.32 |
| 2-3-3j | 43.42 | 47.51 | 49.37 | 61.45 | 66.89 | 81.29 | 96.57 |
| 3-3-3a | 43.27 | 47.36 | 49.21 | 61.27 | 66.73 | 81.26 | 96.80 |
| 3-3-3b | 43.55 | 47.61 | 49.42 | 61.21 | 66.58 | 80.84 | 96.11 |
| 3-3-3c | 43.54 | 47.63 | 49.46 | 61.49 | 66.93 | 81.45 | 97.04 |
| 3-3-3d | 43.49 | 47.57 | 49.40 | 61.40 | 66.84 | 81.32 | 96.86 |

**Table 5.14:** Solution energies (eV) for divalent cations in $\alpha$-$Al_2O_3$ via neutral interstitial compensation (reaction 5.7).

| Divalent Cation | $Mg^{2+}$ | $Co^{2+}$ | $Fe^{2+}$ | $Cd^{2+}$ | $Ca^{2+}$ | $Sr^{2+}$ | $Ba^{2+}$ |
|---|---|---|---|---|---|---|---|
| Cation Radii (Å) | 0.72 | 0.75 | 0.780 | 0.95 | 1.00 | 1.18 | 1.35 |
| Isolated | 2.62 | 2.72 | 2.82 | 3.77 | 4.32 | 6.15 | 8.72 |
| 1-1-2a | **1.68** | **1.84** | 2.07 | 3.62 | 4.32 | 6.36 | 9.06 |
| 1-1-3a | 1.71 | 1.84 | 2.05 | 3.47 | 4.13 | 6.09 | 8.75 |
| 1-2-2a | 1.79 | 1.90 | 2.07 | 3.26 | 3.85 | 5.74 | 7.97 |
| 1-2-2b | 1.76 | 1.89 | 2.06 | 3.34 | 3.97 | 5.84 | 8.44 |
| 1-2-2c | 1.74 | 1.86 | 2.03 | 3.25 | 3.86 | 5.55 | 7.96 |
| 1-2-2d | 1.76 | 1.89 | 2.06 | 3.31 | 3.94 | 5.98 | 8.48 |
| 1-2-3a | 1.84 | 1.95 | 2.11 | 3.27 | 3.86 | 5.55 | 7.94 |
| 1-2-3b | 1.75 | 1.87 | 2.04 | 3.25 | 3.86 | 5.66 | 8.16 |

*(continued on next page)*

**Embolded** results indicate the lowest solution energy geometry.

*(continued from previous page)*

| Divalent Cation | $Mg^{2+}$ | $Co^{2+}$ | $Fe^{2+}$ | $Cd^{2+}$ | $Ca^{2+}$ | $Sr^{2+}$ | $Ba^{2+}$ |
|---|---|---|---|---|---|---|---|
| Cation Radii (Å) | 0.72 | 0.75 | 0.780 | 0.95 | 1.00 | 1.18 | 1.35 |
| 1-2-3c | 1.85 | 1.95 | 2.11 | 3.28 | 3.86 | 5.73 | 8.28 |
| 1-2-3d | 1.80 | 1.89 | 2.05 | 3.19 | 3.77 | 5.61 | 8.13 |
| 1-2-3e | 1.78 | 1.90 | 2.07 | 3.27 | 3.88 | *pnc* | 8.19 |
| 1-2-3f | 1.84 | 1.95 | 2.11 | 3.27 | 3.86 | 5.55 | 7.94 |
| 1-2-3g | 1.81 | 1.92 | 2.08 | 3.23 | 3.82 | 5.72 | 8.32 |
| 1-2-3h | 1.84 | 1.93 | 2.09 | 3.21 | 3.77 | 5.58 | 8.05 |
| 1-3-3a | 1.79 | 1.89 | 2.05 | 3.23 | 3.84 | 5.64 | 8.19 |
| 1-3-3b | 1.88 | 1.96 | 2.10 | 3.15 | 3.69 | 5.46 | 7.91 |
| 1-3-3c | 1.83 | 1.92 | 2.08 | 3.20 | 3.78 | 5.65 | 8.24 |
| 1-3-3d | 1.81 | 1.91 | 2.06 | 3.17 | 3.75 | 5.62 | 8.19 |
| 2-2-2a | 1.86 | 1.93 | 2.02 | **2.84** | **3.34** | 4.97 | 7.23 |
| 2-2-2b | 1.83 | 1.91 | 2.01 | 2.91 | 3.44 | 5.20 | 7.67 |
| 2-2-2c | 1.78 | 1.87 | **1.97** | 2.85 | 3.39 | 5.17 | 7.65 |
| 2-2-3a | 1.98 | 2.04 | 2.13 | 2.89 | 3.36 | **4.91** | **7.07** |
| 2-2-3b | 1.91 | 1.99 | 2.09 | 2.96 | 3.47 | 5.14 | 7.45 |
| 2-2-3c | 1.87 | 1.94 | 2.04 | 2.91 | 3.43 | 5.15 | 7.54 |
| 2-2-3d | 2.03 | 2.09 | 2.19 | 3.04 | 3.54 | 5.17 | 7.44 |
| 2-2-3e | 1.86 | 1.93 | 2.03 | 2.89 | 3.41 | 5.11 | 7.47 |
| 2-2-3f | 1.89 | 1.96 | 2.05 | 2.89 | 3.39 | 5.04 | 7.34 |
| 2-2-3g | 1.91 | 2.00 | 2.08 | 2.92 | 3.43 | 5.12 | 7.48 |
| 2-2-3h | 1.83 | 1.91 | 2.01 | 2.91 | 3.45 | 5.23 | 7.73 |
| 2-2-3i | 1.90 | 1.97 | 2.07 | 2.93 | 3.44 | 5.10 | 7.39 |
| 2-2-3j | 1.88 | 1.96 | 2.06 | 2.97 | 3.50 | 5.26 | 7.69 |
| 2-2-3k | 1.93 | 2.01 | 2.11 | 3.00 | 3.53 | 5.31 | 7.82 |
| 2-2-3l | 1.86 | 1.94 | 2.05 | 2.97 | 3.52 | 5.34 | 7.90 |
| 2-2-3m | 1.89 | 1.98 | 2.09 | 3.02 | 3.56 | 5.36 | 7.86 |
| 2-2-3n | 1.93 | 2.01 | 2.11 | 3.00 | 3.53 | 5.31 | 7.82 |
| 2-3-3a | 1.97 | 2.04 | 2.13 | 2.96 | 3.46 | 5.14 | 7.49 |
| 2-3-3b | 1.89 | 1.96 | 2.06 | 2.95 | 3.48 | 5.24 | 7.71 |
| 2-3-3c | 1.94 | 2.01 | 2.11 | 3.01 | 3.53 | 5.28 | 7.70 |
| 2-3-3d | 1.96 | 2.03 | 2.13 | 3.00 | 3.51 | 5.20 | 7.53 |
| 2-3-3e | 2.02 | 2.10 | 2.19 | 3.03 | 3.53 | 5.19 | 7.50 |
| 2-3-3f | 1.95 | 2.03 | 2.12 | 2.96 | 3.47 | 5.16 | 7.53 |
| 2-3-3g | 1.93 | 2.01 | 2.12 | 3.02 | 3.55 | 5.30 | 7.73 |

*(continued on next page)*

**Embolded** results indicate the lowest solution energy geometry.

*(continued from previous page)*

| Divalent Cation | $Mg^{2+}$ | $Co^{2+}$ | $Fe^{2+}$ | $Cd^{2+}$ | $Ca^{2+}$ | $Sr^{2+}$ | $Ba^{2+}$ |
|---|---|---|---|---|---|---|---|
| Cation Radii (Å) | 0.72 | 0.75 | 0.780 | 0.95 | 1.00 | 1.18 | 1.35 |
| 2-3-3h | 1.88 | 1.96 | 2.06 | 2.97 | 3.51 | 5.32 | 7.84 |
| 2-3-3i | 1.89 | 1.97 | 2.06 | 2.93 | 3.46 | 5.19 | 7.59 |
| 2-3-3j | 1.92 | 2.00 | 2.10 | 2.99 | 3.52 | 5.25 | 7.65 |
| 3-3-3a | 1.89 | 1.96 | 2.06 | 2.95 | 3.48 | 5.24 | 7.71 |
| 3-3-3b | 1.96 | 2.02 | 2.11 | 2.93 | 3.44 | 5.14 | 7.54 |
| 3-3-3c | 1.95 | 2.03 | 2.13 | 3.00 | 3.53 | 5.29 | 7.77 |
| 3-3-3d | 1.94 | 2.01 | 2.11 | 2.98 | 3.51 | 5.26 | 7.73 |

**Embolded** results indicate the lowest solution energy geometry.

**Table 5.15:** Binding energies (eV) for neutral clusters in $\alpha$-$Al_2O_3$: interstitial compensation of 2+ cations (reaction 5.7).

| Divalent Cation | $Mg^{2+}$ | $Co^{2+}$ | $Fe^{2+}$ | $Cd^{2+}$ | $Ca^{2+}$ | $Sr^{2+}$ | $Ba^{2+}$ |
|---|---|---|---|---|---|---|---|
| Cation Radii (Å) | 0.72 | 0.75 | 0.780 | 0.95 | 1.00 | 1.18 | 1.35 |
| 1-1-2a | **3.74** | **3.50** | 3.00 | 0.62 | 0.01 | -0.85 | -1.38 |
| 1-1-3a | 3.65 | 3.50 | 3.08 | 1.19 | 0.76 | 0.23 | -0.15 |
| 1-2-2a | 3.32 | 3.26 | 3.02 | 2.04 | 1.89 | 1.64 | 2.97 |
| 1-2-2b | 3.42 | 3.32 | 3.03 | 1.72 | 1.40 | 1.24 | 1.09 |
| 1-2-2c | 3.49 | 3.43 | 3.16 | 2.07 | 1.85 | 2.39 | 3.04 |
| 1-2-2d | 3.44 | 3.32 | 3.06 | 1.84 | 1.52 | 0.66 | 0.92 |
| 1-2-3a | 3.10 | 3.05 | 2.84 | 2.00 | 1.87 | 2.40 | 3.11 |
| 1-2-3b | 3.45 | 3.40 | 3.15 | 2.07 | 1.83 | 1.98 | 2.21 |
| 1-2-3c | 3.06 | 3.07 | 2.84 | 1.95 | 1.83 | 1.67 | 1.76 |
| 1-2-3d | 3.29 | 3.30 | 3.09 | 2.32 | 2.23 | 2.15 | 2.34 |
| 1-2-3e | 3.33 | 3.26 | 3.02 | 2.01 | 1.79 | *pnc* | 2.08 |
| 1-2-3f | 3.10 | 3.05 | 2.84 | 2.00 | 1.87 | 2.40 | 3.11 |
| 1-2-3g | 3.22 | 3.19 | 2.99 | 2.16 | 2.01 | 1.73 | 1.57 |
| 1-2-3h | 3.12 | 3.14 | 2.93 | 2.23 | 2.19 | 2.27 | 2.65 |
| 1-3-3a | 3.33 | 3.29 | 3.07 | 2.15 | 1.93 | 2.04 | 2.12 |
| 1-3-3b | 2.94 | 3.02 | 2.88 | 2.47 | 2.51 | 2.76 | 3.23 |
| 1-3-3c | 3.15 | 3.17 | 2.98 | 2.29 | 2.19 | 2.00 | 1.92 |
| 1-3-3d | 3.22 | 3.23 | 3.05 | 2.38 | 2.28 | 2.12 | 2.09 |
| 2-2-2a | 3.03 | 3.15 | 3.21 | **3.71** | **3.94** | 4.72 | 5.93 |

*(continued on next page)*

**Embolded** results indicate the highest binding energy geometry.

*(continued from previous page)*

| Divalent Cation | $Mg^{2+}$ | $Co^{2+}$ | $Fe^{2+}$ | $Cd^{2+}$ | $Ca^{2+}$ | $Sr^{2+}$ | $Ba^{2+}$ |
|---|---|---|---|---|---|---|---|
| Cation Radii (Å) | 0.72 | 0.75 | 0.780 | 0.95 | 1.00 | 1.18 | 1.35 |
| 2-2-2b | 3.13 | 3.21 | 3.23 | 3.44 | 3.52 | 3.78 | 4.18 |
| 2-2-2c | 3.34 | 3.40 | **3.43** | 3.69 | 3.75 | 3.94 | 4.28 |
| 2-2-3a | 2.57 | 2.69 | 2.79 | 3.51 | 3.84 | **4.95** | **6.57** |
| 2-2-3b | 2.81 | 2.92 | 2.94 | 3.24 | 3.41 | 4.03 | 5.06 |
| 2-2-3c | 3.00 | 3.10 | 3.13 | 3.43 | 3.56 | 4.00 | 4.68 |
| 2-2-3d | 2.37 | 2.49 | 2.53 | 2.91 | 3.13 | 3.90 | 5.10 |
| 2-2-3e | 3.03 | 3.14 | 3.17 | 3.50 | 3.65 | 4.17 | 5.00 |
| 2-2-3f | 2.91 | 3.02 | 3.07 | 3.52 | 3.73 | 4.44 | 5.51 |
| 2-2-3g | 2.81 | 2.88 | 2.96 | 3.40 | 3.56 | 4.11 | 4.93 |
| 2-2-3h | 3.16 | 3.23 | 3.25 | 3.44 | 3.49 | 3.67 | 3.96 |
| 2-2-3i | 2.88 | 2.97 | 3.00 | 3.36 | 3.54 | 4.19 | 5.32 |
| 2-2-3j | 2.96 | 3.04 | 3.05 | 3.22 | 3.29 | 3.57 | 4.10 |
| 2-2-3k | 2.77 | 2.82 | 2.86 | 3.08 | 3.16 | 3.38 | 3.57 |
| 2-2-3l | 3.03 | 3.09 | 3.09 | 3.18 | 3.20 | 3.25 | 3.27 |
| 2-2-3m | 2.90 | 2.96 | 2.95 | 3.00 | 3.03 | 3.17 | 3.44 |
| 2-2-3n | 2.77 | 2.82 | 2.86 | 3.08 | 3.16 | 3.38 | 3.56 |
| 2-3-3a | 2.60 | 2.70 | 2.77 | 3.25 | 3.44 | 4.05 | 4.91 |
| 2-3-3b | 2.92 | 3.01 | 3.04 | 3.30 | 3.37 | 3.62 | 4.01 |
| 2-3-3c | 2.73 | 2.83 | 2.84 | 3.05 | 3.15 | 3.49 | 4.05 |
| 2-3-3d | 2.63 | 2.73 | 2.76 | 3.08 | 3.24 | 3.81 | 4.72 |
| 2-3-3e | 2.39 | 2.47 | 2.53 | 2.94 | 3.15 | 3.83 | 4.87 |
| 2-3-3f | 2.67 | 2.75 | 2.82 | 3.24 | 3.41 | 3.95 | 4.75 |
| 2-3-3g | 2.74 | 2.82 | 2.83 | 2.99 | 3.08 | 3.39 | 3.96 |
| 2-3-3h | 2.96 | 3.04 | 3.05 | 3.20 | 3.23 | 3.33 | 3.49 |
| 2-3-3i | 2.91 | 3.00 | 3.03 | 3.34 | 3.45 | 3.85 | 4.50 |
| 2-3-3j | 2.78 | 2.87 | 2.88 | 3.11 | 3.21 | 3.59 | 4.24 |
| 3-3-3a | 2.92 | 3.01 | 3.04 | 3.30 | 3.37 | 3.62 | 4.01 |
| 3-3-3b | 2.64 | 2.77 | 2.84 | 3.35 | 3.52 | 4.04 | 4.71 |
| 3-3-3c | 2.66 | 2.75 | 2.79 | 3.08 | 3.17 | 3.43 | 3.78 |
| 3-3-3d | 2.71 | 2.81 | 2.85 | 3.17 | 3.27 | 3.56 | 3.95 |

**Embolded** results indicate the highest binding energy geometry.

**Table 5.16:** Cluster energies (eV) for divalent cation solution in α-$Al_2O_3$ via neutral vacancy compensation.

| Divalent Cation | $Mg^{2+}$ | $Co^{2+}$ | $Fe^{2+}$ | $Cd^{2+}$ | $Ca^{2+}$ | $Sr^{2+}$ | $Ba^{2+}$ |
|---|---|---|---|---|---|---|---|
| Cation Radii (Å) | 0.72 | 0.75 | 0.780 | 0.95 | 1.00 | 1.18 | 1.35 |
| Isolated | 82.99 | 85.77 | 87.02 | 95.23 | 98.92 | 108.78 | 119.40 |
| 1-1a | 80.28 | 82.82 | 84.08 | 91.74 | 95.09 | 103.83 | 112.90 |
| 1-2a | 80.78 | 83.32 | 84.59 | 92.40 | 95.80 | 104.68 | 113.97 |
| 1-2b | 80.57 | 83.10 | 84.35 | 92.00 | 95.35 | 104.12 | 113.23 |
| 1-3a | 81.36 | 84.00 | 85.28 | 93.22 | 96.67 | 105.71 | 115.11 |
| 1-3b | 81.13 | 83.80 | 85.04 | 92.87 | 96.34 | 105.44 | 114.95 |
| 1-4a | 81.16 | 83.81 | 85.07 | 92.97 | 96.43 | 105.51 | 115.01 |
| 1-4b | 81.46 | 84.14 | 85.43 | 93.51 | 97.02 | 106.24 | 117.78 |
| 2-2a | 81.22 | 83.78 | 85.03 | 92.85 | 96.28 | 105.33 | 114.91 |
| 2-3a | 81.68 | 84.34 | 85.61 | 93.70 | 97.26 | 106.64 | 116.54 |
| 2-3b | 81.81 | 84.44 | 85.68 | 93.61 | 97.10 | 106.33 | 116.14 |
| 2-4a | 81.51 | 84.17 | 85.44 | 93.54 | 97.13 | 106.67 | 116.90 |
| 2-4b | 81.70 | 84.32 | 85.62 | 93.80 | 97.37 | 106.82 | 116.93 |
| 3-3a | 82.20 | 84.98 | 86.27 | 94.69 | 98.43 | 108.45 | 119.09 |
| 3-4a | 82.27 | 85.05 | 86.31 | 91.99 | 95.35 | 104.12 | 113.24 |
| 3-4b | 82.00 | 84.77 | 86.02 | 94.20 | 97.85 | 107.58 | 118.06 |
| 4-4a | 81.97 | 84.74 | 85.99 | 94.14 | 97.79 | 107.51 | 117.95 |

**Table 5.17:** Solution energies (eV) for divalent cations in α-$Al_2O_3$ via neutral vacancy compensation (reaction 5.8)

| Divalent Cation | $Mg^{2+}$ | $Co^{2+}$ | $Fe^{2+}$ | $Cd^{2+}$ | $Ca^{2+}$ | $Sr^{2+}$ | $Ba^{2+}$ |
|---|---|---|---|---|---|---|---|
| Cation Radii (Å) | 0.72 | 0.75 | 0.780 | 0.95 | 1.00 | 1.18 | 1.35 |
| Isolated | 1.98 | 2.07 | 2.17 | 3.01 | 3.50 | 5.12 | 7.40 |
| 1-1a | **1.08** | **1.09** | **1.18** | **1.84** | **2.22** | **3.47** | **5.24** |
| 1-2a | 1.25 | 1.25 | 1.36 | 2.06 | 2.46 | 3.76 | 5.59 |
| 1-2b | 1.18 | 1.18 | 1.28 | 1.93 | 2.31 | 3.57 | 5.35 |
| 1-3a | 1.44 | 1.48 | 1.58 | 2.34 | 2.75 | 4.10 | 5.98 |
| 1-3b | 1.37 | 1.41 | 1.51 | 2.22 | 2.64 | 4.01 | 5.92 |
| 1-4a | 1.38 | 1.42 | 1.51 | 2.25 | 2.67 | 4.03 | 5.94 |

*(continued on next page)*

**Embolded** results indicate the lowest solution energy geometry.

*(continued from previous page)*

| Divalent Cation | $Mg^{2+}$ | $Co^{2+}$ | $Fe^{2+}$ | $Cd^{2+}$ | $Ca^{2+}$ | $Sr^{2+}$ | $Ba^{2+}$ |
|---|---|---|---|---|---|---|---|
| Cation Radii (Å) | 0.72 | 0.75 | 0.780 | 0.95 | 1.00 | 1.18 | 1.35 |
| 1-4b | 1.47 | 1.53 | 1.63 | 2.43 | 2.86 | 4.28 | 6.86 |
| 2-2a | 1.40 | 1.41 | 1.50 | 2.21 | 2.62 | 3.97 | 5.91 |
| 2-3a | 1.55 | 1.59 | 1.70 | 2.50 | 2.94 | 4.41 | 6.45 |
| 2-3b | 1.59 | 1.63 | 1.72 | 2.47 | 2.89 | 4.31 | 6.32 |
| 2-4a | 1.49 | 1.54 | 1.64 | 2.44 | 2.90 | 4.42 | 6.57 |
| 2-4b | 1.56 | 1.59 | 1.70 | 2.53 | 2.98 | 4.47 | 6.58 |
| 3-3a | 1.72 | 1.81 | 1.91 | 2.83 | 3.33 | 5.02 | 7.30 |
| 3-4a | 1.75 | 1.83 | 1.93 | 1.93 | 2.31 | 3.57 | 5.35 |
| 3-4b | 1.66 | 1.74 | 1.83 | 2.66 | 3.14 | 4.72 | 6.96 |
| 4-4a | 1.65 | 1.73 | 1.82 | 2.64 | 3.12 | 4.70 | 6.92 |

**Embolded** results indicate the lowest solution energy geometry.

**Table 5.18:** Binding energies (eV) for neutral clusters in $\alpha$-$Al_2O_3$: vacancy compensation of 2+ cations (reaction 5.8).

| Divalent Cation | $Mg^{2+}$ | $Co^{2+}$ | $Fe^{2+}$ | $Cd^{2+}$ | $Ca^{2+}$ | $Sr^{2+}$ | $Ba^{2+}$ |
|---|---|---|---|---|---|---|---|
| Cation Radii (Å) | 0.72 | 0.75 | 0.780 | 0.95 | 1.00 | 1.18 | 1.35 |
| 1-1a | **2.71** | **2.95** | **2.95** | **3.49** | **3.83** | **4.95** | **6.50** |
| 1-2a | 2.20 | 2.45 | 2.43 | 2.83 | 3.13 | 4.09 | 5.43 |
| 1-2b | 2.42 | 2.67 | 2.67 | 3.24 | 3.57 | 4.65 | 6.17 |
| 1-3a | 1.62 | 1.78 | 1.75 | 2.01 | 2.25 | 3.07 | 4.28 |
| 1-3b | 1.85 | 1.97 | 1.98 | 2.36 | 2.59 | 3.33 | 4.45 |
| 1-4a | 1.83 | 1.96 | 1.96 | 2.26 | 2.50 | 3.27 | 4.39 |
| 1-4b | 1.53 | 1.64 | 1.59 | 1.73 | 1.90 | 2.54 | 1.62 |
| 2-2a | 1.76 | 1.99 | 2.00 | 2.38 | 2.64 | 3.45 | 4.49 |
| 2-3a | 1.30 | 1.44 | 1.41 | 1.53 | 1.67 | 2.13 | 2.86 |
| 2-3b | 1.18 | 1.34 | 1.34 | 1.63 | 1.83 | 2.44 | 3.26 |
| 2-4a | 1.48 | 1.60 | 1.58 | 1.69 | 1.79 | 2.11 | 2.50 |
| 2-4b | 1.28 | 1.45 | 1.41 | 1.43 | 1.56 | 1.95 | 2.47 |
| 3-3a | 0.78 | 0.79 | 0.76 | 0.54 | 0.49 | 0.32 | 0.31 |
| 3-4a | 0.71 | 0.72 | 0.71 | 3.24 | 3.57 | 4.66 | 6.16 |
| 3-4b | 0.98 | 1.00 | 1.00 | 1.04 | 1.08 | 1.20 | 1.34 |
| 4-4a | 1.02 | 1.03 | 1.04 | 1.09 | 1.13 | 1.27 | 1.44 |

**Embolded** results indicate the highest binding energy geometry.

**Table 5.19:** Isolated interstitial defect, substitutional defect and oxide lattice energies (eV) for divalent cations in $\alpha$-$Cr_2O_3$

| Divalent Cation | $Mg^{2+}$ | $Co^{2+}$ | $Fe^{2+}$ | $Cd^{2+}$ | $Ca^{2+}$ | $Sr^{2+}$ | $Ba^{2+}$ |
|---|---|---|---|---|---|---|---|
| Cation Radii (Å) | 0.72 | 0.75 | 0.780 | 0.95 | 1.00 | 1.18 | 1.35 |
| iso $B_i^{\bullet\bullet}$ | -16.86 | -15.34 | -14.52 | -9.43 | -7.37 | -1.77 | 4.46 |
| iso $B_{Cr}^{\prime}$ | 26.31 | 27.56 | 28.08 | 31.55 | 33.14 | 37.31 | 41.68 |
| Lattice Energy | -41.31 | -40.05 | -39.56 | -36.72 | -35.61 | -33.12 | -31.23 |

**Table 5.20:** Cluster energies (eV) for divalent cation solution in $\alpha$-$Cr_2O_3$ via neutral dopant interstitial compensation.

| Divalent Cation | $Mg^{2+}$ | $Co^{2+}$ | $Fe^{2+}$ | $Cd^{2+}$ | $Ca^{2+}$ | $Sr^{2+}$ | $Ba^{2+}$ |
|---|---|---|---|---|---|---|---|
| Cation Radii (Å) | 0.72 | 0.75 | 0.780 | 0.95 | 1.00 | 1.18 | 1.35 |
| Isolated | 35.77 | 39.78 | 41.63 | 53.68 | 58.90 | 72.85 | 87.82 |
| 1-1a | 32.02 | 36.22 | 38.25 | 51.02 | 56.35 | 70.39 | 85.13 |
| 1-2a | 32.94 | 36.98 | 38.93 | 51.32 | 56.55 | 70.39 | 82.82 |
| 1-2b | 32.96 | 37.03 | 38.98 | 51.33 | 56.54 | 70.30 | 84.65 |
| 1-3a | 33.00 | 37.06 | 39.03 | 51.49 | 56.77 | 70.81 | *pnc* |
| 1-3b | 33.32 | 37.33 | 39.27 | 51.55 | 56.74 | 70.45 | 84.90 |
| 1-4a | 33.07 | 36.94 | 38.90 | 50.92 | 55.98 | 69.26 | 83.32 |
| 1-4b | 32.61 | 36.64 | 38.62 | 51.05 | 56.32 | 70.34 | 85.29 |
| 2-2a | 34.10 | 37.98 | 39.79 | 51.41 | 56.43 | 69.73 | 83.84 |
| 2-2b | 33.86 | 37.78 | 39.59 | 51.27 | 56.34 | 69.76 | 83.97 |
| 2-2c | 33.86 | 37.78 | 39.59 | 51.27 | 56.34 | 69.76 | 83.97 |
| 2-3a | 34.54 | 38.50 | 40.30 | 52.00 | 57.06 | 70.46 | 84.49 |
| 2-3b | 33.99 | 37.93 | 39.78 | 51.70 | 56.87 | 70.60 | 85.14 |
| 2-3c | 34.54 | 38.50 | 40.30 | 52.00 | 57.06 | 70.46 | 84.49 |
| 2-3d | 33.99 | 37.93 | 39.78 | 51.70 | 56.87 | 70.60 | 85.14 |
| 2-4a | 33.59 | 37.46 | 39.32 | 51.11 | 56.23 | 69.81 | 84.21 |
| 2-4b | 33.60 | 37.50 | 39.36 | 51.23 | 56.37 | 70.03 | 84.58 |
| 3-3a | 34.29 | 38.24 | 40.10 | 52.15 | 57.36 | 71.33 | 86.24 |
| 3-3b | 34.26 | 38.23 | 40.10 | 52.22 | 57.47 | 71.49 | 86.26 |
| 3-3c | 34.20 | 38.16 | 40.03 | 52.13 | 57.37 | 71.40 | 86.23 |
| 3-4a | 33.74 | 37.65 | 39.54 | 51.57 | 56.79 | 70.74 | 85.75 |
| 3-4b | 34.00 | 37.92 | 39.82 | 51.88 | 57.09 | 70.96 | 85.14 |
| 4-4a | 33.29 | 37.15 | 39.05 | 51.03 | 56.23 | 70.13 | 85.15 |

**Table 5.21:** Solution energies (eV) for divalent cations in $\alpha$-$Cr_2O_3$ via neutral dopant interstitial compensation (reaction 5.6).

| Divalent Cation | $Mg^{2+}$ | $Co^{2+}$ | $Fe^{2+}$ | $Cd^{2+}$ | $Ca^{2+}$ | $Sr^{2+}$ | $Ba^{2+}$ |
|---|---|---|---|---|---|---|---|
| Cation Radii (Å) | 0.72 | 0.75 | 0.780 | 0.95 | 1.00 | 1.18 | 1.35 |
| Isolated | 2.39 | 2.46 | 2.60 | 3.77 | 4.40 | 6.56 | 9.66 |
| 1-1a | **1.14** | **1.28** | **1.47** | 2.88 | 3.55 | 5.74 | 8.76 |
| 1-2a | 1.44 | 1.53 | 1.70 | 2.98 | 3.61 | 5.74 | 7.99 |
| 1-2b | 1.45 | 1.55 | 1.71 | 2.98 | 3.61 | 5.71 | **8.61** |
| 1-3a | 1.46 | 1.56 | 1.73 | 3.04 | 3.69 | 5.88 | *pnc* |
| 1-3b | 1.57 | 1.64 | 1.81 | 3.06 | 3.68 | 5.76 | 8.69 |
| 1-4a | 1.49 | 1.52 | 1.68 | **2.85** | **3.42** | **5.36** | 8.16 |
| 1-4b | 1.33 | 1.42 | 1.59 | 2.89 | 3.54 | 5.72 | 8.82 |
| 2-2a | 1.83 | 1.86 | 1.98 | 3.01 | 3.58 | 5.52 | 8.33 |
| 2-2b | 1.75 | 1.80 | 1.91 | 2.97 | 3.54 | 5.53 | 8.38 |
| 2-2c | 1.75 | 1.80 | 1.91 | 2.97 | 3.54 | 5.53 | 8.38 |
| 2-3a | 1.98 | 2.03 | 2.15 | 3.21 | 3.78 | 5.76 | 8.55 |
| 2-3b | 1.79 | 1.85 | 1.98 | 3.11 | 3.72 | 5.81 | 8.77 |
| 2-3c | 1.98 | 2.03 | 2.15 | 3.21 | 3.78 | 5.76 | 8.55 |
| 2-3d | 1.79 | 1.85 | 1.98 | 3.11 | 3.72 | 5.81 | 8.77 |
| 2-4a | 1.66 | 1.69 | 1.82 | 2.91 | 3.51 | 5.55 | 8.46 |
| 2-4b | 1.66 | 1.70 | 1.84 | 2.95 | 3.56 | 5.62 | 8.58 |
| 3-3a | 1.89 | 1.95 | 2.09 | 3.26 | 3.89 | 6.05 | 9.13 |
| 3-3b | 1.88 | 1.94 | 2.09 | 3.28 | 3.92 | 6.11 | 9.14 |
| 3-3c | 1.86 | 1.92 | 2.06 | 3.25 | 3.89 | 6.07 | 9.13 |
| 3-4a | 1.71 | 1.75 | 1.90 | 3.07 | 3.69 | 5.86 | 8.97 |
| 3-4b | 1.80 | 1.84 | 1.99 | 3.17 | 3.79 | 5.93 | 8.77 |
| 4-4a | 1.56 | 1.58 | 1.73 | 2.89 | 3.51 | 5.65 | 8.77 |

**Embolded** results indicate the lowest solution energy geometry.

**Table 5.22:** Binding energies (eV) for neutral clusters in $\alpha$-$Cr_2O_3$: dopant interstitial compensation of 2+ cations (reaction 5.6).

| Divalent Cation | $Mg^{2+}$ | $Co^{2+}$ | $Fe^{2+}$ | $Cd^{2+}$ | $Ca^{2+}$ | $Sr^{2+}$ | $Ba^{2+}$ |
|---|---|---|---|---|---|---|---|
| Cation Radii (Å) | 0.72 | 0.75 | 0.780 | 0.95 | 1.00 | 1.18 | 1.35 |
| 1-1a | **3.74** | **3.55** | **3.38** | 2.65 | 2.56 | 2.46 | 2.70 |
| 1-2a | 2.83 | 2.79 | 2.70 | 2.36 | 2.36 | 2.46 | 5.00 |
| 1-2b | 2.81 | 2.75 | 2.65 | 2.35 | 2.36 | 2.55 | **3.17** |
| 1-3a | 2.77 | 2.71 | 2.60 | 2.19 | 2.13 | 2.04 | *pnc* |
| 1-3b | 2.44 | 2.45 | 2.36 | 2.13 | 2.17 | 2.40 | 2.93 |
| 1-4a | 2.70 | 2.83 | 2.73 | **2.76** | **2.93** | **3.59** | 4.50 |
| 1-4b | 3.16 | 3.13 | 3.01 | 2.63 | 2.58 | 2.51 | 2.53 |
| 2-2a | 1.67 | 1.79 | 1.85 | 2.27 | 2.47 | 3.12 | 3.99 |
| 2-2b | 1.91 | 1.99 | 2.04 | 2.41 | 2.57 | 3.09 | 3.85 |
| 2-2c | 1.91 | 1.99 | 2.04 | 2.41 | 2.57 | 3.09 | 3.85 |
| 2-3a | 1.23 | 1.28 | 1.34 | 1.68 | 1.85 | 2.39 | 3.34 |
| 2-3b | 1.77 | 1.84 | 1.85 | 1.97 | 2.04 | 2.25 | 2.68 |
| 2-3c | 1.23 | 1.28 | 1.34 | 1.68 | 1.85 | 2.39 | 3.34 |
| 2-3d | 1.77 | 1.84 | 1.85 | 1.97 | 2.04 | 2.25 | 2.68 |
| 2-4a | 2.18 | 2.31 | 2.32 | 2.57 | 2.67 | 3.04 | 3.61 |
| 2-4b | 2.17 | 2.28 | 2.27 | 2.45 | 2.53 | 2.82 | 3.24 |
| 3-3a | 1.48 | 1.54 | 1.53 | 1.53 | 1.54 | 1.52 | 1.58 |
| 3-3b | 1.51 | 1.55 | 1.53 | 1.46 | 1.44 | 1.36 | 1.57 |
| 3-3c | 1.57 | 1.62 | 1.60 | 1.55 | 1.53 | 1.46 | 1.59 |
| 3-4a | 2.02 | 2.12 | 2.09 | 2.11 | 2.12 | 2.11 | 2.07 |
| 3-4b | 1.77 | 1.86 | 1.82 | 1.80 | 1.82 | 1.89 | 2.69 |
| 4-4a | 2.48 | 2.63 | 2.58 | 2.64 | 2.67 | 2.72 | 2.67 |

**Embolded** results indicate the highest binding energy geometry.

**Table 5.23:** Cluster energies (eV) for divalent cation solution in $\alpha$-$Cr_2O_3$ via neutral interstitial compensation.

| Divalent Cation | $Mg^{2+}$ | $Co^{2+}$ | $Fe^{2+}$ | $Cd^{2+}$ | $Ca^{2+}$ | $Sr^{2+}$ | $Ba^{2+}$ |
|---|---|---|---|---|---|---|---|
| Cation Radii (Å) | 0.72 | 0.75 | 0.780 | 0.95 | 1.00 | 1.18 | 1.35 |
| Isolated | 39.70 | 43.44 | 44.99 | 55.42 | 60.17 | 72.69 | 85.81 |
| 1-1-2a | 33.67 | 37.72 | 39.72 | 52.46 | 57.85 | 72.26 | 86.60 |
| 1-1-3a | 34.01 | 37.96 | 39.92 | 52.28 | 57.53 | 71.50 | 85.63 |
| 1-2-2a | 34.93 | 38.77 | 40.57 | 52.14 | 57.14 | 70.34 | *pnc* |
| 1-2-2b | 34.70 | 38.57 | 40.39 | 52.11 | 57.21 | 70.77 | 84.01 |
| 1-2-2c | 34.67 | 38.51 | 40.32 | 51.93 | 56.97 | 70.29 | 82.68 |
| 1-2-2d | 34.74 | 38.62 | 40.43 | 52.09 | 57.18 | 70.71 | 84.18 |
| 1-2-3a | 35.29 | 39.13 | 40.89 | 52.28 | 57.24 | 70.33 | 82.91 |
| 1-2-3b | 34.77 | 38.59 | 40.40 | 51.98 | 57.02 | 70.39 | 83.37 |
| 1-2-3c | 35.28 | 39.05 | 40.84 | 52.26 | 57.21 | 70.27 | 83.93 |
| 1-2-3d | 35.07 | 38.84 | 40.62 | 51.97 | 56.91 | 69.92 | 83.44 |
| 1-2-3e | 34.94 | 38.77 | 40.58 | 52.11 | 57.14 | 70.45 | 83.51 |
| 1-2-3f | 35.29 | 39.13 | 40.89 | 52.28 | 57.24 | 70.33 | 82.91 |
| 1-2-3g | 35.17 | 38.97 | 40.74 | 52.12 | 57.09 | 70.22 | 84.03 |
| 1-2-3h | 35.27 | 39.03 | 40.81 | 52.15 | 57.05 | 69.95 | 83.28 |
| 1-3-3a | 35.01 | 38.79 | 40.58 | 52.00 | 57.01 | 70.28 | 83.30 |
| 1-3-3b | 35.67 | 39.36 | 41.09 | 52.12 | 56.94 | 69.61 | 82.90 |
| 1-3-3c | 35.31 | 39.05 | 40.83 | 52.12 | 57.05 | 70.09 | 83.78 |
| 1-3-3d | 35.24 | 38.99 | 40.76 | 52.02 | 56.94 | 69.95 | 83.62 |
| 2-2-2a | 36.20 | 39.83 | 41.37 | 51.56 | 56.17 | 68.24 | 80.71 |
| 2-2-2b | 35.99 | 39.65 | 41.20 | 51.51 | 56.20 | 68.56 | 81.47 |
| 2-2-2c | 35.76 | 39.43 | 40.97 | 51.23 | 55.92 | 68.26 | 81.01 |
| 2-2-3a | 36.85 | 40.51 | 42.01 | 52.02 | 56.55 | 68.36 | 80.47 |
| 2-2-3b | 36.34 | 39.98 | 41.55 | 51.88 | 56.53 | 68.73 | 81.35 |
| 2-2-3c | 36.16 | 39.80 | 41.36 | 51.67 | 56.34 | 68.66 | 81.51 |
| 2-2-3d | 36.88 | 40.52 | 42.07 | 52.31 | 56.92 | 69.00 | 81.50 |
| 2-2-3e | 36.12 | 39.75 | 41.32 | 51.62 | 56.29 | 68.57 | 81.32 |
| 2-2-3f | 36.32 | 39.96 | 41.51 | 51.72 | 56.34 | 68.44 | 80.96 |
| 2-2-3g | 36.49 | 40.16 | 41.68 | 51.81 | 56.43 | 68.55 | 81.12 |
| 2-2-3h | 35.96 | 39.61 | 41.18 | 51.52 | 56.23 | 68.67 | 81.66 |
| 2-2-3i | 36.27 | 39.92 | 41.49 | 51.76 | 56.40 | 68.51 | 80.88 |
| 2-2-3j | 36.11 | 39.76 | 41.34 | 51.70 | 56.40 | 68.76 | 81.58 |

*(continued on next page)*

*(continued from previous page)*

| Divalent Cation | $Mg^{2+}$ | $Co^{2+}$ | $Fe^{2+}$ | $Cd^{2+}$ | $Ca^{2+}$ | $Sr^{2+}$ | $Ba^{2+}$ |
|---|---|---|---|---|---|---|---|
| Cation Radii (Å) | 0.72 | 0.75 | 0.780 | 0.95 | 1.00 | 1.18 | 1.35 |
| 2-2-3k | 36.45 | 40.14 | 41.66 | 51.92 | 56.59 | 68.94 | 81.92 |
| 2-2-3l | 36.07 | 39.74 | 41.31 | 51.70 | 56.43 | 68.92 | 82.07 |
| 2-2-3m | 36.16 | 39.83 | 41.41 | 51.85 | 56.58 | 69.04 | 82.04 |
| 2-2-3n | 36.45 | 40.14 | 41.66 | 51.92 | 56.59 | 68.94 | 81.92 |
| 2-3-3a | 36.75 | 40.40 | 41.91 | 52.01 | 56.61 | 68.70 | 81.24 |
| 2-3-3b | 36.27 | 39.90 | 41.46 | 51.75 | 56.44 | 68.81 | 81.74 |
| 2-3-3c | 36.42 | 40.05 | 41.61 | 51.93 | 56.60 | 68.89 | 81.65 |
| 2-3-3d | 36.57 | 40.21 | 41.77 | 52.02 | 56.66 | 68.80 | 81.30 |
| 2-3-3e | 36.93 | 40.60 | 42.13 | 52.31 | 56.92 | 69.00 | 81.48 |
| 2-3-3f | 36.65 | 40.32 | 41.84 | 51.98 | 56.61 | 68.78 | 81.46 |
| 2-3-3g | 36.39 | 40.05 | 41.63 | 52.03 | 56.74 | 69.12 | 82.01 |
| 2-3-3h | 36.18 | 39.82 | 41.40 | 51.78 | 56.51 | 69.01 | 82.17 |
| 2-3-3i | 36.29 | 39.94 | 41.50 | 51.78 | 56.45 | 68.76 | 81.59 |
| 2-3-3j | 36.37 | 40.03 | 41.59 | 51.94 | 56.62 | 68.94 | 81.74 |
| 3-3-3a | 36.27 | 39.90 | 41.46 | 51.75 | 56.44 | 68.81 | 81.74 |
| 3-3-3b | 36.70 | 40.29 | 41.82 | 51.90 | 56.51 | 68.60 | 81.10 |
| 3-3-3c | 36.63 | 40.25 | 41.80 | 52.06 | 56.74 | 69.08 | 82.00 |
| 3-3-3d | 36.58 | 40.20 | 41.74 | 51.97 | 56.64 | 68.97 | 81.86 |

**Table 5.24:** Solution energies (eV) for divalent cations in $\alpha$-$Cr_2O_3$ via neutral interstitial compensation (reaction 5.7).

| Divalent Cation | $Mg^{2+}$ | $Co^{2+}$ | $Fe^{2+}$ | $Cd^{2+}$ | $Ca^{2+}$ | $Sr^{2+}$ | $Ba^{2+}$ |
|---|---|---|---|---|---|---|---|
| Cation Radii (Å) | 0.72 | 0.75 | 0.780 | 0.95 | 1.00 | 1.18 | 1.35 |
| Isolated | 2.77 | 2.76 | 2.79 | 3.26 | 3.62 | 4.88 | 6.74 |
| 1-1-2a | **1.26** | **1.33** | **1.47** | 2.52 | 3.04 | 4.77 | 6.94 |
| 1-1-3a | 1.35 | 1.39 | 1.52 | 2.48 | 2.96 | 4.58 | 6.70 |
| 1-2-2a | 1.58 | 1.59 | 1.68 | 2.44 | 2.86 | 4.29 | *pnc* |
| 1-2-2b | 1.52 | 1.54 | 1.64 | 2.44 | 2.88 | 4.40 | 6.29 |
| 1-2-2c | 1.52 | 1.53 | 1.62 | 2.39 | 2.82 | 4.28 | 5.96 |
| 1-2-2d | 1.53 | 1.56 | 1.65 | 2.43 | 2.87 | 4.38 | 6.34 |
| 1-2-3a | 1.67 | 1.68 | 1.76 | 2.48 | 2.88 | 4.29 | 6.02 |
| 1-2-3b | 1.54 | 1.55 | 1.64 | 2.40 | 2.83 | 4.30 | 6.13 |

*(continued on next page)*

**Embolded** results indicate the lowest solution energy geometry.

*(continued from previous page)*

| Divalent Cation | $Mg^{2+}$ | $Co^{2+}$ | $Fe^{2+}$ | $Cd^{2+}$ | $Ca^{2+}$ | $Sr^{2+}$ | $Ba^{2+}$ |
|---|---|---|---|---|---|---|---|
| Cation Radii (Å) | 0.72 | 0.75 | 0.780 | 0.95 | 1.00 | 1.18 | 1.35 |
| 1-2-3c | 1.67 | 1.66 | 1.75 | 2.47 | 2.88 | 4.27 | 6.27 |
| 1-2-3d | 1.61 | 1.61 | 1.69 | 2.40 | 2.80 | 4.19 | 6.15 |
| 1-2-3e | 1.58 | 1.59 | 1.68 | 2.44 | 2.86 | 4.32 | 6.17 |
| 1-2-3f | 1.67 | 1.68 | 1.76 | 2.48 | 2.88 | 4.29 | 6.02 |
| 1-2-3g | 1.64 | 1.64 | 1.72 | 2.44 | 2.85 | 4.26 | 6.30 |
| 1-2-3h | 1.66 | 1.66 | 1.74 | 2.44 | 2.84 | 4.19 | 6.11 |
| 1-3-3a | 1.60 | 1.60 | 1.68 | 2.41 | 2.83 | 4.28 | 6.11 |
| 1-3-3b | 1.76 | 1.74 | 1.81 | 2.44 | 2.81 | 4.11 | 6.02 |
| 1-3-3c | 1.67 | 1.66 | 1.74 | 2.44 | 2.84 | 4.23 | 6.24 |
| 1-3-3d | 1.66 | 1.65 | 1.73 | 2.41 | 2.81 | 4.19 | 6.19 |
| 2-2-2a | 1.90 | 1.86 | 1.88 | 2.30 | 2.62 | **3.77** | 5.47 |
| 2-2-2b | 1.84 | 1.81 | 1.84 | 2.28 | 2.62 | 3.85 | 5.66 |
| 2-2-2c | 1.79 | 1.76 | 1.78 | **2.21** | **2.55** | 3.77 | 5.54 |
| 2-2-3a | 2.06 | 2.03 | 2.04 | 2.41 | 2.71 | 3.80 | **5.41** |
| 2-2-3b | 1.93 | 1.90 | 1.93 | 2.38 | 2.71 | 3.89 | 5.63 |
| 2-2-3c | 1.89 | 1.85 | 1.88 | 2.32 | 2.66 | 3.87 | 5.67 |
| 2-2-3d | 2.07 | 2.03 | 2.05 | 2.48 | 2.80 | 3.96 | 5.66 |
| 2-2-3e | 1.88 | 1.84 | 1.87 | 2.31 | 2.65 | 3.85 | 5.62 |
| 2-2-3f | 1.93 | 1.89 | 1.92 | 2.34 | 2.66 | 3.82 | 5.53 |
| 2-2-3g | 1.97 | 1.94 | 1.96 | 2.36 | 2.68 | 3.85 | 5.57 |
| 2-2-3h | 1.84 | 1.80 | 1.83 | 2.29 | 2.63 | 3.87 | 5.71 |
| 2-2-3i | 1.91 | 1.88 | 1.91 | 2.35 | 2.67 | 3.83 | 5.51 |
| 2-2-3j | 1.87 | 1.84 | 1.87 | 2.33 | 2.67 | 3.90 | 5.68 |
| 2-2-3k | 1.96 | 1.93 | 1.95 | 2.39 | 2.72 | 3.94 | 5.77 |
| 2-2-3l | 1.86 | 1.84 | 1.87 | 2.33 | 2.68 | 3.94 | 5.81 |
| 2-2-3m | 1.89 | 1.86 | 1.89 | 2.37 | 2.72 | 3.97 | 5.80 |
| 2-2-3n | 1.96 | 1.93 | 1.95 | 2.39 | 2.72 | 3.94 | 5.77 |
| 2-3-3a | 2.04 | 2.00 | 2.02 | 2.41 | 2.73 | 3.88 | 5.60 |
| 2-3-3b | 1.92 | 1.88 | 1.90 | 2.34 | 2.68 | 3.91 | 5.72 |
| 2-3-3c | 1.95 | 1.91 | 1.94 | 2.39 | 2.72 | 3.93 | 5.70 |
| 2-3-3d | 1.99 | 1.95 | 1.98 | 2.41 | 2.74 | 3.91 | 5.62 |
| 2-3-3e | 2.08 | 2.05 | 2.07 | 2.48 | 2.80 | 3.96 | 5.66 |
| 2-3-3f | 2.01 | 1.98 | 2.00 | 2.40 | 2.73 | 3.90 | 5.66 |
| 2-3-3g | 1.95 | 1.91 | 1.95 | 2.41 | 2.76 | 3.99 | 5.79 |

*(continued on next page)*

**Embolded** results indicate the lowest solution energy geometry.

*(continued from previous page)*

| Divalent Cation | $Mg^{2+}$ | $Co^{2+}$ | $Fe^{2+}$ | $Cd^{2+}$ | $Ca^{2+}$ | $Sr^{2+}$ | $Ba^{2+}$ |
|---|---|---|---|---|---|---|---|
| Cation Radii (Å) | 0.72 | 0.75 | 0.780 | 0.95 | 1.00 | 1.18 | 1.35 |
| 2-3-3h | 1.89 | 1.86 | 1.89 | 2.35 | 2.70 | 3.96 | 5.83 |
| 2-3-3i | 1.92 | 1.89 | 1.91 | 2.35 | 2.69 | 3.90 | 5.69 |
| 2-3-3j | 1.94 | 1.91 | 1.94 | 2.39 | 2.73 | 3.94 | 5.72 |
| 3-3-3a | 1.92 | 1.88 | 1.90 | 2.34 | 2.68 | 3.91 | 5.72 |
| 3-3-3b | 2.02 | 1.97 | 1.99 | 2.38 | 2.70 | 3.86 | 5.57 |
| 3-3-3c | 2.00 | 1.96 | 1.99 | 2.42 | 2.76 | 3.98 | 5.79 |
| 3-3-3d | 1.99 | 1.95 | 1.97 | 2.40 | 2.73 | 3.95 | 5.75 |

**Embolded** results indicate the lowest solution energy geometry.

**Table 5.25:** Binding energies (eV) for neutral clusters in $\alpha$-$Cr_2O_3$: interstitial compensation of 2+ cations (reaction 5.7).

| Divalent Cation | $Mg^{2+}$ | $Co^{2+}$ | $Fe^{2+}$ | $Cd^{2+}$ | $Ca^{2+}$ | $Sr^{2+}$ | $Ba^{2+}$ |
|---|---|---|---|---|---|---|---|
| Cation Radii (Å) | 0.72 | 0.75 | 0.780 | 0.95 | 1.00 | 1.18 | 1.35 |
| 1-1-2a | **6.03** | **5.72** | **5.27** | 2.97 | 2.32 | 0.43 | -0.79 |
| 1-1-3a | 5.68 | 5.48 | 5.07 | 3.14 | 2.64 | 1.19 | 0.18 |
| 1-2-2a | 4.77 | 4.67 | 4.42 | 3.28 | 3.02 | 2.36 | *pnc* |
| 1-2-2b | 4.99 | 4.87 | 4.60 | 3.31 | 2.95 | 1.93 | 1.80 |
| 1-2-2c | 5.02 | 4.93 | 4.67 | 3.49 | 3.19 | 2.40 | 3.13 |
| 1-2-2d | 4.96 | 4.82 | 4.56 | 3.34 | 2.99 | 1.99 | 1.63 |
| 1-2-3a | 4.41 | 4.31 | 4.10 | 3.14 | 2.93 | 2.36 | 2.90 |
| 1-2-3b | 4.93 | 4.85 | 4.59 | 3.44 | 3.14 | 2.30 | 2.44 |
| 1-2-3c | 4.41 | 4.39 | 4.15 | 3.16 | 2.96 | 2.42 | 1.88 |
| 1-2-3d | 4.63 | 4.60 | 4.37 | 3.45 | 3.26 | 2.77 | 2.37 |
| 1-2-3e | 4.76 | 4.67 | 4.41 | 3.31 | 3.03 | 2.24 | 2.29 |
| 1-2-3f | 4.41 | 4.31 | 4.10 | 3.14 | 2.93 | 2.36 | 2.90 |
| 1-2-3g | 4.53 | 4.47 | 4.25 | 3.30 | 3.08 | 2.47 | 1.78 |
| 1-2-3h | 4.43 | 4.41 | 4.18 | 3.28 | 3.11 | 2.75 | 2.53 |
| 1-3-3a | 4.69 | 4.65 | 4.41 | 3.42 | 3.16 | 2.41 | 2.51 |
| 1-3-3b | 4.03 | 4.08 | 3.90 | 3.30 | 3.23 | 3.08 | 2.91 |
| 1-3-3c | 4.39 | 4.39 | 4.16 | 3.30 | 3.12 | 2.61 | 2.03 |
| 1-3-3d | 4.45 | 4.45 | 4.23 | 3.40 | 3.22 | 2.74 | 2.19 |
| 2-2-2a | 3.49 | 3.61 | 3.62 | 3.87 | 4.00 | **4.45** | 5.10 |

*(continued on next page)*

**Embolded** results indicate the highest binding energy geometry.

*(continued from previous page)*

| Divalent Cation | $Mg^{2+}$ | $Co^{2+}$ | $Fe^{2+}$ | $Cd^{2+}$ | $Ca^{2+}$ | $Sr^{2+}$ | $Ba^{2+}$ |
|---|---|---|---|---|---|---|---|
| Cation Radii (Å) | 0.72 | 0.75 | 0.780 | 0.95 | 1.00 | 1.18 | 1.35 |
| 2-2-2b | 3.71 | 3.79 | 3.79 | 3.91 | 3.96 | 4.13 | 4.34 |
| 2-2-2c | 3.94 | 4.01 | 4.02 | **4.19** | **4.24** | 4.44 | 4.80 |
| 2-2-3a | 2.84 | 2.93 | 2.98 | 3.40 | 3.62 | 4.34 | **5.34** |
| 2-2-3b | 3.36 | 3.46 | 3.44 | 3.55 | 3.64 | 3.96 | 4.46 |
| 2-2-3c | 3.54 | 3.64 | 3.63 | 3.76 | 3.82 | 4.03 | 4.30 |
| 2-2-3d | 2.82 | 2.92 | 2.92 | 3.11 | 3.25 | 3.69 | 4.31 |
| 2-2-3e | 3.58 | 3.69 | 3.67 | 3.80 | 3.87 | 4.12 | 4.48 |
| 2-2-3f | 3.38 | 3.48 | 3.48 | 3.70 | 3.83 | 4.25 | 4.85 |
| 2-2-3g | 3.21 | 3.28 | 3.31 | 3.62 | 3.74 | 4.14 | 4.69 |
| 2-2-3h | 3.74 | 3.83 | 3.81 | 3.90 | 3.93 | 4.03 | 4.15 |
| 2-2-3i | 3.43 | 3.52 | 3.50 | 3.67 | 3.77 | 4.19 | 4.93 |
| 2-2-3j | 3.59 | 3.68 | 3.65 | 3.72 | 3.76 | 3.93 | 4.23 |
| 2-2-3k | 3.25 | 3.30 | 3.33 | 3.51 | 3.58 | 3.76 | 3.89 |
| 2-2-3l | 3.63 | 3.70 | 3.68 | 3.72 | 3.74 | 3.77 | 3.74 |
| 2-2-3m | 3.54 | 3.61 | 3.58 | 3.57 | 3.59 | 3.65 | 3.76 |
| 2-2-3n | 3.25 | 3.30 | 3.33 | 3.51 | 3.58 | 3.76 | 3.89 |
| 2-3-3a | 2.94 | 3.04 | 3.08 | 3.41 | 3.56 | 4.00 | 4.57 |
| 2-3-3b | 3.42 | 3.54 | 3.53 | 3.67 | 3.73 | 3.88 | 4.07 |
| 2-3-3c | 3.28 | 3.39 | 3.38 | 3.50 | 3.56 | 3.80 | 4.16 |
| 2-3-3d | 3.12 | 3.23 | 3.22 | 3.40 | 3.51 | 3.89 | 4.51 |
| 2-3-3e | 2.77 | 2.84 | 2.86 | 3.11 | 3.25 | 3.69 | 4.33 |
| 2-3-3f | 3.04 | 3.12 | 3.15 | 3.44 | 3.56 | 3.91 | 4.35 |
| 2-3-3g | 3.30 | 3.39 | 3.36 | 3.39 | 3.43 | 3.57 | 3.80 |
| 2-3-3h | 3.52 | 3.62 | 3.59 | 3.64 | 3.66 | 3.68 | 3.64 |
| 2-3-3i | 3.41 | 3.50 | 3.49 | 3.64 | 3.71 | 3.93 | 4.22 |
| 2-3-3j | 3.32 | 3.41 | 3.40 | 3.49 | 3.54 | 3.75 | 4.07 |
| 3-3-3a | 3.42 | 3.54 | 3.53 | 3.67 | 3.73 | 3.88 | 4.07 |
| 3-3-3b | 3.00 | 3.15 | 3.18 | 3.53 | 3.66 | 4.10 | 4.70 |
| 3-3-3c | 3.07 | 3.18 | 3.19 | 3.37 | 3.43 | 3.61 | 3.81 |
| 3-3-3d | 3.12 | 3.24 | 3.25 | 3.45 | 3.52 | 3.73 | 3.95 |

**Embolded** results indicate the highest binding energy geometry.

**Table 5.26:** Cluster energies (eV) for divalent cation solution in $\alpha$-$Cr_2O_3$ via neutral vacancy compensation.

| Divalent Cation | $Mg^{2+}$ | $Co^{2+}$ | $Fe^{2+}$ | $Cd^{2+}$ | $Ca^{2+}$ | $Sr^{2+}$ | $Ba^{2+}$ |
|---|---|---|---|---|---|---|---|
| Cation Radii (Å) | 0.72 | 0.75 | 0.780 | 0.95 | 1.00 | 1.18 | 1.35 |
| Isolated | 76.23 | 78.73 | 79.76 | 86.72 | 89.88 | 98.23 | 106.97 |
| 1-1a | 73.02 | 75.36 | 76.47 | 83.33 | 86.28 | 93.88 | 101.54 |
| 1-2a | 73.54 | 75.86 | 76.96 | 83.87 | 86.85 | 94.61 | 102.51 |
| 1-2b | 73.33 | 75.65 | 76.76 | 83.57 | 86.52 | 94.14 | 101.84 |
| 1-3a | 74.20 | 76.59 | 77.69 | 84.71 | 87.77 | 95.70 | 103.74 |
| 1-3b | 74.02 | 76.45 | 77.52 | 84.42 | 87.46 | 95.36 | 103.39 |
| 1-4a | 74.06 | 76.47 | 77.55 | 84.48 | 87.52 | 95.46 | 103.56 |
| 1-4b | 74.25 | 76.70 | 77.81 | 84.93 | 88.02 | 96.08 | *pnc* |
| 2-2a | 74.08 | 76.41 | 77.48 | 84.30 | 87.29 | 95.11 | 103.25 |
| 2-3a | 74.52 | 76.92 | 78.00 | 84.98 | 88.06 | 96.14 | 104.51 |
| 2-3b | 74.78 | 77.16 | 78.21 | 85.08 | 88.12 | 96.13 | 104.51 |
| 2-4a | 74.40 | 76.80 | 77.87 | 84.84 | 87.94 | 96.12 | 104.69 |
| 2-4b | 74.57 | 76.94 | 78.02 | 85.06 | 88.16 | 96.36 | 105.02 |
| 3-3a | 75.11 | 77.61 | 78.67 | 85.78 | 88.99 | 97.56 | 106.77 |
| 3-4a | 75.29 | 77.80 | 78.85 | 85.88 | 89.03 | 94.13 | 101.84 |
| 3-4b | 75.04 | 77.54 | 78.58 | 85.56 | 88.72 | 97.06 | 105.83 |
| 4-4a | 75.04 | 77.55 | 78.58 | 85.56 | 88.71 | 97.04 | 105.73 |

**Table 5.27:** Solution energies (eV) for divalent cations in $\alpha$-$Cr_2O_3$ via neutral vacancy compensation (reaction 5.8).

| Divalent Cation | $Mg^{2+}$ | $Co^{2+}$ | $Fe^{2+}$ | $Cd^{2+}$ | $Ca^{2+}$ | $Sr^{2+}$ | $Ba^{2+}$ |
|---|---|---|---|---|---|---|---|
| Cation Radii (Å) | 0.72 | 0.75 | 0.780 | 0.95 | 1.00 | 1.18 | 1.35 |
| Isolated | 2.10 | 2.09 | 2.12 | 2.54 | 2.85 | 3.98 | 5.63 |
| 1-1a | **1.03** | **0.97** | **1.02** | **1.41** | **1.65** | **2.53** | **3.82** |
| 1-2a | 1.21 | 1.14 | 1.18 | 1.59 | 1.85 | 2.77 | 4.15 |
| 1-2b | 1.14 | 1.07 | 1.11 | 1.49 | 1.73 | 2.61 | 3.92 |
| 1-3a | 1.43 | 1.38 | 1.43 | 1.87 | 2.15 | 3.14 | 4.56 |
| 1-3b | 1.37 | 1.33 | 1.37 | 1.78 | 2.05 | 3.02 | 4.44 |
| 1-4a | 1.38 | 1.34 | 1.38 | 1.80 | 2.07 | 3.05 | 4.50 |

*(continued on next page)*

**Embolded** results indicate the lowest solution energy geometry.

*(continued from previous page)*

| Divalent Cation | $Mg^{2+}$ | $Co^{2+}$ | $Fe^{2+}$ | $Cd^{2+}$ | $Ca^{2+}$ | $Sr^{2+}$ | $Ba^{2+}$ |
|---|---|---|---|---|---|---|---|
| Cation Radii (Å) | 0.72 | 0.75 | 0.780 | 0.95 | 1.00 | 1.18 | 1.35 |
| 1-4b | 1.44 | 1.42 | 1.47 | 1.94 | 2.24 | 3.26 | *pnc* |
| 2-2a | 1.38 | 1.32 | 1.36 | 1.74 | 1.99 | 2.94 | 4.39 |
| 2-3a | 1.53 | 1.49 | 1.53 | 1.96 | 2.25 | 3.28 | 4.81 |
| 2-3b | 1.62 | 1.57 | 1.60 | 1.99 | 2.27 | 3.28 | 4.81 |
| 2-4a | 1.49 | 1.45 | 1.49 | 1.91 | 2.21 | 3.28 | 4.87 |
| 2-4b | 1.55 | 1.50 | 1.54 | 1.99 | 2.28 | 3.36 | 4.98 |
| 3-3a | 1.73 | 1.72 | 1.75 | 2.23 | 2.56 | 3.75 | 5.57 |
| 3-4a | 1.79 | 1.78 | 1.81 | 2.26 | 2.57 | 2.61 | 3.92 |
| 3-4b | 1.71 | 1.70 | 1.72 | 2.16 | 2.47 | 3.59 | 5.25 |
| 4-4a | 1.71 | 1.70 | 1.72 | 2.16 | 2.47 | 3.58 | 5.22 |

**Embolded** results indicate the lowest solution energy geometry.

**Table 5.28:** Binding energies (eV) for neutral clusters in $\alpha$-$Cr_2O_3$: vacancy compensation of 2+ cations (reaction 5.8).

| Divalent Cation | $Mg^{2+}$ | $Co^{2+}$ | $Fe^{2+}$ | $Cd^{2+}$ | $Ca^{2+}$ | $Sr^{2+}$ | $Ba^{2+}$ |
|---|---|---|---|---|---|---|---|
| Cation Radii (Å) | 0.72 | 0.75 | 0.780 | 0.95 | 1.00 | 1.18 | 1.35 |
| 1-1a | **3.21** | **3.37** | **3.29** | **3.39** | **3.60** | **4.35** | **5.44** |
| 1-2a | 2.69 | 2.87 | 2.80 | 2.85 | 3.03 | 3.62 | 4.46 |
| 1-2b | 2.90 | 3.08 | 3.01 | 3.15 | 3.36 | 4.09 | 5.13 |
| 1-3a | 2.04 | 2.14 | 2.07 | 2.00 | 2.11 | 2.53 | 3.23 |
| 1-3b | 2.21 | 2.28 | 2.24 | 2.30 | 2.42 | 2.87 | 3.58 |
| 1-4a | 2.18 | 2.26 | 2.21 | 2.24 | 2.36 | 2.77 | 3.41 |
| 1-4b | 1.98 | 2.03 | 1.95 | 1.79 | 1.86 | 2.15 | *pnc* |
| 2-2a | 2.16 | 2.32 | 2.28 | 2.42 | 2.59 | 3.12 | 3.72 |
| 2-3a | 1.72 | 1.81 | 1.76 | 1.74 | 1.82 | 2.09 | 2.47 |
| 2-3b | 1.46 | 1.57 | 1.55 | 1.64 | 1.76 | 2.10 | 2.47 |
| 2-4a | 1.84 | 1.92 | 1.89 | 1.88 | 1.94 | 2.11 | 2.28 |
| 2-4b | 1.67 | 1.79 | 1.74 | 1.65 | 1.71 | 1.87 | 1.96 |
| 3-3a | 1.12 | 1.12 | 1.10 | 0.93 | 0.89 | 0.67 | 0.20 |
| 3-4a | 0.95 | 0.93 | 0.91 | 0.84 | 0.85 | 4.10 | 5.14 |
| 3-4b | 1.19 | 1.19 | 1.19 | 1.15 | 1.16 | 1.17 | 1.15 |
| 4-4a | 1.19 | 1.18 | 1.18 | 1.16 | 1.17 | 1.19 | 1.24 |

**Embolded** results indicate the highest binding energy geometry.

**Table 5.29:** Isolated interstitial defect, substitutional defect and oxide lattice energies (eV) for divalent cations in α-$Fe_2O_3$

| Divalent Cation | $Mg^{2+}$ | $Co^{2+}$ | $Cd^{2+}$ | $Ca^{2+}$ | $Sr^{2+}$ | $Ba^{2+}$ |
|---|---|---|---|---|---|---|
| Cation Radii (Å) | 0.72 | 0.75 | 0.95 | 1.00 | 1.18 | 1.35 |
| iso $B_i^{\bullet\bullet}$ | -16.79 | -15.28 | -9.39 | -7.33 | -1.74 | 4.48 |
| iso $B'_{Fe}$ | 26.38 | 27.62 | 31.60 | 33.17 | 37.33 | 41.68 |
| Lattice Energy | -41.31 | -40.05 | -36.72 | -35.61 | -33.12 | -31.23 |

**Table 5.30:** Cluster energies (eV) for divalent cation solution in α-$Fe_2O_3$ via neutral dopant interstitial compensation.

| Divalent Cation | $Mg^{2+}$ | $Co^{2+}$ | $Cd^{2+}$ | $Ca^{2+}$ | $Sr^{2+}$ | $Ba^{2+}$ |
|---|---|---|---|---|---|---|
| Cation Radii (Å) | 0.72 | 0.75 | 0.95 | 1.00 | 1.18 | 1.35 |
| Isolated | 35.97 | 39.97 | 53.81 | 59.01 | 72.91 | 87.83 |
| 1-1a | 32.03 | 36.22 | 50.95 | 56.25 | 70.24 | 84.92 |
| 1-2a | 32.98 | 37.01 | 51.28 | 56.49 | 70.29 | 82.81 |
| 1-2b | 33.00 | 37.06 | 51.30 | 56.49 | 70.21 | 84.52 |
| 1-3a | 33.04 | 37.10 | 51.46 | 56.73 | 70.72 | 85.61 |
| 1-3b | 33.38 | 37.37 | 51.54 | 56.71 | 70.39 | 84.81 |
| 1-4a | 33.14 | 37.00 | 50.92 | 55.95 | 69.16 | 83.14 |
| 1-4b | 32.66 | 36.68 | 51.02 | 56.28 | 70.24 | 85.13 |
| 2-2a | 34.20 | 38.06 | 51.44 | 56.44 | 69.69 | 83.76 |
| 2-2b | 33.95 | 37.86 | 51.28 | 56.33 | 69.71 | 83.89 |
| 2-2c | 33.95 | 37.86 | 51.28 | 56.33 | 69.71 | 83.89 |
| 2-3a | 34.66 | 38.61 | 52.05 | 57.10 | 70.46 | 84.46 |
| 2-3b | 34.09 | 38.01 | 51.73 | 56.87 | 70.57 | 85.10 |
| 2-3c | 34.66 | 38.61 | 52.05 | 57.10 | 70.46 | 84.46 |
| 2-3d | 34.09 | 38.01 | 51.73 | 56.87 | 70.57 | 85.10 |
| 2-4a | 33.69 | 37.55 | 51.14 | 56.23 | 69.76 | 84.11 |
| 2-4b | 33.70 | 37.58 | 51.26 | 56.38 | 69.99 | 84.49 |
| 3-3a | 34.39 | 38.33 | 52.18 | 57.38 | 71.30 | 86.18 |
| 3-3b | 34.36 | 38.32 | 52.27 | 57.49 | 71.48 | 86.24 |
| 3-3c | 34.30 | 38.24 | 52.17 | 57.39 | 71.38 | 86.20 |
| 3-4a | 33.85 | 37.74 | 51.61 | 56.81 | 70.71 | 85.67 |
| 3-4b | 34.11 | 38.01 | 51.93 | 57.11 | 70.92 | 85.12 |

*(continued on next page)*

**Embolded** results indicate the highest binding energy geometry.

*(continued from previous page)*

| Divalent Cation | $Mg^{2+}$ | $Co^{2+}$ | $Cd^{2+}$ | $Ca^{2+}$ | $Sr^{2+}$ | $Ba^{2+}$ |
|---|---|---|---|---|---|---|
| Cation Radii (Å) | 0.72 | 0.75 | 0.95 | 1.00 | 1.18 | 1.35 |
| 4-4a | 33.39 | 37.24 | 51.07 | 56.25 | 70.09 | 85.04 |

**Embolded** results indicate the highest binding energy geometry.

**Table 5.31:** Solution energies (eV) for divalent cations in $\alpha$-$Fe_2O_3$ via neutral dopant interstitial compensation (reaction 5.6).

| Divalent Cation | $Mg^{2+}$ | $Co^{2+}$ | $Cd^{2+}$ | $Ca^{2+}$ | $Sr^{2+}$ | $Ba^{2+}$ |
|---|---|---|---|---|---|---|
| Cation Radii (Å) | 0.72 | 0.75 | 0.95 | 1.00 | 1.18 | 1.35 |
| Isolated | 2.44 | 2.51 | 3.80 | 4.43 | 6.57 | 9.66 |
| 1-1a | **1.13** | **1.26** | 2.85 | 3.51 | 5.68 | 8.68 |
| 1-2a | 1.45 | 1.53 | 2.96 | 3.59 | 5.70 | **7.98** |
| 1-2b | 1.45 | 1.55 | 2.97 | 3.59 | 5.67 | 8.55 |
| 1-3a | 1.47 | 1.56 | 3.02 | 3.67 | 5.84 | 8.91 |
| 1-3b | 1.58 | 1.65 | 3.05 | 3.66 | 5.73 | 8.65 |
| 1-4a | 1.50 | 1.52 | **2.84** | **3.41** | **5.32** | 8.09 |
| 1-4b | 1.34 | 1.42 | 2.87 | 3.52 | 5.68 | 8.75 |
| 2-2a | 1.85 | 1.88 | 3.01 | 3.57 | 5.50 | 8.30 |
| 2-2b | 1.77 | 1.81 | 2.96 | 3.53 | 5.50 | 8.34 |
| 2-2c | 1.77 | 1.81 | 2.96 | 3.53 | 5.50 | 8.34 |
| 2-3a | 2.01 | 2.06 | 3.22 | 3.79 | 5.75 | 8.53 |
| 2-3b | 1.82 | 1.86 | 3.11 | 3.71 | 5.79 | 8.74 |
| 2-3c | 2.01 | 2.06 | 3.22 | 3.79 | 5.75 | 8.53 |
| 2-3d | 1.82 | 1.86 | 3.11 | 3.71 | 5.79 | 8.74 |
| 2-4a | 1.68 | 1.71 | 2.91 | 3.50 | 5.52 | 8.41 |
| 2-4b | 1.69 | 1.72 | 2.95 | 3.55 | 5.60 | 8.54 |
| 3-3a | 1.92 | 1.97 | 3.26 | 3.88 | 6.04 | 9.11 |
| 3-3b | 1.91 | 1.96 | 3.29 | 3.92 | 6.10 | 9.12 |
| 3-3c | 1.89 | 1.94 | 3.26 | 3.89 | 6.06 | 9.11 |
| 3-4a | 1.74 | 1.77 | 3.07 | 3.69 | 5.84 | 8.94 |
| 3-4b | 1.82 | 1.86 | 3.18 | 3.79 | 5.91 | 8.75 |
| 4-4a | 1.58 | 1.60 | 2.89 | 3.51 | 5.63 | 8.72 |

**Embolded** results indicate the lowest solution energy geometry.

**Table 5.32:** Binding energies (eV) for neutral clusters in $\alpha$-$Fe_2O_3$: dopant interstitial compensation of 2+ cations (reaction 5.6).

| Divalent Cation | $Mg^{2+}$ | $Co^{2+}$ | $Cd^{2+}$ | $Ca^{2+}$ | $Sr^{2+}$ | $Ba^{2+}$ |
|---|---|---|---|---|---|---|
| Cation Radii (Å) | 0.72 | 0.75 | 0.95 | 1.00 | 1.18 | 1.35 |
| 1-1a | **3.94** | **3.75** | 2.86 | 2.76 | 2.67 | 2.92 |
| 1-2a | 2.99 | 2.96 | 2.53 | 2.52 | 2.62 | **5.02** |
| 1-2b | 2.97 | 2.91 | 2.51 | 2.52 | 2.71 | 3.31 |
| 1-3a | 2.93 | 2.87 | 2.35 | 2.29 | 2.19 | 2.23 |
| 1-3b | 2.59 | 2.59 | 2.27 | 2.30 | 2.52 | 3.03 |
| 1-4a | 2.83 | 2.97 | **2.90** | **3.07** | **3.75** | 4.70 |
| 1-4b | 3.31 | 3.28 | 2.79 | 2.73 | 2.67 | 2.71 |
| 2-2a | 1.77 | 1.90 | 2.37 | 2.57 | 3.22 | 4.07 |
| 2-2b | 2.02 | 2.11 | 2.53 | 2.68 | 3.20 | 3.94 |
| 2-2c | 2.02 | 2.11 | 2.53 | 2.68 | 3.20 | 3.94 |
| 2-3a | 1.31 | 1.36 | 1.76 | 1.92 | 2.45 | 3.38 |
| 2-3b | 1.88 | 1.96 | 2.08 | 2.14 | 2.34 | 2.73 |
| 2-3c | 1.31 | 1.36 | 1.76 | 1.92 | 2.45 | 3.37 |
| 2-3d | 1.88 | 1.96 | 2.08 | 2.14 | 2.34 | 2.73 |
| 2-4a | 2.28 | 2.42 | 2.67 | 2.78 | 3.15 | 3.73 |
| 2-4b | 2.27 | 2.39 | 2.55 | 2.63 | 2.92 | 3.35 |
| 3-3a | 1.58 | 1.64 | 1.63 | 1.63 | 1.61 | 1.65 |
| 3-3b | 1.61 | 1.65 | 1.54 | 1.52 | 1.43 | 1.60 |
| 3-3c | 1.67 | 1.73 | 1.64 | 1.63 | 1.53 | 1.64 |
| 3-4a | 2.12 | 2.22 | 2.20 | 2.21 | 2.20 | 2.16 |
| 3-4b | 1.86 | 1.95 | 1.88 | 1.90 | 1.99 | 2.71 |
| 4-4a | 2.58 | 2.73 | 2.74 | 2.77 | 2.82 | 2.79 |

**Embolded** results indicate the highest binding energy geometry.

**Table 5.33:** Cluster energies (eV) for divalent cation solution in $\alpha$-$Fe_2O_3$ via neutral interstitial compensation.

| Divalent Cation | $Mg^{2+}$ | $Co^{2+}$ | $Cd^{2+}$ | $Ca^{2+}$ | $Sr^{2+}$ | $Ba^{2+}$ |
|---|---|---|---|---|---|---|
| Cation Radii (Å) | 0.72 | 0.75 | 0.95 | 1.00 | 1.18 | 1.35 |
| Isolated | 40.13 | 43.86 | 55.79 | 60.51 | 72.97 | 86.02 |
| 1-1-2a | 33.72 | 37.76 | 52.44 | 57.81 | 72.19 | 86.59 |
| 1-1-3a | 34.08 | 38.02 | 52.29 | 57.53 | 71.47 | *pnc* |
| 1-2-2a | 35.05 | 38.88 | 52.22 | 57.21 | 70.37 | 84.17 |
| 1-2-2b | 34.81 | 38.67 | 52.16 | 57.24 | 70.75 | 83.98 |
| 1-2-2c | 34.79 | 38.61 | 51.98 | 57.01 | 70.29 | 82.68 |
| 1-2-2d | 34.85 | 38.72 | 52.14 | 57.21 | 70.70 | 84.17 |
| 1-2-3a | 35.44 | 39.27 | 52.37 | 57.31 | 70.37 | 82.96 |
| 1-2-3b | 34.89 | 38.69 | 52.05 | 57.07 | 70.40 | 83.39 |
| 1-2-3c | 35.42 | 39.18 | 52.34 | 57.27 | 70.29 | 83.92 |
| 1-2-3d | 35.20 | 38.95 | 52.05 | 56.97 | 69.95 | 83.44 |
| 1-2-3e | 35.06 | 38.89 | 52.19 | 57.20 | 70.47 | 83.53 |
| 1-2-3f | 35.44 | 39.27 | 52.37 | 57.31 | 70.37 | 82.96 |
| 1-2-3g | 35.31 | 39.10 | 52.21 | 57.16 | 70.26 | 84.05 |
| 1-2-3h | 35.41 | 39.16 | 52.24 | 57.13 | 69.99 | 83.30 |
| 1-3-3a | 35.14 | 38.91 | 52.08 | 57.06 | 70.30 | 83.31 |
| 1-3-3b | 35.83 | 39.51 | 52.23 | 57.03 | 69.67 | 82.94 |
| 1-3-3c | 35.45 | 39.19 | 52.22 | 57.14 | 70.15 | 83.83 |
| 1-3-3d | 35.39 | 39.12 | 52.12 | 57.03 | 70.00 | 83.65 |
| 2-2-2a | 36.41 | 40.02 | 51.72 | 56.31 | 68.36 | 80.81 |
| 2-2-2b | 36.18 | 39.83 | 51.65 | 56.32 | 68.63 | 81.49 |
| 2-2-2c | 35.94 | 39.59 | 51.35 | 56.02 | 68.30 | 80.98 |
| 2-2-3a | 37.10 | 40.74 | 52.23 | 56.74 | 68.52 | 80.60 |
| 2-2-3b | 36.55 | 40.17 | 52.04 | 56.67 | 68.83 | 81.42 |
| 2-2-3c | 36.36 | 39.98 | 51.82 | 56.48 | 68.76 | 81.59 |
| 2-2-3d | 37.11 | 40.74 | 52.49 | 57.08 | 69.12 | 81.59 |
| 2-2-3e | 36.32 | 39.94 | 51.78 | 56.43 | 68.68 | 81.42 |
| 2-2-3f | 36.54 | 40.16 | 51.89 | 56.49 | 68.56 | 81.05 |
| 2-2-3g | 36.71 | 40.37 | 51.98 | 56.58 | 68.66 | 81.17 |
| 2-2-3h | 36.15 | 39.79 | 51.66 | 56.36 | 68.74 | 81.69 |
| 2-2-3i | 36.48 | 40.12 | 51.91 | 56.53 | 68.59 | 80.92 |
| 2-2-3j | 36.30 | 39.94 | 51.84 | 56.52 | 68.82 | 81.57 |

*(continued on next page)*

*(continued from previous page)*

| Divalent Cation | $Mg^{2+}$ | $Co^{2+}$ | $Cd^{2+}$ | $Ca^{2+}$ | $Sr^{2+}$ | $Ba^{2+}$ |
|---|---|---|---|---|---|---|
| Cation Radii (Å) | 0.72 | 0.75 | 0.95 | 1.00 | 1.18 | 1.35 |
| 2-2-3k | 36.67 | 40.34 | 52.07 | 56.73 | 69.01 | 81.92 |
| 2-2-3l | 36.27 | 39.92 | 51.85 | 56.55 | 68.99 | 82.07 |
| 2-2-3m | 36.36 | 40.02 | 51.99 | 56.70 | 69.10 | 82.04 |
| 2-2-3n | 36.67 | 40.34 | 52.07 | 56.73 | 69.01 | 81.92 |
| 2-3-3a | 37.00 | 40.63 | 52.20 | 56.78 | 68.81 | 81.30 |
| 2-3-3b | 36.49 | 40.10 | 51.91 | 56.58 | 68.90 | 81.78 |
| 2-3-3c | 36.63 | 40.25 | 52.08 | 56.73 | 68.96 | 81.65 |
| 2-3-3d | 36.80 | 40.42 | 52.19 | 56.80 | 68.89 | 81.33 |
| 2-3-3e | 37.18 | 40.83 | 52.51 | 57.10 | 69.12 | 81.55 |
| 2-3-3f | 36.89 | 40.54 | 52.17 | 56.78 | 68.91 | 81.55 |
| 2-3-3g | 36.61 | 40.25 | 52.20 | 56.88 | 69.22 | 82.07 |
| 2-3-3h | 36.39 | 40.02 | 51.94 | 56.65 | 69.11 | 82.23 |
| 2-3-3i | 36.51 | 40.14 | 51.95 | 56.61 | 68.87 | 81.67 |
| 2-3-3j | 36.59 | 40.23 | 52.10 | 56.77 | 69.04 | 81.79 |
| 3-3-3a | 36.49 | 40.10 | 51.91 | 56.58 | 68.90 | 81.78 |
| 3-3-3b | 36.93 | 40.51 | 52.08 | 56.66 | 68.70 | 81.14 |
| 3-3-3c | 36.87 | 40.48 | 52.24 | 56.90 | 69.20 | 82.07 |
| 3-3-3d | 36.81 | 40.42 | 52.15 | 56.80 | 69.08 | 81.93 |

**Table 5.34:** Solution energies (eV) for divalent cations in $\alpha$-$Fe_2O_3$ via neutral interstitial compensation (reaction 5.7).

| Divalent Cation | $Mg^{2+}$ | $Co^{2+}$ | $Cd^{2+}$ | $Ca^{2+}$ | $Sr^{2+}$ | $Ba^{2+}$ |
|---|---|---|---|---|---|---|
| Cation Radii (Å) | 0.72 | 0.75 | 0.95 | 1.00 | 1.18 | 1.35 |
| Isolated | 2.87 | 2.86 | 3.35 | 3.69 | 4.94 | 6.79 |
| 1-1-2a | **1.27** | **1.33** | 2.51 | 3.02 | 4.75 | 6.93 |
| 1-1-3a | 1.36 | 1.40 | 2.47 | 2.95 | 4.57 | *pnc* |
| 1-2-2a | 1.60 | 1.61 | 2.45 | 2.87 | 4.29 | 6.33 |
| 1-2-2b | 1.54 | 1.56 | 2.44 | 2.88 | 4.39 | 6.28 |
| 1-2-2c | 1.54 | 1.55 | 2.40 | 2.82 | 4.27 | 5.95 |
| 1-2-2d | 1.55 | 1.57 | 2.44 | 2.87 | 4.38 | 6.33 |
| 1-2-3a | 1.70 | 1.71 | 2.49 | 2.90 | 4.29 | 6.02 |
| 1-2-3b | 1.56 | 1.57 | 2.41 | 2.83 | 4.30 | 6.13 |

*(continued on next page)*

**Embolded** results indicate the lowest solution energy geometry.

*(continued from previous page)*

| Divalent Cation | $Mg^{2+}$ | $Co^{2+}$ | $Cd^{2+}$ | $Ca^{2+}$ | $Sr^{2+}$ | $Ba^{2+}$ |
|---|---|---|---|---|---|---|
| Cation Radii (Å) | 0.72 | 0.75 | 0.95 | 1.00 | 1.18 | 1.35 |
| 1-2-3c | 1.70 | 1.69 | 2.49 | 2.88 | 4.27 | 6.26 |
| 1-2-3d | 1.64 | 1.63 | 2.41 | 2.81 | 4.19 | 6.14 |
| 1-2-3e | 1.61 | 1.62 | 2.45 | 2.87 | 4.32 | 6.17 |
| 1-2-3f | 1.70 | 1.71 | 2.49 | 2.90 | 4.29 | 6.02 |
| 1-2-3g | 1.67 | 1.67 | 2.45 | 2.86 | 4.26 | 6.30 |
| 1-2-3h | 1.69 | 1.68 | 2.46 | 2.85 | 4.20 | 6.11 |
| 1-3-3a | 1.62 | 1.62 | 2.42 | 2.83 | 4.27 | 6.11 |
| 1-3-3b | 1.80 | 1.77 | 2.46 | 2.83 | 4.12 | 6.02 |
| 1-3-3c | 1.70 | 1.69 | 2.46 | 2.85 | 4.24 | 6.24 |
| 1-3-3d | 1.69 | 1.67 | 2.43 | 2.82 | 4.20 | 6.20 |
| 2-2-2a | 1.94 | 1.90 | 2.33 | 2.65 | 3.79 | 5.49 |
| 2-2-2b | 1.89 | 1.85 | 2.31 | 2.65 | 3.86 | 5.65 |
| 2-2-2c | 1.83 | 1.79 | **2.24** | **2.57** | **3.77** | 5.53 |
| 2-2-3a | 2.12 | 2.08 | 2.46 | 2.75 | 3.83 | **5.43** |
| 2-2-3b | 1.98 | 1.94 | 2.41 | 2.74 | 3.91 | 5.64 |
| 2-2-3c | 1.93 | 1.89 | 2.35 | 2.69 | 3.89 | 5.68 |
| 2-2-3d | 2.12 | 2.08 | 2.52 | 2.84 | 3.98 | 5.68 |
| 2-2-3e | 1.92 | 1.88 | 2.34 | 2.68 | 3.87 | 5.64 |
| 2-2-3f | 1.97 | 1.93 | 2.37 | 2.69 | 3.84 | 5.55 |
| 2-2-3g | 2.02 | 1.99 | 2.39 | 2.71 | 3.86 | 5.58 |
| 2-2-3h | 1.88 | 1.84 | 2.32 | 2.66 | 3.89 | 5.71 |
| 2-2-3i | 1.96 | 1.92 | 2.38 | 2.70 | 3.85 | 5.51 |
| 2-2-3j | 1.92 | 1.88 | 2.36 | 2.70 | 3.90 | 5.68 |
| 2-2-3k | 2.01 | 1.98 | 2.42 | 2.75 | 3.95 | 5.76 |
| 2-2-3l | 1.91 | 1.87 | 2.36 | 2.71 | 3.95 | 5.80 |
| 2-2-3m | 1.93 | 1.90 | 2.40 | 2.74 | 3.98 | 5.79 |
| 2-2-3n | 2.01 | 1.98 | 2.42 | 2.75 | 3.95 | 5.76 |
| 2-3-3a | 2.09 | 2.05 | 2.45 | 2.76 | 3.90 | 5.61 |
| 2-3-3b | 1.96 | 1.92 | 2.38 | 2.71 | 3.93 | 5.73 |
| 2-3-3c | 2.00 | 1.96 | 2.42 | 2.75 | 3.94 | 5.70 |
| 2-3-3d | 2.04 | 2.00 | 2.45 | 2.77 | 3.92 | 5.62 |
| 2-3-3e | 2.13 | 2.10 | 2.53 | 2.84 | 3.98 | 5.67 |
| 2-3-3f | 2.06 | 2.03 | 2.44 | 2.76 | 3.93 | 5.67 |
| 2-3-3g | 1.99 | 1.96 | 2.45 | 2.79 | 4.01 | 5.80 |

*(continued on next page)*

**Embolded** results indicate the lowest solution energy geometry.

*(continued from previous page)*

| Divalent Cation | $Mg^{2+}$ | $Co^{2+}$ | $Cd^{2+}$ | $Ca^{2+}$ | $Sr^{2+}$ | $Ba^{2+}$ |
|---|---|---|---|---|---|---|
| Cation Radii (Å) | 0.72 | 0.75 | 0.95 | 1.00 | 1.18 | 1.35 |
| 2-3-3h | 1.94 | 1.90 | 2.38 | 2.73 | 3.98 | 5.84 |
| 2-3-3i | 1.97 | 1.93 | 2.39 | 2.72 | 3.92 | 5.70 |
| 2-3-3j | 1.99 | 1.95 | 2.42 | 2.76 | 3.96 | 5.73 |
| 3-3-3a | 1.96 | 1.92 | 2.38 | 2.71 | 3.93 | 5.73 |
| 3-3-3b | 2.07 | 2.02 | 2.42 | 2.73 | 3.87 | 5.57 |
| 3-3-3c | 2.06 | 2.01 | 2.46 | 2.79 | 4.00 | 5.80 |
| 3-3-3d | 2.04 | 2.00 | 2.44 | 2.77 | 3.97 | 5.77 |

**Embolded** results indicate the lowest solution energy geometry.

**Table 5.35:** Binding energies (eV) for neutral clusters in $\alpha$-$Fe_2O_3$: interstitial compensation of 2+ cations (reaction 5.7).

| Divalent Cation | $Mg^{2+}$ | $Co^{2+}$ | $Cd^{2+}$ | $Ca^{2+}$ | $Sr^{2+}$ | $Ba^{2+}$ |
|---|---|---|---|---|---|---|
| Cation Radii (Å) | 0.72 | 0.75 | 0.95 | 1.00 | 1.18 | 1.35 |
| 1-1-2a | **6.41** | **6.11** | 3.34 | 2.69 | 0.79 | -0.58 |
| 1-1-3a | 6.05 | 5.84 | 3.49 | 2.98 | 1.51 | *pnc* |
| 1-2-2a | 5.08 | 4.98 | 3.57 | 3.30 | 2.60 | 1.85 |
| 1-2-2b | 5.32 | 5.19 | 3.63 | 3.27 | 2.22 | 2.03 |
| 1-2-2c | 5.35 | 5.25 | 3.80 | 3.50 | 2.68 | 3.34 |
| 1-2-2d | 5.28 | 5.14 | 3.64 | 3.29 | 2.27 | 1.85 |
| 1-2-3a | 4.69 | 4.60 | 3.41 | 3.19 | 2.60 | 3.06 |
| 1-2-3b | 5.25 | 5.17 | 3.74 | 3.44 | 2.57 | 2.63 |
| 1-2-3c | 4.71 | 4.68 | 3.45 | 3.24 | 2.68 | 2.10 |
| 1-2-3d | 4.93 | 4.91 | 3.74 | 3.54 | 3.02 | 2.58 |
| 1-2-3e | 5.07 | 4.98 | 3.60 | 3.31 | 2.50 | 2.49 |
| 1-2-3f | 4.69 | 4.60 | 3.41 | 3.19 | 2.60 | 3.06 |
| 1-2-3g | 4.82 | 4.77 | 3.58 | 3.35 | 2.71 | 1.96 |
| 1-2-3h | 4.73 | 4.70 | 3.55 | 3.38 | 2.98 | 2.71 |
| 1-3-3a | 5.00 | 4.96 | 3.71 | 3.44 | 2.68 | 2.71 |
| 1-3-3b | 4.30 | 4.35 | 3.55 | 3.48 | 3.30 | 3.08 |
| 1-3-3c | 4.68 | 4.68 | 3.57 | 3.37 | 2.82 | 2.19 |
| 1-3-3d | 4.75 | 4.74 | 3.67 | 3.48 | 2.97 | 2.36 |
| 2-2-2a | 3.73 | 3.84 | 4.07 | 4.19 | 4.62 | 5.20 |

*(continued on next page)*

**Embolded** results indicate the highest binding energy geometry.

*(continued from previous page)*

| Divalent Cation | $Mg^{2+}$ | $Co^{2+}$ | $Cd^{2+}$ | $Ca^{2+}$ | $Sr^{2+}$ | $Ba^{2+}$ |
|---|---|---|---|---|---|---|
| Cation Radii (Å) | 0.72 | 0.75 | 0.95 | 1.00 | 1.18 | 1.35 |
| 2-2-2b | 3.95 | 4.04 | 4.14 | 4.19 | 4.34 | 4.53 |
| 2-2-2c | 4.19 | 4.27 | **4.44** | **4.48** | **4.67** | 5.03 |
| 2-2-3a | 3.03 | 3.12 | 3.56 | 3.77 | 4.45 | **5.41** |
| 2-2-3b | 3.59 | 3.69 | 3.75 | 3.84 | 4.14 | 4.60 |
| 2-2-3c | 3.77 | 3.88 | 3.97 | 4.03 | 4.21 | 4.43 |
| 2-2-3d | 3.02 | 3.12 | 3.30 | 3.43 | 3.85 | 4.43 |
| 2-2-3e | 3.81 | 3.92 | 4.01 | 4.07 | 4.29 | 4.59 |
| 2-2-3f | 3.60 | 3.70 | 3.90 | 4.01 | 4.41 | 4.97 |
| 2-2-3g | 3.42 | 3.49 | 3.81 | 3.93 | 4.31 | 4.85 |
| 2-2-3h | 3.98 | 4.07 | 4.13 | 4.15 | 4.23 | 4.32 |
| 2-2-3i | 3.66 | 3.75 | 3.88 | 3.98 | 4.38 | 5.10 |
| 2-2-3j | 3.83 | 3.92 | 3.95 | 3.99 | 4.15 | 4.44 |
| 2-2-3k | 3.46 | 3.52 | 3.71 | 3.78 | 3.96 | 4.09 |
| 2-2-3l | 3.86 | 3.94 | 3.94 | 3.96 | 3.98 | 3.95 |
| 2-2-3m | 3.77 | 3.85 | 3.80 | 3.81 | 3.87 | 3.98 |
| 2-2-3n | 3.46 | 3.52 | 3.71 | 3.78 | 3.96 | 4.09 |
| 2-3-3a | 3.14 | 3.24 | 3.59 | 3.73 | 4.16 | 4.71 |
| 2-3-3b | 3.65 | 3.76 | 3.88 | 3.93 | 4.07 | 4.23 |
| 2-3-3c | 3.50 | 3.62 | 3.71 | 3.78 | 4.01 | 4.37 |
| 2-3-3d | 3.33 | 3.45 | 3.60 | 3.71 | 4.08 | 4.69 |
| 2-3-3e | 2.96 | 3.03 | 3.28 | 3.41 | 3.85 | 4.46 |
| 2-3-3f | 3.24 | 3.32 | 3.62 | 3.73 | 4.07 | 4.47 |
| 2-3-3g | 3.52 | 3.61 | 3.59 | 3.62 | 3.75 | 3.95 |
| 2-3-3h | 3.74 | 3.85 | 3.85 | 3.86 | 3.87 | 3.79 |
| 2-3-3i | 3.63 | 3.72 | 3.84 | 3.90 | 4.10 | 4.34 |
| 2-3-3j | 3.54 | 3.64 | 3.69 | 3.74 | 3.93 | 4.23 |
| 3-3-3a | 3.65 | 3.76 | 3.88 | 3.93 | 4.07 | 4.23 |
| 3-3-3b | 3.20 | 3.36 | 3.71 | 3.85 | 4.27 | 4.87 |
| 3-3-3c | 3.27 | 3.39 | 3.54 | 3.60 | 3.77 | 3.94 |
| 3-3-3d | 3.32 | 3.44 | 3.64 | 3.70 | 3.89 | 4.09 |

**Embolded** results indicate the highest binding energy geometry.

**Table 5.36:** Cluster energies (eV) for divalent cation solution in $\alpha$-$Fe_2O_3$ via neutral vacancy compensation.

| Divalent Cation | $Mg^{2+}$ | $Co^{2+}$ | $Cd^{2+}$ | $Ca^{2+}$ | $Sr^{2+}$ | $Ba^{2+}$ |
|---|---|---|---|---|---|---|
| Cation Radii (Å) | 0.72 | 0.75 | 0.95 | 1.00 | 1.18 | 1.35 |
| Isolated | 76.55 | 79.04 | 86.99 | 90.13 | 98.44 | 107.14 |
| 1-1a | 73.14 | 75.48 | 83.44 | 86.38 | 93.96 | 101.59 |
| 1-2a | 73.67 | 75.98 | 83.98 | 86.95 | 94.69 | 102.57 |
| 1-2b | 73.45 | 75.77 | 83.67 | 86.61 | 94.22 | 101.90 |
| 1-3a | 74.38 | 76.76 | 84.87 | 87.92 | 95.84 | 103.88 |
| 1-3b | 74.19 | 76.62 | 84.58 | 87.61 | 95.50 | 103.51 |
| 1-4a | 74.24 | 76.64 | 84.63 | 87.67 | 95.58 | 103.66 |
| 1-4b | 74.43 | 76.88 | 85.09 | 88.18 | 96.22 | *pnc* |
| 2-2a | 74.23 | 76.56 | 84.43 | 87.40 | 95.20 | 103.32 |
| 2-3a | 74.70 | 77.09 | 85.12 | 88.19 | 96.24 | 104.57 |
| 2-3b | 74.97 | 77.35 | 83.99 | 88.29 | 96.27 | 104.64 |
| 2-4a | 74.58 | 76.98 | 84.99 | 88.08 | 96.23 | 104.77 |
| 2-4b | 74.76 | 77.12 | 85.21 | 88.30 | 96.47 | 105.11 |
| 3-3a | 75.33 | 77.83 | 85.96 | 89.16 | 97.69 | 106.87 |
| 3-4a | 75.53 | 78.04 | 86.09 | 89.22 | 94.21 | 101.90 |
| 3-4b | 75.28 | 77.77 | 85.77 | 88.91 | 97.23 | 105.96 |
| 4-4a | 75.28 | 77.78 | 85.77 | 88.91 | 97.21 | 105.87 |

**Table 5.37:** Solution energies (eV) for divalent cations in $\alpha$-$Fe_2O_3$ via neutral vacancy compensation (reaction 5.8).

| Divalent Cation | $Mg^{2+}$ | $Co^{2+}$ | $Cd^{2+}$ | $Ca^{2+}$ | $Sr^{2+}$ | $Ba^{2+}$ |
|---|---|---|---|---|---|---|
| Cation Radii (Å) | 0.72 | 0.75 | 0.95 | 1.00 | 1.18 | 1.35 |
| Isolated | 2.20 | 2.19 | 2.62 | 2.93 | 4.04 | 5.68 |
| 1-1a | **1.07** | **1.00** | **1.44** | **1.68** | **2.55** | **3.83** |
| 1-2a | 1.24 | 1.17 | 1.62 | 1.87 | 2.79 | 4.16 |
| 1-2b | 1.17 | 1.10 | 1.52 | 1.76 | 2.63 | 3.93 |
| 1-3a | 1.48 | 1.43 | 1.91 | 2.19 | 3.17 | 4.59 |
| 1-3b | 1.42 | 1.38 | 1.82 | 2.09 | 3.06 | 4.47 |
| 1-4a | 1.43 | 1.39 | 1.84 | 2.11 | 3.09 | 4.52 |

*(continued on next page)*

**Embolded** results indicate the lowest solution energy geometry.

*(continued from previous page)*

| Divalent Cation | $Mg^{2+}$ | $Co^{2+}$ | $Cd^{2+}$ | $Ca^{2+}$ | $Sr^{2+}$ | $Ba^{2+}$ |
|---|---|---|---|---|---|---|
| Cation Radii (Å) | 0.72 | 0.75 | 0.95 | 1.00 | 1.18 | 1.35 |
| 1-4b | 1.50 | 1.47 | 1.99 | 2.28 | 3.30 | *pnc* |
| 2-2a | 1.43 | 1.36 | 1.77 | 2.02 | 2.96 | 4.41 |
| 2-3a | 1.58 | 1.54 | 2.00 | 2.28 | 3.31 | 4.82 |
| 2-3b | 1.68 | 1.63 | 1.62 | 2.31 | 3.32 | 4.85 |
| 2-4a | 1.54 | 1.50 | 1.96 | 2.25 | 3.30 | 4.89 |
| 2-4b | 1.60 | 1.55 | 2.03 | 2.32 | 3.38 | 5.00 |
| 3-3a | 1.79 | 1.78 | 2.28 | 2.61 | 3.79 | 5.59 |
| 3-4a | 1.86 | 1.85 | 2.32 | 2.63 | 2.63 | 3.93 |
| 3-4b | 1.78 | 1.77 | 2.21 | 2.52 | 3.64 | 5.29 |
| 4-4a | 1.78 | 1.77 | 2.22 | 2.52 | 3.63 | 5.26 |

**Embolded** results indicate the lowest solution energy geometry.

**Table 5.38:** Binding energies (eV) for neutral clusters in $\alpha$-$Fe_2O_3$: vacancy compensation of 2+ cations (reaction 5.8).

| Divalent Cation | $Mg^{2+}$ | $Co^{2+}$ | $Cd^{2+}$ | $Ca^{2+}$ | $Sr^{2+}$ | $Ba^{2+}$ |
|---|---|---|---|---|---|---|
| Cation Radii (Å) | 0.72 | 0.75 | 0.95 | 1.00 | 1.18 | 1.35 |
| 1-1a | **3.41** | **3.56** | **3.55** | **3.76** | **4.49** | **5.56** |
| 1-2a | 2.88 | 3.06 | 3.01 | 3.18 | 3.76 | 4.57 |
| 1-2b | 3.10 | 3.27 | 3.32 | 3.52 | 4.23 | 5.24 |
| 1-3a | 2.18 | 2.28 | 2.12 | 2.22 | 2.61 | 3.27 |
| 1-3b | 2.36 | 2.42 | 2.41 | 2.52 | 2.95 | 3.63 |
| 1-4a | 2.31 | 2.39 | 2.35 | 2.47 | 2.87 | 3.48 |
| 1-4b | 2.12 | 2.16 | 1.90 | 1.96 | 2.23 | *pnc* |
| 2-2a | 2.33 | 2.48 | 2.56 | 2.73 | 3.24 | 3.82 |
| 2-3a | 1.85 | 1.95 | 1.87 | 1.95 | 2.20 | 2.57 |
| 2-3b | 1.58 | 1.69 | 3.00 | 1.85 | 2.17 | 2.50 |
| 2-4a | 1.97 | 2.06 | 2.00 | 2.06 | 2.21 | 2.37 |
| 2-4b | 1.80 | 1.92 | 1.77 | 1.83 | 1.97 | 2.03 |
| 3-3a | 1.22 | 1.21 | 1.02 | 0.97 | 0.76 | 0.27 |
| 3-4a | 1.02 | 1.00 | 0.90 | 0.91 | 4.23 | 5.24 |
| 3-4b | 1.28 | 1.27 | 1.22 | 1.23 | 1.22 | 1.18 |
| 4-4a | 1.27 | 1.26 | 1.22 | 1.22 | 1.24 | 1.27 |

**Embolded** results indicate the highest binding energy geometry.

**Table 5.39:** Isolated interstitial defect, substitutional defect and oxide lattice energies (eV) for tetravalent cations in α-$Al_2O_3$.

| Quadvalent Cation | $Rh^{4+}$ | $Ti^{4+}$ | $Ru^{4+}$ | $Mo^{4+}$ | $Sn^{4+}$ | $Pu^{4+}$ |
|---|---|---|---|---|---|---|
| Cation Radii (Å) | 0.600 | 0.605 | 0.620 | 0.650 | 0.690 | 0.860 |
| iso $D_i^{\bullet\bullet\bullet\bullet}$ | -66.08 | -64.65 | -63.70 | -64.49 | -61.62 | -47.99 |
| iso $D_{Al}^{\bullet}$ | -28.22 | -27.00 | -26.20 | -24.63 | -21.56 | -12.04 |
| Lattice En. | -118.83 | -117.76 | -117.06 | -115.71 | -113.18 | -106.15 |

**Table 5.40:** Cluster energies (eV) for tetravalent cations solution in α-$Al_2O_3$ via neutral interstitial compensation.

| Quadvalent Cation | $Rh^{4+}$ | $Ti^{4+}$ | $Ru^{4+}$ | $Mo^{4+}$ | $Sn^{4+}$ | $Pu^{4+}$ |
|---|---|---|---|---|---|---|
| Cation Radii (Å) | 0.600 | 0.605 | 0.620 | 0.650 | 0.690 | 0.860 |
| Isolated | -69.53 | -67.09 | -65.49 | -62.35 | -56.21 | -37.17 |
| 1-1a | -71.58 | -69.00 | -67.65 | -64.58 | -58.61 | -39.47 |
| 1-2a | -71.42 | -69.04 | -67.48 | -64.40 | -58.41 | -37.95 |
| 1-2b | -71.46 | -69.13 | -67.59 | -64.57 | -58.31 | -39.96 |
| 1-3a | -70.96 | -68.69 | -67.16 | -63.79 | -57.96 | -39.12 |
| 1-3b | -70.83 | -68.31 | -66.71 | -63.56 | -57.45 | -38.67 |
| 1-4a | -70.71 | -68.37 | -66.70 | *pnc* | *pnc* | -39.08 |
| 1-4b | -71.24 | -68.92 | *pnc* | -64.15 | *pnc* | *pnc* |
| 2-2a | -70.70 | -68.28 | -66.68 | -63.59 | -57.68 | -38.99 |
| 2-2b | -71.12 | -68.73 | -67.17 | -64.10 | -58.17 | -39.63 |
| 2-2c | -71.12 | -68.73 | -67.17 | -64.10 | -58.17 | -39.63 |
| 2-3a | -70.71 | -68.28 | -66.70 | -63.58 | -56.91 | -38.47 |
| 2-3b | -71.16 | -68.16 | -67.19 | -64.10 | -57.43 | -39.05 |
| 2-3c | -70.71 | -68.28 | -66.70 | -63.58 | -56.91 | -38.20 |
| 2-3d | -71.16 | -68.16 | -66.58 | -63.47 | -57.43 | -38.61 |
| 2-4a | -70.65 | -68.28 | -67.19 | -64.07 | -57.61 | -38.35 |
| 2-4b | -70.70 | -68.92 | -67.34 | -64.24 | -58.17 | -38.49 |
| 3-3a | -70.73 | -68.25 | -67.15 | -64.08 | -57.28 | -39.63 |
| 3-3b | -70.47 | -68.28 | -66.70 | -63.16 | -57.33 | -38.28 |
| 3-3c | *pnc* | -68.17 | -66.57 | *pnc* | -57.36 | -38.60 |
| 3-4a | -70.71 | -68.39 | -66.79 | -63.66 | -57.56 | -38.41 |
| 3-4b | *pnc* | *pnc* | *pnc* | -63.56 | -57.33 | -38.62 |
| 4-4a | *pnc* | *pnc* | *pnc* | *pnc* | *pnc* | *pnc* |

**Table 5.41:** Solution energies (eV) for tetravalent cations in $\alpha$-$Al_2O_3$ via neutral interstitial compensation (reaction 5.9).

| Quadvalent Cation | $Rh^{4+}$ | $Ti^{4+}$ | $Ru^{4+}$ | $Mo^{4+}$ | $Sn^{4+}$ | $Pu^{4+}$ |
|---|---|---|---|---|---|---|
| Cation Radii (Å) | 0.600 | 0.605 | 0.620 | 0.650 | 0.690 | 0.860 |
| Isolated | 2.83 | 2.92 | 2.99 | 3.14 | 3.50 | 5.16 |
| 1-1a | **2.14** | 2.28 | **2.27** | **2.40** | **2.70** | 4.39 |
| 1-2a | 2.20 | 2.27 | 2.33 | 2.46 | 2.76 | 4.90 |
| 1-2b | 2.18 | **2.24** | 2.29 | 2.40 | 2.80 | **4.23** |
| 1-3a | 2.35 | 2.39 | 2.44 | 2.66 | 2.91 | 4.51 |
| 1-3b | 2.39 | 2.52 | 2.58 | 2.74 | 3.08 | 4.66 |
| 1-4a | 2.43 | 2.50 | 2.59 | *pnc* | *pnc* | 4.52 |
| 1-4b | 2.25 | 2.31 | *pnc* | 2.54 | *pnc* | *pnc* |
| 2-2a | 2.43 | 2.53 | 2.59 | 2.73 | 3.01 | 4.55 |
| 2-2b | 2.30 | 2.37 | 2.43 | 2.56 | 2.84 | 4.34 |
| 2-2c | 2.30 | 2.37 | 2.43 | 2.56 | 2.84 | 4.34 |
| 2-3a | 2.43 | 2.52 | 2.59 | 2.73 | 3.26 | 4.73 |
| 2-3b | 2.28 | 2.57 | 2.42 | 2.56 | 3.09 | 4.53 |
| 2-3c | 2.43 | 2.52 | 2.59 | 2.73 | 3.26 | 4.82 |
| 2-3d | 2.28 | 2.57 | 2.63 | 2.77 | 3.09 | 4.68 |
| 2-4a | 2.45 | 2.53 | 2.43 | 2.57 | 3.03 | 4.77 |
| 2-4b | 2.44 | 2.31 | 2.37 | 2.51 | 2.84 | 4.72 |
| 3-3a | 2.42 | 2.54 | 2.44 | 2.56 | 3.14 | 4.34 |
| 3-3b | 2.51 | 2.53 | 2.59 | 2.87 | 3.12 | 4.79 |
| 3-3c | *pnc* | 2.56 | 2.63 | *pnc* | 3.11 | 4.68 |
| 3-4a | 2.43 | 2.49 | 2.56 | 2.70 | 3.05 | 4.75 |
| 3-4b | *pnc* | *pnc* | *pnc* | 2.74 | 3.12 | 4.68 |

**Embolded** results indicate the lowest solution energy geometry.

**Table 5.42:** Binding energies (eV) for neutral clusters in α-$Al_2O_3$: interstitial compensation of 4+ cations (reaction 5.9).

| Quadvalent Cation | $Rh^{4+}$ | $Ti^{4+}$ | $Ru^{4+}$ | $Mo^{4+}$ | $Sn^{4+}$ | $Pu^{4+}$ |
|---|---|---|---|---|---|---|
| Cation Radii (Å) | 0.600 | 0.605 | 0.620 | 0.650 | 0.690 | 0.860 |
| 1-1a | **2.05** | 1.92 | **2.17** | **2.24** | **2.40** | 2.30 |
| 1-2a | 1.89 | 1.96 | 2.00 | 2.06 | 2.20 | 0.78 |
| 1-2b | 1.94 | **2.04** | 2.11 | 2.22 | 2.10 | **2.78** |
| 1-3a | 1.43 | 1.60 | 1.67 | 1.45 | 1.75 | 1.95 |
| 1-3b | 1.30 | 1.23 | 1.23 | 1.21 | 1.24 | 1.50 |
| 1-4a | 1.18 | 1.28 | 1.22 | *pnc* | *pnc* | 1.91 |
| 1-4b | 1.72 | 1.83 | *pnc* | 1.81 | *pnc* | *pnc* |
| 2-2a | 1.18 | 1.19 | 1.20 | 1.24 | 1.47 | 1.82 |
| 2-2b | 1.59 | 1.65 | 1.68 | 1.75 | 1.96 | 2.46 |
| 2-2c | 1.59 | 1.65 | 1.68 | 1.75 | 1.96 | 2.46 |
| 2-3a | 1.18 | 1.20 | 1.21 | 1.24 | 0.70 | 1.30 |
| 2-3b | 1.63 | 1.07 | 1.71 | 1.76 | 1.22 | 1.88 |
| 2-3c | 1.18 | 1.20 | 1.21 | 1.24 | 0.70 | 1.03 |
| 2-3d | 1.63 | 1.07 | 1.09 | 1.13 | 1.22 | 1.43 |
| 2-4a | 1.12 | 1.19 | 1.70 | 1.73 | 1.39 | 1.18 |
| 2-4b | 1.17 | 1.83 | 1.86 | 1.89 | 1.96 | 1.32 |
| 3-3a | 1.20 | 1.17 | 1.67 | 1.74 | 1.07 | 2.46 |
| 3-3b | 0.94 | 1.19 | 1.21 | 0.81 | 1.12 | 1.11 |
| 3-3c | *pnc* | 1.08 | 1.08 | *pnc* | 1.15 | 1.43 |
| 3-4a | 1.18 | 1.30 | 1.30 | 1.31 | 1.35 | 1.23 |
| 3-4b | *pnc* | *pnc* | *pnc* | 1.21 | 1.12 | 1.45 |
| 4-4a | *pnc* | *pnc* | *pnc* | *pnc* | *pnc* | *pnc* |

**Embolded** results indicate the highest binding energy geometry.

**Table 5.43:** Cluster energies (eV) for tetravalent cations solution in $\alpha$-$Al_2O_3$ via neutral vacancy compensation.

| Quadvalent Cation | $Rh^{4+}$ | $Ti^{4+}$ | $Ru^{4+}$ | $Mo^{4+}$ | $Sn^{4+}$ | $Pu^{4+}$ |
|---|---|---|---|---|---|---|
| Cation Radii (Å) | 0.600 | 0.605 | 0.620 | 0.650 | 0.690 | 0.860 |
| Isolated | -28.19 | -24.53 | -22.12 | -17.41 | -8.21 | 20.35 |
| 1-2-2a | -32.84 | -29.31 | -26.99 | -22.44 | -13.56 | 13.74 |
| 1-2-3a | -32.22 | -28.64 | -26.29 | -21.67 | -12.61 | 15.48 |
| 1-2-3b | -32.46 | -28.90 | -26.56 | -21.98 | -13.03 | 14.42 |
| 2-2-2a | -33.18 | -29.72 | -27.45 | -23.03 | -14.53 | 11.03 |
| 2-2-3a | -32.12 | -28.56 | -26.23 | -21.65 | -12.69 | 14.97 |
| 2-2-3b | -32.34 | -28.79 | -26.47 | -21.91 | -13.02 | 14.27 |
| 2-3-3a | -31.66 | -28.07 | -25.72 | -21.11 | -12.12 | 15.21 |
| 2-3-3b | -31.43 | -27.84 | -25.48 | -20.85 | -11.79 | 15.80 |
| 3-3-3a | -31.14 | -27.57 | -25.24 | -20.68 | -11.95 | 13.58 |

**Table 5.44:** Solution energies (eV) for tetravalent cations in $\alpha$-$Al_2O_3$ via neutral vacancy compensation (reaction 5.10).

| Quadvalent Cation | $Rh^{4+}$ | $Ti^{4+}$ | $Ru^{4+}$ | $Mo^{4+}$ | $Sn^{4+}$ | $Pu^{4+}$ |
|---|---|---|---|---|---|---|
| Cation Radii (Å) | 0.600 | 0.605 | 0.620 | 0.650 | 0.690 | 0.860 |
| Isolated | 2.25 | 2.36 | 2.44 | 2.60 | 3.00 | 4.87 |
| 1-2-2a | **1.09** | **1.16** | **1.22** | **1.35** | **1.67** | **3.22** |
| 1-2-3a | 1.24 | 1.33 | 1.40 | 1.54 | 1.90 | 3.65 |
| 1-2-3b | 1.18 | 1.27 | 1.33 | 1.46 | 1.80 | 3.39 |
| 2-2-2a | 1.00 | 1.06 | 1.11 | 1.20 | 1.42 | 2.54 |
| 2-2-3a | 1.26 | 1.35 | 1.41 | 1.55 | 1.88 | 3.53 |
| 2-2-3b | 1.21 | 1.29 | 1.35 | 1.48 | 1.80 | 3.35 |
| 2-3-3a | 1.38 | 1.47 | 1.54 | 1.68 | 2.03 | 3.59 |
| 2-3-3b | 1.44 | 1.53 | 1.60 | 1.75 | 2.11 | 3.73 |
| 3-3-3a | 1.51 | 1.60 | 1.66 | 1.79 | 2.07 | 3.18 |

**Embolded** results indicate the lowest solution energy geometry.

**Table 5.45:** Binding energies (eV) for neutral clusters in $\alpha$-$Al_2O_3$: vacancy compensation of 4+ cations (reaction 5.10).

| Quadvalent Cation | $Rh^{4+}$ | $Ti^{4+}$ | $Ru^{4+}$ | $Mo^{4+}$ | $Sn^{4+}$ | $Pu^{4+}$ |
|---|---|---|---|---|---|---|
| Cation Radii (Å) | 0.600 | 0.605 | 0.620 | 0.650 | 0.690 | 0.860 |
| 1-2-2a | **4.65** | **4.78** | **4.87** | **5.03** | **5.35** | **6.61** |
| 1-2-3a | 4.03 | 4.11 | 4.16 | 4.26 | 4.40 | 4.87 |
| 1-2-3b | 4.27 | 4.37 | 4.43 | 4.56 | 4.82 | 5.93 |
| 2-2-2a | 5.00 | 5.19 | 5.33 | 5.61 | 6.31 | 9.32 |
| 2-2-3a | 3.93 | 4.04 | 4.11 | 4.24 | 4.48 | 5.38 |
| 2-2-3b | 4.15 | 4.27 | 4.34 | 4.49 | 4.81 | 6.07 |
| 2-3-3a | 3.47 | 3.54 | 3.59 | 3.70 | 3.91 | 5.13 |
| 2-3-3b | 3.25 | 3.31 | 3.35 | 3.43 | 3.58 | 4.55 |
| 3-3-3a | 2.95 | 3.05 | 3.11 | 3.27 | 3.74 | 6.77 |

**Embolded** results indicate the highest binding energy geometry.

**Table 5.46:** Isolated interstitial defect, substitutional defect and oxide lattice energies (eV) for tetravalent cations in α-$Cr_2O_3$

| Quadvalent Cation | $Rh^{4+}$ | $Ti^{4+}$ | $Ru^{4+}$ | $Mo^{4+}$ | $Sn^{4+}$ | $Pu^{4+}$ |
|---|---|---|---|---|---|---|
| Cation Radii (Å) | 0.600 | 0.605 | 0.620 | 0.650 | 0.690 | 0.860 |
| iso $D_i^{\bullet\bullet\bullet\bullet}$ | -68.45 | -68.33 | -67.58 | -64.59 | -61.10 | -55.37 |
| iso $D_{Cr}^{\bullet}$ | -32.72 | -31.58 | -30.84 | -29.37 | -26.51 | -17.74 |
| Lattice En. | -118.83 | -117.76 | -117.06 | -115.71 | -113.18 | -106.15 |

**Table 5.47:** Cluster energies (eV) for tetravalent cations solution in α-$Cr_2O_3$ via neutral interstitial compensation.

| Quadvalent Cation | $Rh^{4+}$ | $Ti^{4+}$ | $Ru^{4+}$ | $Mo^{4+}$ | $Sn^{4+}$ | $Pu^{4+}$ |
|---|---|---|---|---|---|---|
| Cation Radii (Å) | 0.600 | 0.605 | 0.620 | 0.650 | 0.690 | 0.860 |
| Isolated | -78.37 | -76.09 | -74.60 | -71.67 | -65.95 | -48.40 |
| 1-1a | -80.23 | -78.04 | -76.60 | -73.82 | -68.43 | pnc |
| 1-2a | -80.06 | -77.90 | -76.48 | -73.68 | -68.25 | -50.55 |
| 1-2b | -80.00 | -77.85 | -76.44 | -73.68 | -68.36 | -51.10 |
| 1-3a | -80.15 | -77.72 | -76.24 | -73.35 | -67.79 | -50.72 |
| 1-3b | -79.73 | -77.48 | -76.01 | -73.11 | -67.58 | -49.89 |
| 1-4a | -79.65 | -77.48 | -75.94 | -73.10 | *pnc* | *pnc* |
| 1-4b | *pnc* | -77.95 | -76.49 | -73.56 | -67.99 | pnc |
| 2-2a | -79.73 | -77.48 | -76.00 | -73.11 | -67.48 | -49.88 |
| 2-2b | -79.75 | -77.45 | -75.94 | -73.40 | -67.90 | -50.92 |
| 2-2c | -79.90 | -77.45 | -76.24 | -73.40 | -67.90 | -50.92 |
| 2-3a | -79.73 | -77.47 | -75.52 | -73.09 | -67.47 | -49.46 |
| 2-3b | -79.76 | -77.49 | -76.00 | -73.04 | -67.89 | -50.56 |
| 2-3c | -79.34 | -77.03 | -75.99 | -72.56 | -67.47 | -49.46 |
| 2-3d | -79.76 | -77.52 | -76.00 | -73.44 | -67.22 | -50.56 |
| 2-4a | -79.77 | -77.88 | -76.41 | -73.53 | -67.29 | -49.59 |
| 2-4b | -80.11 | -77.90 | -76.04 | -73.59 | -68.02 | -49.77 |
| 3-3a | -79.76 | -77.36 | -76.12 | -73.13 | -67.89 | -50.21 |
| 3-3b | -79.85 | -77.55 | -76.04 | -73.09 | -67.13 | -50.17 |
| 3-3c | -79.86 | *pnc* | *pnc* | -73.13 | -67.27 | -49.80 |
| 3-4a | -79.99 | -77.70 | -76.25 | -73.27 | -67.51 | -49.28 |
| 3-4b | -79.80 | -77.52 | -76.03 | -73.10 | -67.38 | -49.53 |
| 4-4a | *pnc* | *pnc* | *pnc* | *pnc* | *pnc* | *pnc* |

**Table 5.48:** Solution energies (eV) for tetravalent cations in α-$Cr_2O_3$ via neutral interstitial compensation (reaction 5.9).

| Quadvalent Cation | $Rh^{4+}$ | $Ti^{4+}$ | $Ru^{4+}$ | $Mo^{4+}$ | $Sn^{4+}$ | $Pu^{4+}$ |
|---|---|---|---|---|---|---|
| Cation Radii (Å) | 0.600 | 0.605 | 0.620 | 0.650 | 0.690 | 0.860 |
| Isolated | 2.25 | 2.29 | 2.33 | 2.40 | 2.62 | 3.79 |
| 1-1a | **1.63** | **1.64** | **1.66** | **1.69** | **1.80** | *pnc* |
| 1-2a | 1.69 | 1.69 | 1.70 | 1.74 | 1.85 | **3.07** |
| 1-2b | 1.71 | 1.71 | 1.71 | 1.74 | 1.82 | 2.89 |
| 1-3a | 1.66 | 1.75 | 1.78 | 1.85 | 2.01 | 3.01 |
| 1-3b | 1.80 | 1.83 | 1.86 | 1.93 | 2.08 | 3.29 |
| 1-4a | 1.82 | 1.83 | 1.88 | 1.93 | pnc | *pnc* |
| 1-4b | *pnc* | 1.67 | 1.70 | 1.78 | 1.94 | *pnc* |
| 2-2a | 1.80 | 1.83 | 1.86 | 1.93 | 2.11 | 3.29 |
| 2-2b | 1.79 | 1.84 | 1.88 | 1.83 | 1.97 | 2.95 |
| 2-2c | 1.74 | 1.84 | 1.78 | 1.83 | 1.97 | 2.95 |
| 2-3a | 1.80 | 1.83 | 2.02 | 1.93 | 2.12 | 3.43 |
| 2-3b | 1.79 | 1.83 | 1.86 | 1.95 | 1.97 | 3.07 |
| 2-3c | 1.93 | 1.98 | 1.86 | 2.11 | 2.12 | 3.43 |
| 2-3d | 1.79 | 1.82 | 1.86 | 1.82 | 2.20 | 3.07 |
| 2-4a | 1.78 | 1.70 | 1.72 | 1.79 | 2.17 | 3.39 |
| 2-4b | 1.67 | 1.69 | 1.85 | 1.77 | 1.93 | 3.33 |
| 3-3a | 1.79 | 1.87 | 1.82 | 1.92 | 1.98 | 3.18 |
| 3-3b | 1.76 | 1.81 | 1.85 | 1.93 | 2.23 | 3.20 |
| 3-3c | 1.75 | *pnc* | *pnc* | 1.92 | 2.18 | 3.32 |
| 3-4a | 1.71 | 1.76 | 1.78 | 1.87 | 2.10 | 3.49 |
| 3-4b | 1.77 | 1.82 | 1.85 | 1.93 | 2.14 | 3.41 |
| 4-4a | *pnc* | *pnc* | *pnc* | *pnc* | *pnc* | *pnc* |

**Embolded** results indicate the lowest solution energy geometry.

**Table 5.49:** Binding energies (eV) for neutral clusters in $\alpha$-$Cr_2O_3$: interstitial compensation of 4+ cations (reaction 5.9).

| Quadvalent Cation | $Rh^{4+}$ | $Ti^{4+}$ | $Ru^{4+}$ | $Mo^{4+}$ | $Sn^{4+}$ | $Pu^{4+}$ |
|---|---|---|---|---|---|---|
| Cation Radii (Å) | 0.600 | 0.605 | 0.620 | 0.650 | 0.690 | 0.860 |
| 1-1a | **1.86** | **1.95** | **2.00** | **2.15** | **2.48** | *pnc* |
| 1-2a | 1.69 | 1.80 | 1.88 | 2.00 | 2.31 | **2.15** |
| 1-2b | 1.63 | 1.76 | 1.84 | 2.00 | 2.41 | 2.70 |
| 1-3a | 1.78 | 1.63 | 1.64 | 1.68 | 1.84 | 2.32 |
| 1-3b | 1.36 | 1.39 | 1.41 | 1.44 | 1.64 | 1.49 |
| 1-4a | 1.28 | 1.39 | 1.35 | 1.43 | pnc | *pnc* |
| 1-4b | pnc | 1.86 | 1.89 | 1.88 | 2.04 | *pnc* |
| 2-2a | 1.36 | 1.39 | 1.40 | 1.43 | 1.53 | 1.49 |
| 2-2b | 1.39 | 1.36 | 1.34 | 1.73 | 1.96 | 2.53 |
| 2-2c | 1.53 | 1.36 | 1.65 | 1.73 | 1.96 | 2.53 |
| 2-3a | 1.36 | 1.38 | 0.92 | 1.42 | 1.52 | 1.07 |
| 2-3b | 1.39 | 1.40 | 1.40 | 1.36 | 1.94 | 2.16 |
| 2-3c | 0.97 | 0.94 | 1.39 | 0.89 | 1.52 | 1.07 |
| 2-3d | 1.39 | 1.43 | 1.41 | 1.76 | 1.27 | 2.16 |
| 2-4a | 1.40 | 1.79 | 1.81 | 1.86 | 1.34 | 1.20 |
| 2-4b | 1.74 | 1.81 | 1.45 | 1.91 | 2.07 | 1.38 |
| 3-3a | 1.39 | 1.26 | 1.52 | 1.46 | 1.94 | 1.81 |
| 3-3b | 1.48 | 1.46 | 1.44 | 1.41 | 1.19 | 1.77 |
| 3-3c | 1.50 | pnc | pnc | 1.45 | 1.33 | 1.41 |
| 3-4a | 1.62 | 1.61 | 1.66 | 1.59 | 1.56 | 0.88 |
| 3-4b | 1.43 | 1.43 | 1.43 | 1.42 | 1.44 | 1.13 |
| 4-4a | *pnc* | *pnc* | *pnc* | *pnc* | *pnc* | *pnc* |

**Embolded** results indicate the highest binding energy geometry.

**Table 5.50:** Cluster energies (eV) for tetravalent cations solution in α-$Cr_2O_3$ via neutral vacancy compensation.

| Quadvalent Cation | $Rh^{4+}$ | $Ti^{4+}$ | $Ru^{4+}$ | $Mo^{4+}$ | $Sn^{4+}$ | $Pu^{4+}$ |
|---|---|---|---|---|---|---|
| Cation Radii (Å) | 0.600 | 0.605 | 0.620 | 0.650 | 0.690 | 0.860 |
| Isolated | -43.33 | -39.91 | -37.67 | -33.29 | -24.70 | 1.63 |
| 1-2-2a | -47.86 | -44.57 | -42.40 | -38.17 | -29.86 | -4.32 |
| 1-2-3a | -47.41 | -44.09 | -41.91 | -37.64 | -29.23 | -3.25 |
| 1-2-3b | -47.72 | -44.38 | -42.19 | -37.91 | -29.52 | -3.86 |
| 2-2-2a | -48.12 | -44.82 | -42.66 | -38.44 | -30.24 | -5.87 |
| 2-2-3a | -47.22 | -43.90 | -41.73 | -37.47 | -29.10 | -3.33 |
| 2-2-3b | -47.48 | -44.15 | -41.98 | -37.71 | -29.35 | -3.80 |
| 2-3-3a | -46.95 | -43.60 | -41.41 | -37.11 | -28.67 | -2.94 |
| 2-3-3b | -46.71 | -43.37 | -41.17 | -36.87 | -28.40 | -2.48 |
| 3-3-3a | -46.55 | -43.17 | -40.95 | -36.63 | -28.20 | -3.49 |

**Table 5.51:** Solution energies (eV) for tetravalent cations in α-$Cr_2O_3$ via neutral vacancy compensation(reaction 5.10).

| Quadvalent Cation | $Rh^{4+}$ | $Ti^{4+}$ | $Ru^{4+}$ | $Mo^{4+}$ | $Sn^{4+}$ | $Pu^{4+}$ |
|---|---|---|---|---|---|---|
| Cation Radii (Å) | 0.600 | 0.605 | 0.620 | 0.650 | 0.690 | 0.860 |
| Isolated | 2.02 | 2.07 | 2.11 | 2.19 | 2.44 | 3.75 |
| 1-2-2a | **0.89** | **0.91** | **0.92** | **0.97** | **1.15** | **2.26** |
| 1-2-3a | 1.00 | 1.02 | 1.05 | 1.11 | 1.30 | 2.53 |
| 1-2-3b | 0.92 | 0.95 | 0.98 | 1.04 | 1.23 | 2.38 |
| 2-2-2a | 0.82 | 0.84 | 0.86 | 0.91 | 1.05 | 1.87 |
| 2-2-3a | 1.05 | 1.07 | 1.09 | 1.15 | 1.34 | 2.51 |
| 2-2-3b | 0.98 | 1.01 | 1.03 | 1.09 | 1.27 | 2.39 |
| 2-3-3a | 1.11 | 1.15 | 1.17 | 1.24 | 1.44 | 2.61 |
| 2-3-3b | 1.17 | 1.21 | 1.23 | 1.30 | 1.51 | 2.72 |
| 3-3-3a | 1.21 | 1.25 | 1.29 | 1.36 | 1.56 | 2.47 |

**Embolded** results indicate the lowest solution energy geometry.

**Table 5.52:** Binding energies (eV) for neutral clusters in $\alpha$-$Cr_2O_3$: vacancy compensation of 4+ cations (reaction 5.10).

| Quadvalent Cation | $Rh^{4+}$ | $Ti^{4+}$ | $Ru^{4+}$ | $Mo^{4+}$ | $Sn^{4+}$ | $Pu^{4+}$ |
|---|---|---|---|---|---|---|
| Cation Radii (Å) | 0.600 | 0.605 | 0.620 | 0.650 | 0.690 | 0.860 |
| 1-2-2a | **4.53** | **4.65** | **4.73** | **4.88** | **5.16** | **5.95** |
| 1-2-3a | 4.08 | 4.18 | 4.24 | 4.35 | 4.53 | 4.88 |
| 1-2-3b | 4.39 | 4.47 | 4.52 | 4.63 | 4.82 | 5.49 |
| 2-2-2a | 4.79 | 4.91 | 4.99 | 5.15 | 5.54 | 7.50 |
| 2-2-3a | 3.89 | 3.99 | 4.06 | 4.18 | 4.40 | 4.96 |
| 2-2-3b | 4.15 | 4.24 | 4.31 | 4.43 | 4.66 | 5.43 |
| 2-3-3a | 3.62 | 3.69 | 3.74 | 3.83 | 3.98 | 4.57 |
| 2-3-3b | 3.38 | 3.45 | 3.50 | 3.58 | 3.71 | 4.11 |
| 3-3-3a | 3.23 | 3.26 | 3.28 | 3.34 | 3.51 | 5.13 |

**Embolded** results indicate the highest binding energy geometry.

**Table 5.53:** Isolated interstitial defect, substitutional defect and oxide lattice energies (eV) for tetravalent cations in α-$Fe_2O_3$

| Quadvalent Cation | $Rh^{4+}$ | $Ti^{4+}$ | $Ru^{4+}$ | $Mo^{4+}$ | $Sn^{4+}$ | $Pu^{4+}$ |
|---|---|---|---|---|---|---|
| Cation Radii (Å) | 0.600 | 0.605 | 0.620 | 0.650 | 0.690 | 0.860 |
| iso $D_i^{\bullet\bullet\bullet\bullet}$ | -68.13 | -66.72 | -65.80 | -65.83 | -60.75 | -55.13 |
| iso $D_{Fe}^{\bullet}$ | -32.72 | -31.58 | -30.84 | -29.38 | -26.52 | -17.76 |
| Lattice En. | -118.83 | -117.76 | -117.06 | -115.71 | -113.18 | -106.15 |

**Table 5.54:** Cluster energies (eV) for tetravalent cations solution in α-$Fe_2O_3$ via neutral interstitial compensation.

| Quadvalent Cation | $Rh^{4+}$ | $Ti^{4+}$ | $Ru^{4+}$ | $Mo^{4+}$ | $Sn^{4+}$ | $Pu^{4+}$ |
|---|---|---|---|---|---|---|
| Cation Radii (Å) | 0.600 | 0.605 | 0.620 | 0.650 | 0.690 | 0.860 |
| Isolated | -78.36 | -76.09 | -74.60 | -71.68 | -65.97 | -48.45 |
| 1-1a | -80.27 | -78.09 | -76.65 | -73.89 | -68.51 | -51.36 |
| 1-2a | -80.10 | -77.94 | -76.53 | -73.74 | -68.33 | -49.88 |
| 1-2b | -80.05 | -77.90 | -76.50 | -73.74 | -68.44 | -50.70 |
| 1-3a | -80.23 | -77.95 | -76.33 | -73.62 | -67.87 | -50.86 |
| 1-3b | -79.87 | -77.56 | -76.12 | -73.21 | -67.58 | -50.33 |
| 1-4a | *pnc* | *pnc* | *pnc* | *pnc* | *pnc* | -50.53 |
| 1-4b | *pnc* | -78.01 | -76.49 | -73.64 | -68.09 | *pnc* |
| 2-2a | -79.80 | -77.55 | -76.08 | -73.20 | -67.58 | -50.02 |
| 2-2b | -79.85 | -77.76 | -76.05 | -73.48 | -67.99 | -51.05 |
| 2-2c | -79.85 | -77.76 | -76.31 | -73.48 | -67.99 | -51.05 |
| 2-3a | -79.81 | -77.56 | -76.08 | -72.67 | -67.57 | -49.39 |
| 2-3b | -79.83 | -77.56 | -76.11 | -73.15 | -67.98 | -50.68 |
| 2-3c | -79.81 | -77.14 | -75.63 | -72.67 | -67.57 | -49.58 |
| 2-3d | -79.83 | -77.62 | -76.11 | -73.16 | -67.35 | -50.68 |
| 2-4a | -79.84 | -77.57 | -76.49 | -73.17 | -67.30 | -49.70 |
| 2-4b | -79.95 | -77.96 | -76.51 | -73.19 | -68.10 | -49.88 |
| 3-3a | -79.85 | -77.73 | -76.05 | -73.10 | -67.37 | -50.29 |
| 3-3b | -79.95 | -77.59 | *pnc* | -73.09 | -67.43 | -49.71 |
| 3-3c | -80.10 | -77.66 | *pnc* | -73.22 | -67.45 | -49.73 |
| 3-4a | -80.07 | -77.78 | -76.29 | -73.40 | -67.61 | -49.80 |
| 3-4b | -79.71 | -77.60 | -76.11 | -73.18 | -67.45 | -50.80 |
| 4-4a | *pnc* | *pnc* | *pnc* | -73.42 | *pnc* | -49.96 |

**Table 5.55:** Solution energies (eV) for tetravalent cations in α-$Fe_2O_3$ via neutral interstitial compensation (reaction 5.9).

| Quadvalent Cation | $Rh^{4+}$ | $Ti^{4+}$ | $Ru^{4+}$ | $Mo^{4+}$ | $Sn^{4+}$ | $Pu^{4+}$ |
|---|---|---|---|---|---|---|
| Cation Radii (Å) | 0.600 | 0.605 | 0.620 | 0.650 | 0.690 | 0.860 |
| Isolated | 2.24 | 2.28 | 2.32 | 2.39 | 2.61 | 3.76 |
| 1-1a | **1.61** | **1.62** | **1.63** | **1.66** | **1.76** | **2.79** |
| 1-2a | 1.66 | 1.67 | 1.67 | 1.71 | 1.82 | 3.28 |
| 1-2b | 1.68 | 1.68 | 1.68 | 1.71 | 1.78 | 3.01 |
| 1-3a | 1.62 | 1.66 | 1.74 | 1.75 | 1.97 | 2.96 |
| 1-3b | 1.74 | 1.80 | 1.81 | 1.88 | 2.07 | 3.13 |
| 1-4a | *pnc* | *pnc* | *pnc* | *pnc* | *pnc* | 3.07 |
| 1-4b | pnc | 1.64 | 1.69 | 1.74 | 1.90 | *pnc* |
| 2-2a | 1.77 | 1.80 | 1.82 | 1.89 | 2.07 | 3.24 |
| 2-2b | 1.75 | 1.73 | 1.84 | 1.79 | 1.93 | 2.90 |
| 2-2c | 1.75 | 1.73 | 1.75 | 1.79 | 1.93 | 2.90 |
| 2-3a | 1.76 | 1.80 | 1.82 | 2.06 | 2.07 | 3.45 |
| 2-3b | 1.75 | 1.80 | 1.81 | 1.90 | 1.94 | 3.02 |
| 2-3c | 1.76 | 1.94 | 1.97 | 2.06 | 2.07 | 3.38 |
| 2-3d | 1.75 | 1.77 | 1.81 | 1.90 | 2.14 | 3.02 |
| 2-4a | 1.75 | 1.79 | 1.69 | 1.90 | 2.16 | 3.34 |
| 2-4b | 1.71 | 1.66 | 1.68 | 1.89 | 1.89 | 3.28 |
| 3-3a | 1.75 | 1.74 | 1.83 | 1.92 | 2.14 | 3.15 |
| 3-3b | 1.71 | 1.79 | *pnc* | 1.92 | 2.12 | 3.34 |
| 3-3c | 1.67 | 1.76 | *pnc* | 1.88 | 2.11 | 3.33 |
| 3-4a | 1.68 | 1.72 | 1.75 | 1.82 | 2.06 | 3.31 |
| 3-4b | 1.79 | 1.78 | 1.81 | 1.89 | 2.11 | 2.98 |
| 4-4a | *pnc* | *pnc* | *pnc* | 1.81 | *pnc* | 3.26 |

**Embolded** results indicate the lowest solution energy geometry.

**Table 5.56:** Binding energies (eV) for neutral clusters in $\alpha$-$Fe_2O_3$: interstitial compensation of 4+ cations (reaction 5.9).

| Quadvalent Cation | $Rh^{4+}$ | $Ti^{4+}$ | $Ru^{4+}$ | $Mo^{4+}$ | $Sn^{4+}$ | $Pu^{4+}$ |
|---|---|---|---|---|---|---|
| Cation Radii (Å) | 0.600 | 0.605 | 0.620 | 0.650 | 0.690 | 0.860 |
| 1-1a | **1.91** | **2.00** | **2.05** | **2.20** | **2.54** | **2.91** |
| 1-2a | 1.74 | 1.85 | 1.93 | 2.05 | 2.37 | 1.43 |
| 1-2b | 1.68 | 1.81 | 1.90 | 2.06 | 2.47 | 2.25 |
| 1-3a | 1.86 | 1.86 | 1.72 | 1.93 | 1.90 | 2.41 |
| 1-3b | 1.50 | 1.47 | 1.52 | 1.52 | 1.61 | 1.89 |
| 1-4a | *pnc* | *pnc* | *pnc* | *pnc* | *pnc* | 2.09 |
| 1-4b | pnc | 1.92 | 1.89 | 1.96 | 2.12 | *pnc* |
| 2-2a | 1.43 | 1.46 | 1.48 | 1.51 | 1.61 | 1.57 |
| 2-2b | 1.49 | 1.67 | 1.44 | 1.80 | 2.03 | 2.60 |
| 2-2c | 1.49 | 1.67 | 1.71 | 1.80 | 2.03 | 2.60 |
| 2-3a | 1.45 | 1.47 | 1.48 | 0.99 | 1.60 | 0.94 |
| 2-3b | 1.47 | 1.47 | 1.51 | 1.47 | 2.01 | 2.24 |
| 2-3c | 1.45 | 1.05 | 1.03 | 0.99 | 1.60 | 1.13 |
| 2-3d | 1.47 | 1.53 | 1.51 | 1.48 | 1.38 | 2.24 |
| 2-4a | 1.47 | 1.47 | 1.89 | 1.48 | 1.33 | 1.25 |
| 2-4b | 1.59 | 1.87 | 1.91 | 1.51 | 2.13 | 1.43 |
| 3-3a | 1.49 | 1.64 | 1.45 | 1.42 | 1.40 | 1.85 |
| 3-3b | 1.58 | 1.50 | *pnc* | 1.41 | 1.46 | 1.27 |
| 3-3c | 1.73 | 1.57 | *pnc* | 1.54 | 1.48 | 1.29 |
| 3-4a | 1.70 | 1.69 | 1.69 | 1.71 | 1.64 | 1.35 |
| 3-4b | 1.35 | 1.51 | 1.51 | 1.50 | 1.48 | 2.35 |
| 4-4a | *pnc* | *pnc* | *pnc* | 1.74 | *pnc* | 1.51 |

**Embolded** results indicate the highest binding energy geometry.

**Table 5.57:** Cluster energies (eV) for tetravalent cations solution in α-$Fe_2O_3$ via neutral vacancy compensation.

| Quadvalent Cation | $Rh^{4+}$ | $Ti^{4+}$ | $Ru^{4+}$ | $Mo^{4+}$ | $Sn^{4+}$ | $Pu^{4+}$ |
|---|---|---|---|---|---|---|
| Cation Radii (Å) | 0.600 | 0.605 | 0.620 | 0.650 | 0.690 | 0.860 |
| Isolated | -42.99 | -39.58 | -37.35 | -32.97 | -24.40 | 1.88 |
| 1-2-2a | -47.75 | -44.46 | -42.30 | -38.07 | -29.77 | -4.23 |
| 1-2-3a | -47.29 | -43.97 | -41.80 | -37.54 | -29.15 | -3.21 |
| 1-2-3b | -47.62 | -44.29 | -42.10 | -37.83 | -29.45 | -3.82 |
| 2-2-2a | -48.04 | -44.74 | -42.58 | -38.36 | -30.16 | -5.75 |
| 2-2-3a | -47.10 | -43.79 | -41.62 | -37.36 | -29.00 | -3.26 |
| 2-2-3b | -47.37 | -44.05 | -41.88 | -37.62 | -29.27 | -3.73 |
| 2-3-3a | -46.84 | -43.49 | -41.30 | -37.01 | -28.59 | -2.89 |
| 2-3-3b | -46.58 | -43.24 | -41.05 | -36.76 | -28.31 | -2.41 |
| 3-3-3a | -46.44 | -43.06 | -40.85 | -36.53 | -28.12 | -3.41 |

**Table 5.58:** Solution energies (eV) for tetravalent cations in α-$Fe_2O_3$ via neutral vacancy compensation (reaction 5.10).

| Quadvalent Cation | $Rh^{4+}$ | $Ti^{4+}$ | $Ru^{4+}$ | $Mo^{4+}$ | $Sn^{4+}$ | $Pu^{4+}$ |
|---|---|---|---|---|---|---|
| Cation Radii (Å) | 0.600 | 0.605 | 0.620 | 0.650 | 0.690 | 0.860 |
| Isolated | 2.09 | 2.14 | 2.17 | 2.26 | 2.50 | 3.80 |
| 1-2-2a | **0.90** | **0.92** | **0.94** | **0.98** | **1.16** | **2.27** |
| 1-2-3a | 1.02 | 1.04 | 1.06 | 1.12 | 1.31 | 2.53 |
| 1-2-3b | 0.93 | 0.96 | 0.98 | 1.04 | 1.24 | 2.37 |
| 2-2-2a | 0.83 | 0.85 | 0.87 | 0.91 | 1.06 | 1.89 |
| 2-2-3a | 1.06 | 1.09 | 1.11 | 1.16 | 1.35 | 2.51 |
| 2-2-3b | 1.00 | 1.02 | 1.04 | 1.10 | 1.28 | 2.40 |
| 2-3-3a | 1.13 | 1.16 | 1.18 | 1.25 | 1.45 | 2.61 |
| 2-3-3b | 1.19 | 1.22 | 1.25 | 1.31 | 1.52 | 2.73 |
| 3-3-3a | 1.23 | 1.27 | 1.30 | 1.37 | 1.57 | 2.48 |

**Embolded** results indicate the lowest solution energy geometry.

**Table 5.59:** Binding energies (eV) for neutral clusters in $\alpha$-$Fe_2O_3$: vacancy compensation of 4+ cations (reaction 5.10).

| Quadvalent Cation | $Rh^{4+}$ | $Ti^{4+}$ | $Ru^{4+}$ | $Mo^{4+}$ | $Sn^{4+}$ | $Pu^{4+}$ |
|---|---|---|---|---|---|---|
| Cation Radii (Å) | 0.600 | 0.605 | 0.620 | 0.650 | 0.690 | 0.860 |
| 1-2-2a | **4.75** | **4.87** | **4.95** | **5.10** | **5.37** | **6.11** |
| 1-2-3a | 4.29 | 4.39 | 4.45 | 4.57 | 4.75 | 5.09 |
| 1-2-3b | 4.62 | 4.70 | 4.76 | 4.86 | 5.05 | 5.70 |
| 2-2-2a | 5.05 | 5.15 | 5.23 | 5.38 | 5.76 | 7.63 |
| 2-2-3a | 4.10 | 4.20 | 4.27 | 4.39 | 4.60 | 5.14 |
| 2-2-3b | 4.37 | 4.47 | 4.53 | 4.65 | 4.87 | 5.61 |
| 2-3-3a | 3.84 | 3.91 | 3.95 | 4.04 | 4.19 | 4.77 |
| 2-3-3b | 3.59 | 3.66 | 3.70 | 3.78 | 3.91 | 4.29 |
| 3-3-3a | 3.45 | 3.48 | 3.50 | 3.56 | 3.72 | 5.29 |

**Embolded** results indicate the highest binding energy geometry.

#### 5.4.2.2 General Comments on Aliovalent Results

Comparing the three systems, solution energies for $\alpha$-$Al_2O_3$ are slightly higher and the dopant ion radii dependency is stronger than in $\alpha$-$Cr_2O_3$ and $\alpha$-$Fe_2O_3$. This is apparent from the higher values and steeper gradients in figure 5.2, compared to figures 5.3 and 5.4. This indicates that if dopants become incorporated in the lattice, they will thermodynamically form a second phase more easily if that lattice is $\alpha$-$Al_2O_3$. In other words their equilibrium dopant concentrations in $\alpha$-$Al_2O_3$ will be lower than in $\alpha$-$Cr_2O_3$ and $\alpha$-$Fe_2O_3$.

Generally $\alpha$-$Cr_2O_3$ and $\alpha$-$Fe_2O_3$ yield very similar results. This can be explained by the very close match between the two lattice volumes (see table 5.1). As such, it is difficult to resolve any appreciable variation between the two with respect to solution energies. Of course in low $p_{O_2}$ it is much easier to reduce $Fe^{3+}$ than $Cr^{3+}$ which will lead to alternative mechanisms in the iron system not considered here. Consequently distinct differences between defect mechanisms can be expected in $\alpha$-$Cr_2O_3$ and $\alpha$-$Fe_2O_3$ at specific oxygen

partial pressures.

#### 5.4.2.3 Solution of Isovalent Cations

Isovalent solution will not create charged defects in the lattice (reaction 5.5). Hence, these dopant species are not expected to increase the concentration of those defects (e.g. vacancies or interstitials) which might aid mass transport through the lattice [78, 79, 82, 93, 102, 103]. However, the large solution energies for large dopant cations (i.e. $Yb^{3+}$, $Y^{3+}$, $Sm^{3+}$ and $La^{3+}$ which range from 2.4eV to 5eV in $\alpha$-$Al_2O_3$ and 1.2eV to 3eV in $\alpha$-$Cr_2O_3$ and $\alpha$-$Fe_2O_3$) mean that such dopants will not stay in solution but will overwhelmingly form a second (or grain boundary) phase. The formation of a second phase will lead to complex grain boundary structures. Grain boundaries are likely to provide a lower energy pathway for atomic transport than through the bulk, and so are considered undesirable.

Dopant cations with radii close to that of the host lattice cation, exhibit small solution energies. Evidence of a minimum is visible in figures 5.3 and 5.4 where the host cation radii lies between the minimum and maximum range of 3+ dopants studied. Solution energies increase rapidly as the dopant cation size differs from that of the host. Thus, only ions with radii very close to the host lattice radii are likely to exhibit appreciable solubility in these lattices (e.g. $Cr^{3+}$, $Ga^{3+}$, $Fe^{3+}$ in $\alpha$-$Al_2O_3$; $Al^{3+}$, $Cr^{3+}$, $Ga^{3+}$ in $\alpha$-$Fe_2O_3$ and; $Al^{3+}$, $Fe^{3+}$, $Ga^{3+}$ in $\alpha$-$Cr_2O_3$ all of which have solution energies less than 0.5eV).

#### 5.4.2.4 Aliovalent Substitution

**Compensation Effects.** Aliovalent substitution requires intrinsic charge compensating defects (reactions 5.7-5.10) or extrinsic charge compensating defects (reaction 5.6) to be formed. This may increase the concentration of those species responsible for mediating transport in these host materials. However, there is also the potential to produce defects that will either reduce the mobile species concentration (through the intrinsic defect equi-

libria) or hinder their transport mechanisms (through defect cluster formation which will be discussed later). Again care must exercised over ions with excessively large solution energies since they will result in second phase formation.

**Divalent Substitution.** For all divalent cations investigated here, anion vacancy compensation (reaction 5.8) is the dominant mechanism for the three host oxides (see figures 5.2-5.4). Reaction 5.6, which assumes compensation via dopant interstitial ions, is close in energy for $Mg^{2+}$ solution (especially in $\alpha$-$Cr_2O_3$ and $\alpha$-$Fe_2O_3$). However, the preference for vacancies (reaction 5.8) over dopant interstitials (reaction 5.6) increases substantially for larger cations.

The solution energy range for divalent ions, assuming isolated defects, is 2.0eV to 7.4eV, for $Al_2O_3$, and 2.2eV to 5.6eV, for $\alpha$-$Cr_2O_3$ and $\alpha$-$Fe_2O_3$. As a result of these differences the range of divalent ion radii for which there is any practical solution will be smaller in $\alpha$-$Al_2O_3$ than in the other materials. However, in all three host materials only the smallest cations will exhibit any solution concentration. The larger 2+ ions will tend to either form a second phase or will segregate to grain boundaries.

The lowest solution energies are predicted for substitutional ions with smaller radii for all three host lattices, as would be expected, since the smaller radii cations are closer in size to the host lattice cations. However, the effective size of the substitution site is not exactly the same as that of the host lattice ion that is being replaced. This is because relaxation of the near neighbour oxygen ions is outward, away from the 2+ substitutional ion, since the effective charge of the defect is minus one. This creates a slightly larger substitutional site. Consequently the curves depicting 2+ ion solution as a function of dopant ion radius would exhibit a minimum at a radius larger than that of the host lattice cation. Some evidence of this is seen in figures 5.3 and 5.4.

It is now possible to assess when, assuming equilibrium, the extrinsic equilibrium

solution of binary oxides, $BO$, results in the formation of greater concentrations of oxygen vacancies, $V_O^{\bullet\bullet}$, than the corresponding lowest energy intrinsic reaction. Since both Schottky and anion Frenkel processes produce oxygen vacancies, and since they exhibit similar energies, both must be compared to the favoured divalent solution mechanism.

The equation that describes the equilibrium oxygen vacancy concentration, if oxygen vacancies are formed primarily through solution of dopant ions, has already been derived; this is equation 5.18. Conversely if Schottky disorder is dominant (as may be the case in α-$Al_2O_3$), equation 5.14 will govern oxygen vacancy concentration. However, if anion Frenkel disorder is dominant (as may be the case for α-$Cr_2O_3$ and α-$Fe_2O_3$), then,

$$[V_O^{\bullet\bullet}] = e^{\frac{-\Delta H_{an-fr}}{2kT}} \tag{5.23}$$

is appropriate where $\Delta H_{an-fr}$ is the anion Frenkel reaction energy.

Since the pre-exponential factors in equations 5.14, 5.18 and 5.23 are numerically close and the equations are dominated by the energy term in the exponential, the extrinsic reaction will effectively dominate when $\frac{1}{3}\Delta H_{sol(5.8)} < \frac{1}{5}\Delta H_{sh}$ or $< \frac{1}{2}\Delta H_{an-fr}$. Energies for $\frac{1}{3}\Delta H_{sol(5.8)}$ are given in figures 5.2a-5.4a and tables 5.17, 5.27 5.37. The normalised Schottky and anion Frenkel energies from table 5.6 are also indicated in figures 5.2-5.4 by dotted lines parallel to the x-axis. Thus, when isolated, the extrinsic solution reaction 5.8 is responsible for oxygen vacancy formation in all three materials except when the dopant 2+ cations are vary large (i.e. $Sr^{2+}$ and $Ba^{2+}$ for α-$Al_2O_3$ and $Ba^{2+}$ in α-$Cr_2O_3$ and α-$Fe_2O_3$). Clearly the solution energies for these large cations are sufficiently large and their resulting equilibrium solution concentrations will be so small they will not alter the intrinsic equilibria.

**Tetravalent Substitution.** For tetravalent cation solution in α-$Al_2O_3$, host cation vacancy compensation (reaction 5.10) is the dominant solution mechanism for all dopant ions

(see figure 5.2). This agrees with available experimental evidence for $Ti^{4+}$ solution in $\alpha$-$Al_2O_3$ [77, 98, 99]. The solution energies for this solution mechanism, assuming isolated defects, range from 2.2eV to 4.8eV. Again, smaller ions exhibit higher equilibrium solution concentrations (i.e. have lower solution energies) than larger dopant ions. Furthermore, there is a sharp increase in solution energy as the 4+ dopant radius increases. This is because, in the case of a 4+ dopant ion, the effective size of the substitutional site is smaller than the host lattice ion. The smaller site is a consequence of the effective charge of the dopant being positive one, so that the near neighbour oxygen ions are drawn inward slightly. Thus even the smallest 4+ ion is larger than the substitutional site.

For tetravalent ion accommodation in $\alpha$-$Cr_2O_3$ and $\alpha$-$Fe_2O_3$ the difference between solution energies for reactions 5.9 and 5.10 is small for the isolated case. Conversely in the clustered case reaction 5.10 exhibits a substantially lower energy than reaction 5.9. Solution energies for both reactions yield values for $\alpha$-$Cr_2O_3$ and $\alpha$-$Fe_2O_3$ of between 2.0eV and 3.8eV with smaller cations exhibiting the lower solution energies. In fact, reactions 5.9 and 5.10 are connected through the Schottky and anion Frenkel reactions,

$$\Delta H_{sol(5.9)} = \frac{2}{3}\Delta H_{sol(5.10)} + \Delta H_{an-fr} + \frac{3}{4}\Delta H_{sh} \tag{5.24}$$

Therefore, whichever reaction is dominant, both the metal vacancy and oxygen interstitial concentrations will increase (see table 5.3).

A prediction may now be made of the tetravalent dopant ions for which solution via reactions 5.9 and 5.10 will result in the formation of a greater concentration of metal vacancies than the equivalent intrinsic mass action equilibrium relationship, assuming defects are spatially separated.

The relationship that governs the metal vacancy concentration, assuming solution defects are dominant, is equation 5.22 (which can be modified to yield equivalent equations for oxygen interstitials through equation 5.24). This must be compared to the equivalent

lowest energy intrinsic reaction that results in metal vacancy formation. In all three host lattices this is the Schottky process (reaction 5.1) and therefore equation 5.13 must be compared to equation 5.22. Again since the pre-exponential factors are numerically similar the extrinsic doping reaction will effectively dominate when $\frac{1}{4}\Delta H_{sol(5.10)} < \frac{1}{5}\Delta H_{sh}$. This inequality can be investigated by comparing energies given in figures 5.2-5.4 and tables 5.45, 5.52 5.59. Therefore, through the equilibrium solution of any 4+ cation included here, the resulting population of $V_M'''$ (and through reaction 5.24, $O_i''$) dominates concentrations derived from intrinsic reactions. Since the equilibrium 4+ dopant solution populations are small (i.e. the solution energies are high), there only has to be a small impurity content for the equilibrium solution to be achieved and the intrinsic reaction to be dominated. In α-$Cr_2O_3$ and α-$Fe_2O_3$ such an analysis will need to be modified for $p_{O_2}$ and temperature regimes where electronic reactions are important (for α-$Al_2O_3$ this will not be necessary given its large band gap,8.8eV [107]). For example, electronic defects may well offer a lower energy compensation mechanism for 4+ ion substitution (e.g. via $Fe'_{Fe}$ compensation) so that the $V_M'''$ and $O_i''$ concentrations will not be modified to the same degree.

### 5.4.3 Defect Cluster Formation

The extent to which defects will form clusters or remain isolated depends on the magnitude of binding energy. For example, the defects associated with reaction 5.8 may form neutral clusters of the type,

$$2B'_M + V_O^{\bullet\bullet} \underset{sol(5.8)}{\longrightarrow} \{2B'_M : V_O^{\bullet\bullet}\}^{\times} \tag{5.25}$$

in which case a mass action equation can be defined,

$$\frac{[\{2B'_M : V_O^{\bullet\bullet}\}^{\times}]}{[B'_M]^2[V_O^{\bullet\bullet}]} = e^{\frac{-\Delta H^{clst}_{sol(5.8)}}{kT}} \tag{5.26}$$

where $\Delta H^{clst}_{sol(5.8)}$ is the energy for reaction 5.25. In fact this energy, the binding energy, is the difference between solution energies for reaction 5.8 assuming isolated defects and

assuming clustered defects. Since the binding energy for reaction 5.25 is positive, as for all mechanisms studied here, it is clear that clusters are most stable at low temperatures but tend to break up at high temperatures. This has been studied in detail for $Mg^{2+}$ and $Ti^{4+}$ solution in $\alpha$-$Al_2O_3$ previously by Lagerlöf and Grimes [63] who also considered a variety of possible charged defect clusters. Since defect cluster formation lowers solution energies it is important to determine if the lowest energy solution mechanism is changed through defect association.

In the case of divalent substitution three mechanisms are considered, 5.6, 5.7 and 5.8. Thus, two equilibria between cluster types are needed to solve the concentration relationship, provided some assumptions are made. First consider, the equilibrium between the dopant interstitial mechanism (reaction 5.6) and the vacancy mechanism (reaction 5.8),

$$\frac{3}{2}\{2B'_M : V_O^{\bullet\bullet}\}^{\times} + \frac{1}{2}M_2O_3 \rightleftharpoons \{2B'_M : B_i^{\bullet\bullet}\}^{\times} + M_M^{\times} + \frac{3}{2}O_O^{\times} \tag{5.27}$$

the corresponding mass action relationship is,

$$\frac{[\{2B'_M : B_i^{\bullet\bullet}\}^{\times}]}{[\{2B'_M : V_O^{\bullet\bullet}\}^{\times}]^{\frac{3}{2}}} = e^{\frac{-\Delta H_{5.27}}{kT}} \tag{5.28}$$

Second, consider the equilibrium between the interstitial mechanism (reaction 5.7) and the vacancy mechanism (reaction 5.8),

$$\frac{3}{2}\{2B'_M : V_O^{\bullet\bullet}\}^{\times} + \frac{1}{2}M_2O_3 \rightleftharpoons \{3B'_M : M_i^{\bullet\bullet\bullet}\}^{\times} + \frac{3}{2}O_O^{\times} \tag{5.29}$$

the corresponding mass action relationship is,

$$\frac{[\{3B'_M : M_i^{\bullet\bullet\bullet}\}^{\times}]}{[\{2B'_M : V_O^{\bullet\bullet}\}^{\times}]^{\frac{3}{2}}} = e^{\frac{-\Delta H_{5.29}}{kT}} \tag{5.30}$$

For reaction 5.27 and 5.29 the energies (i.e. $\Delta H_{5.27}$ and $\Delta H_{5.29}$) are presented in tables 5.60 and 5.61. All reaction energies are positive indicating that the vacancy mechanism (reaction 5.8) will proceed in preference to either the dopant interstitial (reaction 5.6) or the interstitial (reaction 5.7) mechanism.

It is also important to gauge by how much the vacancy mechanism dominates. This can be done by assuming the vacancy cluster concentration, $[\{2B'_M : V_O^{\bullet\bullet}\}^{\times}]$, is of the order of $10^{-4}$ (by analogy to the results of Lagerlöf and Grimes) and calculating the corresponding cluster concentration of the other types of cluster in α-$Al_2O_3$. This is done for equations 5.27 and 5.29 in tables 5.60 and 5.61 respectively at temperatures of 600K, 1000K, 1400K and 1800K. Since all these concentrations are much smaller than $10^{-4}$ it is reasonable to assume that the vacancy mechanism greatly dominates the other two divalent solution mechanisms (as was the case when isolated defects were assumed).

**Table 5.60:** Reaction energies for the equilibrium between the vacancy and dopant interstitial solution mechanisms with corresponding concentration of dopant interstitial clusters assuming $[\{2B'_M : V_O^{\bullet\bullet}\}^{\times}]$ is $10^{-4}$.

| 2+ cation | $Mg^{2+}$ | $Co^{2+}$ | $Fe^{2+}$ | $Cd^{2+}$ | $Ca^{2+}$ | $Sr^{2+}$ | $Ba^{2+}$ |
|---|---|---|---|---|---|---|---|
| $\Delta H_{5.28}$ | 0.48 | 1.18 | 1.67 | 4.00 | 4.76 | 6.38 | 7.63 |
| Temp. (K) | | | | | | | |
| 600 | $9.1\text{x}10^{-11}$ | $1.3\text{x}10^{-16}$ | $1.0\text{x}10^{-20}$ | $2.5\text{x}10^{-40}$ | $1.1\text{x}10^{-46}$ | $2.5\text{x}10^{-60}$ | $8.4\text{x}10^{-71}$ |
| 1000 | $3.8\text{x}10^{-09}$ | $1.2\text{x}10^{-12}$ | $4.0\text{x}10^{-15}$ | $6.9\text{x}10^{-27}$ | $1.1\text{x}10^{-30}$ | $6.9\text{x}10^{-39}$ | $3.6\text{x}10^{-45}$ |
| 1400 | $1.9\text{x}10^{-08}$ | $5.8\text{x}10^{-11}$ | $1.0\text{x}10^{-12}$ | $4.0\text{x}10^{-21}$ | $7.5\text{x}10^{-24}$ | $1.1\text{x}10^{-29}$ | $3.5\text{x}10^{-34}$ |
| 1800 | $4.5\text{x}10^{-08}$ | $5.1\text{x}10^{-10}$ | $2.2\text{x}10^{-11}$ | $6.3\text{x}10^{-18}$ | $4.8\text{x}10^{-20}$ | $1.4\text{x}10^{-24}$ | $4.4\text{x}10^{-28}$ |

**Table 5.61:** Reaction energies for the equilibrium between the vacancy and interstitial solution mechanisms with corresponding concentration of interstitial clusters assuming $[\{2B'_M : V_O^{\bullet\bullet}\}^{\times}]$ is $10^{-4}$.

| 2+ cation | $Mg^{2+}$ | $Co^{2+}$ | $Fe^{2+}$ | $Cd^{2+}$ | $Ca^{2+}$ | $Sr^{2+}$ | $Ba^{2+}$ |
|---|---|---|---|---|---|---|---|
| $\Delta H_{5.30}$ | 1.87 | 2.47 | 2.54 | 3.07 | 3.36 | 4.02 | 4.73 |
| Temp. (K) | | | | | | | |
| 600 | $2.1\text{x}10^{-22}$ | $1.8\text{x}10^{-27}$ | $5.1\text{x}10^{-28}$ | $1.6\text{x}10^{-32}$ | $6.0\text{x}10^{-35}$ | $1.7\text{x}10^{-40}$ | $2.0\text{x}10^{-46}$ |
| 1000 | $3.9\text{x}10^{-16}$ | $3.5\text{x}10^{-19}$ | $1.7\text{x}10^{-19}$ | $3.3\text{x}10^{-22}$ | $1.2\text{x}10^{-23}$ | $5.5\text{x}10^{-27}$ | $1.5\text{x}10^{-30}$ |
| 1400 | $1.9\text{x}10^{-13}$ | $1.3\text{x}10^{-15}$ | $7.5\text{x}10^{-16}$ | $8.7\text{x}10^{-18}$ | $8.0\text{x}10^{-19}$ | $3.4\text{x}10^{-21}$ | $9.7\text{x}10^{-24}$ |
| 1800 | $5.9\text{x}10^{-12}$ | $1.2\text{x}10^{-13}$ | $8.0\text{x}10^{-14}$ | $2.5\text{x}10^{-15}$ | $3.9\text{x}10^{-16}$ | $5.5\text{x}10^{-18}$ | $5.9\text{x}10^{-20}$ |

In the case of tetravalent substitution only two solution mechanisms are considered, 5.9 and 5.10. To be able to compare these reactions consider the equilibrium between

them,

$$\{3D_M^{\bullet} : V_M^{'''}\}^{\times} + \frac{1}{2}M_2O_3 \rightleftharpoons \frac{3}{2}\{2D_M^{\bullet} : O_i^{''}\}^{\times} + M_M^{\times} \tag{5.31}$$

the corresponding mass action relationship is therefore,

$$\frac{[\{2D_M^{\bullet} : O_i^{''}\}^{\times}]^{\frac{3}{2}}}{[\{3D_M^{\bullet} : V_M^{'''}\}^{\times}]} = e^{\frac{-\Delta H_{5.31}}{kT}} \tag{5.32}$$

where $\Delta H_{5.31}$ is the reaction energy when the cluster associated with vacancies (reaction 5.10) is transformed into the cluster associated with interstitials (reaction 5.9). Using the appropriate calculated cluster energies, $\Delta H_{5.31}$ have been evaluated for $\alpha$-$Al_2O_3$. These are all positive and are presented in table 5.62. Again if it is assumed that $[\{3D_M^{\bullet} : V_M^{'''}\}^{\times}]$ is $10^{-4}$. As such, metal vacancy compensation dominates the solution of tetravalent dopant ions.

**Table 5.62:** Reaction energies for the equilibrium between the vacancy and interstitial solution mechanisms with corresponding concentration of interstitial clusters assuming $[\{3D_M^{\bullet} : V_M^{'''}\}^{\times}]$ is $10^{-4}$.

| 4+ cation | $Rh^{4+}$ | $Ti^{4+}$ | $Ru^{4+}$ | $Mo^{4+}$ | $Sn^{4+}$ | $Pu^{4+}$ |
|---|---|---|---|---|---|---|
| $\Delta H_{5.31}$ | 5.30 | 5.44 | 5.34 | 5.40 | 5.47 | 6.16 |
| Temp. (K) | | | | | | |
| 600 | $7.1\text{x}10^{-39}$ | $1.1\text{x}10^{-39}$ | $4.3\text{x}10^{-39}$ | $2.0\text{x}10^{-39}$ | $7.9\text{x}10^{-40}$ | $1.1\text{x}10^{-43}$ |
| 1000 | $5.2\text{x}10^{-27}$ | $1.7\text{x}10^{-27}$ | $3.9\text{x}10^{-27}$ | $2.4\text{x}10^{-27}$ | $1.4\text{x}10^{-27}$ | $6.8\text{x}10^{-30}$ |
| 1400 | $6.4\text{x}10^{-22}$ | $2.9\text{x}10^{-22}$ | $5.2\text{x}10^{-22}$ | $3.7\text{x}10^{-22}$ | $2.5\text{x}10^{-22}$ | $5.6\text{x}10^{-24}$ |
| 1800 | $4.3\text{x}10^{-19}$ | $2.3\text{x}10^{-19}$ | $3.6\text{x}10^{-19}$ | $2.8\text{x}10^{-19}$ | $2.1\text{x}10^{-19}$ | $1.1\text{x}10^{-20}$ |

For further details of equilibria between clustered, partly clustered (i.e. charged defect clusters) and isolated defect reactions see previous studies of MgO and $TiO_2$ solution in $\alpha$-$Al_2O_3$ [63].

## 5.5 Summary

The analysis presented above, while rigorous, is not complete. Currently discussion and conclusions are only valid under conditions where ionic defects dominate electronic defects

in the host materials. Furthermore, equilibrium is assumed that, while possible at high temperatures, may well not be attainable at low temperatures or for samples that have been quenched from high temperatures. Nevertheless, these results (energies) provide useful data for analysis of non-equilibrium materials since they are the driving forces for solution and cluster formation.

The solution mechanisms and corresponding energies for isovalent and aliovalent dopant ions have been predicted. In all cases, energies increase dramatically with increasing dopant ion radius. Fortunately, despite there being a number of possible solution mechanisms, the lowest energy mechanism for divalent ion substitution is through compensation by oxygen vacancies for the whole range of dopant ion size (from $Mg^{2+}$ to $Ba^{2+}$). For tetravalent substitution, compensation is predicted to always occur through compensation by host metal cation vacancies (with ionic radii in the range 0.6Å to 0.86Å) for $\alpha$-$Al_2O_3$ but through metal vacancy or oxygen interstitial compensation in $\alpha$-$Cr_2O_3$ and $\alpha$-$Fe_2O_3$ depending on the dopant radius. However, defect clustering will result in metal vacancy compensation being dominant across the range of ion sizes studied here.

Isovalent ion substitution does not require charge compensation. Nevertheless energies associated with solution of large trivalent ions are high and consequently the equilibrium solution limits of these ions will be very small. Most large isovalent cations will therefore contribute to second phase formation, possibly as grain boundary phases. The same holds true for most aliovalent dopant ions, so that for all but the smallest aliovalent ions, solution limits will be small.

Despite low solution limits, most aliovalent cations exhibit sufficient concentration that, at equilibrium, their presence in the three corundum lattices will result in concentrations of vacancies that will dominate intrinsic equilibria. Consequently the concentrations of vacancies and interstitial host lattice ions will be dictated entirely by the balance between the total inventories of divalent and tetravalent dopant ions. Evaluation of the balance

will be a difficult task for two reasons; first, the equilibrium concentrations of different aliovalent ions are so different, and second, divalent and tetravalent substitutional ions will themselves form bound defect clusters which will depend strongly on their respective radii [63]. Nevertheless, as shown previously for $Mg^{2+}$ and $Ti^{4+}$ solution, such analysis while complex, is possible [63].

Some useful general trends are clear. If divalent ions are substituted into a lattice, the oxygen vacancy concentration is driven up. Through the Schottky and Frenkel equilibria this means that metal vacancy and oxygen interstitial concentrations are forced down and metal interstitial concentrations driven up (though the latter will still be small). The opposite situation will evolve through reaction 5.10 for tetravalent ion solution. These observations are summarised in table 5.63.

**Table 5.63:** Relative change in concentration of important defects due to incorporation of dopant ions via predicted dominant reactions. † indicates the primary defect introduced by the mechanism.

| Dominant | Dopant | | Intrinsic Species | | | |
|---|---|---|---|---|---|---|
| Equation | $B'_M$ | $D^{\bullet}_M$ | $M^{\bullet\bullet\bullet}_i$ | $V'''_M$ | $O''_i$ | $V^{\bullet\bullet}_O$ |
| 5.8 | ↑ | - | ↑ | ↓ | ↓ | ↑ † |
| 5.10 | - | ↑ | ↓ | ↑† | ↑ | ↓ |

The results of this study are in general agreement with available experimental data. It has already been mentioned that in $\alpha$-$Al_2O_3$ the similarity between Schottky and anion Frenkel energies is consistent with the observations of El-Aiat and Kröger [89]. Furthermore, the present prediction that solution of titanium in $\alpha$-$Al_2O_3$ is via cation vacancies is in agreement with the experimental data of Perot-Ervas *et al.* [77].

The summary of table 5.63 is also consistent with oxygen self diffusion increasing through $Mg^{2+}$ doping and decreasing through $Ti^{2+}$ doping as reported by Lagerlöf *et al.* [95, 96] and Haneda *et al.* [97]. This is, of course, assuming that oxygen is transported via

a vacancy mechanism.

Results for α-$Cr_2O_3$ are in broad agreement with previous simulation studies by Lawrence *et al.* [86]. Agreement is also seen with the observation of Hagel and Seybolt [81] that $Y^{3+}$ has a minimal effect on cation diffusion. In contrast the observation that $Ce^{4+}$ does not effect cation diffusion seems at odds with the present results. As intimated earlier Ce may, in fact, adopt a 3+ charge state in α-$Cr_2O_3$, which would then make the present results consistent with the experimental observations. Potentials are available for $Ce^{3+}$ and $Ce^{4+}$ so this is briefly investigated here. Consider the reaction,

$$Ce_M^{\times} \rightarrow Ce_M^{\bullet} + e^{-}(\infty) \tag{5.33}$$

where this process is the ionisation energy of $Ce^{3+}$ within the α-$Cr_2O_3$ lattice. $Ce_M^{\times}$ and $Ce_M^{\bullet}$ are evaluated to be 14.13 eV and -17.06 eV respectively by simulation. However this does not include the electronic contribution, the atomic $4^{th}$ ionisation energy, 36.72eV [108]. Thus, $\Delta H_{5.33}$ is -17.06 + 36.72 -14.13 = 5.53eV. This, is the energy required to remove an electron from a $Ce_M^{\times}$ to the vacuum level creating $Ce_M^{\bullet}$. However, the electron will actually occupy a state at the bottom of the conduction band thus gaining some amount of energy ($x$eV), as illustrated in figure 5.5. Unfortunately, it is not possible here to calculate this energy contribution. It is thought, however, that in an insulator, such as α-$Cr_2O_3$, this energy will be no more than 2eV [109]. Thus, it seems that Ce will actually adopt a 3+ charge state in α-$Cr_2O_3$. As such, the result of Hagel and Seybolt actually relate to $Ce^{3+}$.

Formulation of a model that describes transport through α-$Fe_2O_3$ will clearly require further work. The present results are consistent with previous suggestions [105, 106] that variations in transport properties between samples are due to different impurity contents. That is, the results presented here for α-$Fe_2O_3$ and indeed all three host oxides suggest that the concentrations of those structural defects (vacancies and lattice ion interstitial species) that mediate transport will depend critically on the balance of impurities. Thus, to

some degree, the effectiveness of these oxide films as passive protection against further corrosion will be greatly influenced by impurity content. However, impurity content can lead to complex mechanisms as shown recently in stainless steel passive layers [110].

Unfortunately the literature is not conclusive as to which defects are important for transport. Nevertheless, it does seem that aluminium vacancies are mobile in $\alpha$-$Al_2O_3$ [77–79]. In $\alpha$-$Cr_2O_3$, chromium is believed to be mobile but the mechanism (via interstitial or vacancy) is disputed [80, 101, 102]. Again the host cation is believed to be mobile in $\alpha$-$Fe_2O_3$, possibly via an interstitial mechanism [82, 83, 103, 105, 106], although the valance state of the interstitial is not clear with respect to transport [105, 106]. It is possible to use atomistic techniques to make predictions of activation energies for migration (as demonstrated in chapter 4) and this would certainly be crucial to any continuation of the work presented here.

Finally a comment on isovalent impurity defects. Of course 3+ cations should not impact on the concentration of defects associated with transport in these materials. However,

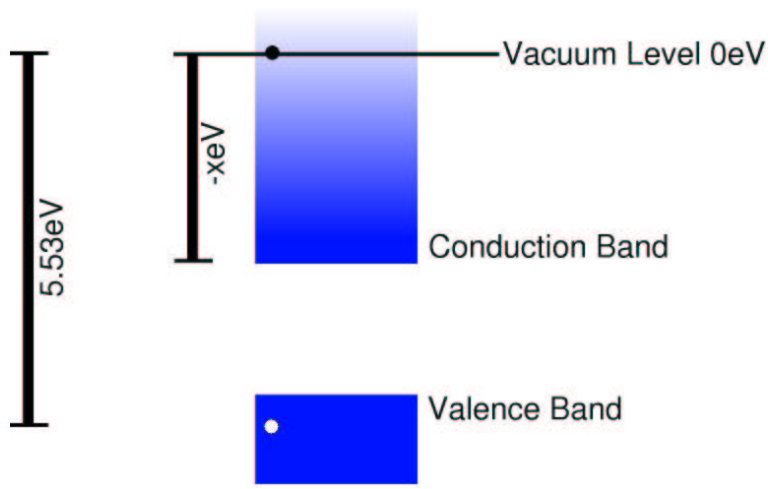


**Figure 5.5:** Representation of the ionisation process of $Ce_M^{\times}$ to $Ce_M^{\bullet}$ by an electron being removed to $\infty$, costing 5.53eV, and then falling to the bottom of the valence band, gaining some amount of energy (-xeV).

qualitatively at least, larger 3+ (and indeed 2+ and 4+) cation dopants have high solution energies and will contribute to the formation of grain boundaries and secondary phases. Either structure may be considered detrimental to corrosion protection and thus should be avoided.

Two uncertainties have prevented the alloy chemistry selection being made in a similar manner to that done for $NiF_2$. These are:

- uncertainty in the exact transport mechanisms responsible for passive layer growth.
- the likelihood that electronic defects, not considered here, may form in $\alpha$-$Cr_2O_3$ and $\alpha$-$Fe_2O_3$.

As such, more effort has been expended in exploring defect equilibria. Nevertheless, important relationships have been established which can be exploited in the future.

## 5.6 Further Work

In reality the structures of passive oxide films are clearly complex [110, 111] and reference to regular corundum structures assumed here cannot be expected to solve complex corrosion issues. The present work then forms the basis from which more complete systems can be modelled in the future. Further investigations should look at other structures that may exist on the surface of these aluminium and steel alloys. For example, a study of the defect chemistry of $Fe_3O_4$ using the potentials used here would be valuable. Studies of surface hydroxylation may also reveal important results. Such studies may include, for example, grain boundary structures which are known to influence the resistance of stainless steels to inter-granular corrosion and 'end grain' attack [112]. Furthermore valence changes of host cations (particularly $Fe^{3+} \rightarrow Fe^{2+}$) and the intrinsic electronic defects could also be included. The effect of negative ion species (i.e. $Cl^-$ and $S^{2-}$) may also

be possible to study as experience with describing these ions with pair potentials grows. Undoubtedly, new simulation techniques will be required to tackle all of these issues and such development is recommended.

As a direct extension of this work it would be interesting to investigate the intrinsic migration hop saddle-point energies. This could be done using the same technique as used for $NiF_2$ in chapter 4.

In this study only neutral clusters were considered, thus, simulation of charged cluster would be of interest. With this information the complex equilibria considered Lagerlöf and Grimes for $\alpha$-$Al_2O_3$ could be extended to $\alpha$-$Cr_2O_3$ and $\alpha$-$Fe_2O_3$.